LBL PUB-5263
SLAC-359
CALT-68-1622

INVESTIGATION
of an
ASYMMETRIC B FACTORY
in the
PEP TUNNEL

March 1990

Lawrence Berkeley Laboratory
1 Cyclotron Road
Berkeley, California 94720

Stanford Linear Accelerator Center
Stanford University • Stanford, California 94305

California Institute of Technology
Pasadena, California 91125

Prepared for the U.S. Department of Energy under Contract Numbers DE-AC03-76SF00098, DE-AC03-76SF00515, and DE-AC03-81-ER40050.

CONTENTS

Summary

This report addresses the feasibility of designing and constructing an asymmetric B-factory—based on the PEP storage ring at SLAC—that can begin operation at a luminosity of 3×10^{33} cm^{-2} s^{-1} and could ultimately reach even higher luminosity. Such a facility, operating at the $\Upsilon(4S)$ resonance, could be used to study mixing, rare decays, and CP violation in the $B\bar{B}$ system, and could also study tau and charm physics. The essential accelerator physics, engineering, and technology issues that must be addressed to successfully build this exciting and challenging facility are identified, and possible solutions, or R&D activities that will reasonably lead to such solutions, are described. Based on this study, it can confidently be concluded that:

- Using state-of-the-art storage ring technology, careful engineering, and a well-thought-out design philosophy, it is possible to begin immediately to design and then construct an asymmetric B-factory that can be operated, after its commissioning period, at a luminosity of 3×10^{33} cm^{-2} s^{-1}

- By keeping the design flexible and providing sufficient "parametric reach" it should be possible to upgrade the collider to reach even higher luminosity, approaching 1×10^{34} cm^{-2} s^{-1}

The investigations performed to date have been quite encouraging. A study of those issues that pertain to the high beam current requirements indicates that the anticipated problems are amenable to well-understood, albeit difficult, engineering solutions; no new phenomena have been uncovered that would lead to the need to develop entirely new technologies. A scheme for separating the closely-spaced beam bunches at the IP has been worked out in detail for the case of head-on collisions of round beams and shown to be feasible, and an alternative scheme based on a nonzero crossing angle scenario with crab-crossing also shows promise. Masking of the detector from the intense synchrotron radiation produced near the IP is not a completely solved problem as yet, although progress is being made in this regard. Feasibility proofs for new rf cavities and feedback systems have been worked out, and the vacuum and heat-load issues have been demonstrated to be solvable by straightforward application of modern storage ring vacuum system technology. An injection system design—using the existing SLC injection system—has been studied and shown to be adequate.

Successfully reaching our design goal requires R&D efforts in a few specialized areas. Primary topics that deserve further study include: high-power windows for delivering the rf power to the fewest possible number of rf cavities; high-power feedback systems to suppress multibunch instabilities; means to remove higher-order modes from the rf cavities and the power deposited into them; crab-crossing techniques; vacuum chamber designs capable of providing good vacuum in the presence of high synchrotron radiation power; and compact, high-gradient superconducting quadrupoles.

In addition to these technology issues, there are several accelerator physics issues where further work is needed. Foremost among these is the continuation of our efforts to understand quantitatively the behavior of the beam-beam interaction for asymmetric beam conditions.

The PEP storage ring is an ideal platform from which to launch an asymmetric B-factory facility, having a well-designed, flexible lattice with suitably long straight sections, a tunnel that permits the siting of a new low-energy storage ring without requiring extensive conventional facilities construction, and access to a powerful injector. These advantages, coupled with the existence—in close proximity—of a highly qualified and enthusiastic team of physicists from SLAC, LBL, LLNL, Caltech, and various University of California campuses, make this an ideal project for the SLAC site.

The design concept presented here provides an unprecedented opportunity for SLAC to extend the cutting edge of high-energy physics research and collider technology worldwide, and would make an ideal use of the PEP storage ring far into the future.

Foreword

In October 1989, LBL PUB-5244 (SLAC-352, CALT-68-1589), "Feasibility Study for an Asymmetric B Factory Based on PEP," was released. This report discussed extensively the technical issues that must be addressed in order to construct an asymmetric B factory running in the $\Upsilon(4S)$ energy region. Solutions, or approaches, to most of these technical problems were outlined, in the context of an example machine design consisting of a newly constructed 733-m circumference low-energy ring colliding with the high-energy PEP ring. At the same time, a companion report (SLAC-353, LBL-27856, CALT-68-1588), "The Physics Program of a High-Luminosity Asymmetric B Factory at SLAC," was issued.

Encouraged by the results of these studies, in December 1989 the Directorates of SLAC and LBL established a new one-year study whose goal is the design of a PEP-based machine with an energy asymmetry of 9 GeV $\times$ 3.1 GeV and a luminosity of 3×10^{33} cm^{-2} s^{-1}. This design study is being coordinated by A. Hutton at SLAC and M. Zisman at LBL; present members of the design team are listed on the following page. This group is now actively pursuing several promising approaches to the design of such a machine, and expects to provide its final design report in January, 1991.

A B factory of this general type is one of the most promising future options for the U.S. high-energy physics program, and thus is under serious consideration by the HEPAP Subpanel chaired by Frank Sciulli. The release of the present report, which is prompted by the visit to SLAC, on March 8–9, 1990, of the HEPAP Subpanel, is intended to provide background material for the Subpanel's deliberations.

In this report, we describe an alternative design example in which both the 9-GeV and 3.1-GeV rings are the same circumference and housed together in the PEP tunnel. Parameters have been chosen to achieve the required luminosity of 3×10^{33} cm^{-2} s^{-1}. The information contained here also serves to update the original Feasibility Study report in those areas where progress has been made in our understanding of the technical issues, e.g., improved masking schemes and an injection scheme based on the existing SLC injector.

The results of the study to date establish the feasibility of a scenario with both rings in the PEP tunnel, although the current design is far from optimized. Nonetheless, this document— together with LBL PUB-5244—serves to frame the issues involved in the design of a high-luminosity asymmetric collider and to record our progress towards a fully optimized design.

This report was prepared under the scientific editorship of M. Zisman (LBL); the technical editor was D. Vaughan (LBL); technical typing was ably carried out at LBL by M. Condon with assistance from D. Gonzales.

B-Factory Machine Design Team

- **California Institute of Technology**
  D. Hitlin; F. Porter

- **Lawrence Berkeley Laboratory**
  S. Chattopadhyay; Y.H. Chin; D. Dell'Orco; E. Forest; M. Furman; A.A. Garren; C. Hearty; A. Jacob; K. Kennedy; K. Kim; G. Lambertson; P. Oddone; M. Ronan; A. Sessler; C. Taylor; F. Voelker; M. Zisman

- **Lawrence Livermore Laboratory and University of California at Los Angeles**
  W. Barletta

- **Stanford Linear Accelerator Center**
  M. Allen; K. Bane; E. Bloom; F. Brenkus; K. Brown; J. Corbett; M. Cornacchia; D. Coupal; W. Davies-White; H. DeStaebler; M. Donald; J. Dorfan; I. Hsu; A. Hutton; T. Jenkins; W. Kozanecki; A. Lisin; G. Loew; R. Miller; P. Morton; J.-L. Pellegrin; T. Raubenheimer; J. Rees; D. Ritson; R. Ruth; A. Saab; W. Savage; H. Schwarz; J. Seeman; K. Thompson; H. Weidner; P. Wilson

- **IIRPA/University of California at San Diego**
  M. Sullivan

- **Fermilab**
  G. Jackson

- **University of Massachusetts**
  S. Hertzbach

- **Caltech Visitors**
  J. Tennyson

- **LBL Visitors**
  A. Zholents (INP, Novosibirsk)

- **SLAC Visitors**
  H. Fitze (Paul-Scherrer Institute, Zurich)

1. Introduction

The study of rare and CP-violating B-meson decays holds great promise as a fundamental probe of the Standard Model and whatever new physics may lie beyond it. An ideal way to carry out such a study is to construct a high-luminosity electron-positron collider to serve as a "B factory." The physics potential of such a facility is discussed in detail in a companion report.[1]

There are various possible approaches to the design of such an electron-positron collider, including storage-ring, linac-on-linac, and linac-on-storage-ring scenarios. At the present time, the linac-based approaches must be considered to be more speculative, since the technologies of linear colliders and high-power, high-repetition-rate, high-brilliance linacs are still in their infancy. Moreover, in the energy range of interest for a B factory, such alternatives do not seem to offer any significant advantages over storage-ring colliders, which correspond to a more straightforward extrapolation of the present state of the art. Consequently, the many major laboratories worldwide that are now enthusiastically pursuing the design of a high-luminosity B-factory, e.g., CESR at Cornell,[2] KEK in Japan,[3] INP at Novosibirsk,[4] Paul Scherrer Institute (now in collaboration with CERN) in Switzerland,[5] and DESY in Germany,[6] have uniformly focused on asymmetric storage-ring colliders.

Because of the rare decay modes that must be observed with good statistics to study CP violations, luminosity is of paramount importance in B-meson physics. The required luminosity for observing CP violation depends on several parameters of the Standard Model that are in a continuous state of refinement. This is discussed in some detail in Chapter Two of the companion report.[1] It appears that an integrated luminosity of ≥ 30 fb^{-1}/year is sufficient for asymmetric storage rings at the $\Upsilon(4S)$ resonance.[1,7] This integrated luminosity corresponds to a collider delivering 3×10^{33} cm^{-2} s^{-1} for 10^7 seconds.

A luminosity of 3×10^{33} cm^{-2} s^{-1} is more than one order of magnitude beyond that provided by existing electron-positron colliders, so a colliding-beam storage ring complex designed to reach luminosities in this range is a bold venture. It sets goals well beyond those that have been approached before, and

naturally suggests the question: Is it plausible that a machine with such high performance can be realized with storage ring technology as we now understand it? We believe the answer is yes. The task confronts us with challenges of many kinds, but we think we understand them well enough to attack them with a good hope of success. This conclusion is strongly supported in the Summary Report of the recent Workshop on Beam Dynamics Issues of High-Luminosity Asymmetric Collider Rings, held at the Lawrence Berkeley Laboratory, February 12-16, 1990.

1.1. Luminosity Requirements and Feasibility

The history of colliding-beam storage rings, since its inception in the 1950s, has offered a mixed bag of successes and disappointments. Many of the machines have reached their beam-energy goals, but some have fallen well short of their luminosity goals. On the other hand, most of the recent electron-positron rings have approached their design luminosities; CESR and BEPC (in a remarkably short time) have even exceeded their design luminosities. Most of these machines are of the single-ring variety in which one or a few bunches are stored in each beam and collide at a few interaction regions.

We recognize, of course, that the few attempts to use double rings and multiple bunches have been disappointing. Most relevant, perhaps, is DORIS as it was originally built at DESY. When DORIS came on line in 1973, difficulties were encountered due to the finite beam crossing angle (i.e., the beams met at an angle rather than head-on) and the large number of bunches in each beam. Although these problems were never completely overcome, and in the end DORIS was converted to a single-ring system, it is noteworthy that currents up to 0.75 A had been successfully stored in a single ring and currents of several hundred mA had been collided in the double-ring configuration. In interpreting these historical data, it is also important to remember the circumstances at the time. SPEAR had been running since 1972 and churning out data in an energy region that turned out to be exceptionally important; the "November revolution" was in the offing and the users at DORIS wanted to get on with the physics. Perhaps a more sustained effort could have solved more of the multibunch problems; we shall never know.

In any case, the physics of B mesons, and especially of their charge- and parity-violating decays, demands that colliding-beam systems of unprecedentedly high luminosity be created for their study. The laws of storage ring behavior force us to use large numbers of bunches in double rings whether we require asymmetric collisions or not. Thus, we are on the luminosity frontier rather than the energy frontier. SPEAR, DORIS, Petra, PEP, and LEP have pushed forward the energy frontier for electron-positron collisions; a B factory would drop back from the energy frontier but push forward the luminosity frontier.

Great strides have been made in the physics of beam instabilities and current limitations in the last decade, and we believe that

there is a good chance that we can achieve the demanding goals of B-meson physics. In this document we will show that—with innovative design approaches and suitable R&D efforts—*it is possible to design a collider that has sufficient design flexibility to begin operation, after its commissioning period, with a luminosity of* 3×10^{33} cm^{-2} s^{-1}, *and that, with ongoing development efforts, can ultimately achieve even higher luminosity*. With progressive R&D and with state-of-the-art technology applied in the initial implementation, construction of such a collider could begin very soon.

2. Collider Design Issues

In this section we discuss machine physics and engineering issues, as summarized previously, that guide and constrain the APIARY design.

2.1. Luminosity

The general expression for luminosity in an asymmetric collider is cumbersome, involving various parameters of both beams at the IP. To simplify the choices, and to elucidate the general issues of luminosity for all B factories, it is helpful to express the luminosity in an energy-transparent way. Here we express luminosity in terms of a single, common beam-beam tune shift parameter, ξ, along with a combination of other parameters taken from *either* the high-energy (e^-) or the low-energy (e^+) ring, irrespective of energy.

With a few plausible assumptions (e.g., complete beam overlap at the IP and equal beam-beam tune shifts for both beams in both transverse planes) such parameters as energy, intensity, emittance, and the values of the beta functions at the IP may be constrained to satisfy certain scaling relationships. (Details of our approach are presented in Appendix A.) It then becomes possible to express luminosity in a simple, energy-transparent form:[8]

$$\mathcal{L} = 2.17 \times 10^{34}\, \xi\, (1 + r) \left(\frac{I \cdot E}{\beta_y^*} \right)_{+,-} \quad [\mathrm{cm}^{-2}\, \mathrm{s}^{-1}] \qquad (2.1\text{–}1)$$

where

- ξ is the maximum saturated dimensionless beam-beam interaction parameter (the same for both beams and for both the horizontal and the vertical transverse planes)
- r is the aspect ratio characterizing the beam shape (1 for round, 0 for flat)
- I is the average circulating current in amperes
- E is the energy in GeV
- β_y^* is the value of the vertical beta function at the IP in cm

The subscript on the combination $(I \cdot E/\beta_y^*)_{+,-}$ means that it may be taken from either ring.

In this report, the scaling relations derived in Appendix A are used to produce self-consistent sets of parameters. After a few basic parameters are chosen, such as the energies, the currents, the aspect ratios, and the lowest beta value at the IP for either ring, most of the other parameters, including the luminosity $\mathcal{L}$, will follow. To a certain extent, the choice of which parameters should be specified and which should be derived is arbitrary. Nonetheless, as discussed below, there are many practical considerations that limit the degrees of freedom in maximizing the luminosity.

Energy. The energies, $E_{+,-}$, are not entirely free parameters; they are constrained kinematically. To take advantage of the cross section enhancement at the $\Upsilon(4S)$ resonance, the collider center-of-mass energy must be 10.58 GeV. Precise determination of the decay vertices with a reasonable detector geometry then limits the energy ratio to the range of about 1:3 to 1:5. Our simulations of the beam-beam interaction (see below) argue for approximately equal damping time per collision ("damping decrement") in the two rings, which is more easily accomplished when the energy asymmetry is reduced. Taken together, these considerations lead to an optimum energy of the high-energy beam of $E \approx 8$–12 GeV, and the corresponding energy of the low-energy beam is thus $E \approx 3.5$–2.3 GeV. For this design study, we have adopted a low asymmetry, that is, $E_- = 9$ GeV and $E_+ = 3.1$ GeV.

Beam-beam tune shift. The beam-beam tune shift parameter ξ is not really a free parameter; it is determined intrinsically by the nature of the beam-beam interaction. The range of maximum beam-beam tune shifts achieved in existing equal-energy e^+e^- colliders is $\xi \approx 0.03$–0.07. A typical choice would be $\xi = 0.03$; this value is the basis of our luminosity estimates. Insofar as considerably higher tune-shift values than this have already been observed in higher energy collisions at PEP, we consider this value to be quite justifiable. There is some indication from computer simulations[9] that ξ may depend intrinsically on the beam aspect ratio; in other words, that $\xi = \xi(r)$. This is a controversial issue, now being debated, but it is certain that an enhancement in ξ (for round beams) of at best a factor of two can be obtained. In the luminosity estimates made here, we did not take this possible enhancement into account; that is, we took $\xi = 0.03$, independent of r.

One implication of this tune-shift limitation is that increased luminosity must perforce come from decreasing the bunch

spacing s_B —that is, increasing the number of bunches. The push towards small bunch spacing has a significant impact on the design of the IR, which must separate the beams sufficiently to avoid unwanted collisions, and it also exacerbates the problem of coupled-bunch beam instabilities.

Beam aspect ratio. The aspect ratio, r, is free to the extent that one can create round beams. However, the physics of the beam-beam interaction is sensitive to the method (coupling resonances, vertical wigglers, etc.) that is used to make the beams round. Although the use of coupling resonances is a straightforward way to obtain a round beam, it is not clear that applying such a constraint in tune space—where the nonlinear effects of the beam-beam interaction manifest themselves—is the best thing to do. The use of wigglers or phase plane rotators offers the potential advantage of giving round beams via a noiselike excitation that should not correlate with the subtleties of the nonlinear tune-space behavior.

In the low-energy ring, one can imagine the practical use of wigglers to create a large vertical emittance corresponding to r = 1. In the case of the high-energy ring, where the synchrotron radiation emission in the horizontal bending magnets is already very large, the addition of sufficient wigglers (in an intentionally created vertically dispersive region) to produce a round beam is nontrivial although it is certainly conceptually possible. This technique may, however, be impractical from the viewpoint of synchrotron radiation power. Therefore, optics changes (via skew quadrupoles) are likely to be the preferable way to create round beams in the high-energy ring. In any case, we take the maximum enhancement from the use of round beams to be only a geometric factor of two—that is, r = 1 gives (1+ r) = 2 in Eq. (2.1–1).

Beam intensity. The average beam current, I, is a relatively free parameter, but not absolutely so. It is determined by various current-dependent coherent effects. The storage rings will have to accept the chosen currents, given certain impedances in the paths of the beams. There are several intensity-dependent issues with which we must be concerned:

- Longitudinal microwave instability, which causes individual beam bunches to grow both in length and in momentum spread; both the resultant center-of-mass energy spread and the increased bunch length can reduce the effective luminosity

- Transverse mode-coupling instability, which limits the maximum current that can be stored in a single beam bunch
- Touschek scattering, which causes particle loss (from large-angle intrabeam scattering) and reduces the beam lifetime
- Coupled-bunch instabilities, which, unless controlled by feedback, can lead to unstable longitudinal or transverse motion and thus to either beam loss or luminosity loss
- Synchrotron-radiation-induced gas desorption, which can lead to very high background gas pressure and thus to beam losses from gas scattering
- Synchrotron radiation heating of the vacuum chamber wall, which can lead to melting of the chamber if the power density is sufficiently high

Based on our present estimates, the issues of most concern to the APIARY design are coupled-bunch instabilities (driven by parasitic higher-order modes of the rf system); synchrotron-radiation heating; and synchrotron-radiation-induced gas desorption. To deal with the first issue, we propose a modern, low-impedance rf cavity design (either superconducting or room temperature). The problems arising from synchrotron radiation will require innovations in vacuum chamber design, but should be manageable if sufficient care is taken in engineering. These problems will be discussed later in this document.

Beta function at the IP. The beta function at the IP, β_y^*, is a free parameter and is easily variable down to a few centimeters, subject to the bunch-length condition $\sigma_\ell \leq \beta_y^*$. As the beta functions are reduced, however, it becomes more difficult to maintain the required short bunches. Either the rf voltage becomes excessive or the IR optics become unmanageable due to the difficulty of refocusing the beam quickly enough to avoid very large beta functions elsewhere in the ring. For this stage of the design, we consider a bunch length of $\sigma_\ell = 1$ cm to be a sensible target value, which then restricts the value of β_y^* to the range of 2–3 cm.

From Eq. (2.1–1), it is clear that the luminosity is maximized by high currents, low β_y^*, and round beams. What are the implications regarding these parameters for a luminosity goal of 3×10^{33} cm^{-2} s^{-1} ? Following a conservative route, we plan initially to consider a typical low β_y^* of a few centimeters;

$\xi \approx 0.03$; and round beams ($r = 1$). These choices imply an average circulating current, I, of several amperes. This is the approach we envision at this point. If the intrinsic maximum tune shift were truly enhanced for round beams, another twofold improvement in luminosity could be expected. On the other hand, we also intend to examine the relative merits of using flat beams and a reduced value of β_y^* to achieve the required luminosity.

An alternative—and much more speculative—approach could employ an extremely low β_y^* of a few mm, implying the need for a beam current of only a few hundred mA to reach our luminosity goal. The hardware issues involved in producing such a low β_y^* are nontrivial. More importantly, submillimeter bunch lengths would be needed as well, since the luminosity degrades unless $\sigma_\ell \leq \beta_y^*$. One way of producing ultrashort bunches is to use a zero-momentum-compaction ($\alpha = 0$) isochronous ring in which the particle path length is independent of energy.[10,11] Bunch length is then determined solely by injection conditions. However, one needs not only a very precise "zero" value for the momentum compaction, but also good control of the effects of higher-order, nonlinear momentum-compaction coefficients. To build such a ring would be quite challenging, requiring substantial technology R&D in precise control of magnetic fields. Studies along these lines are under way, but for now we favor the more traditional and conservative approach outlined above.

2.2. Beam-Beam Interaction

The attainable luminosity in the APIARY collider will be determined to a large extent by the physics of the beam-beam interaction. Nothing is known experimentally about the "beam-beam tune-shift limit" under asymmetric energy conditions. The situation is complicated, since two beams with unequal energies naturally tend to behave differently. Indeed, what is often observed in computer simulations is that one beam blows up badly while the other beam suffers practically no blowup. This is a serious problem, since the significant blowup in the weaker beam imposes an unnaturally low beam-beam tune shift limit on the stronger beam.

Probably the best cure is to bring the beam-beam interaction into the "strong-strong" regime where the two beams blow up in a similar manner, reducing the beam-beam force on both beams simultaneously. In this way—putting the two beams on an equal footing as far as transverse dynamics is concerned—we might expect to reach the same maximum beam-beam tune shift limit set by nature in equal-energy colliders. Such circumstances, if they can be created, would provide the best possible rationale for the design of an asymmetric collider based on the only fact we know about the actual behavior of the beam-beam effect under symmetric conditions—the beam-beam tune shift limit, ξ, in equal-energy electron-positron colliders.

The beam-beam interaction in the strong-strong regime is not well understood in a quantitative sense at present. The only systematic tool to understand it is provided by computer simulations. Consequently, one must allow for the maximum possible flexibility and freedom in adjusting those parameters which, as indicated by numerical simulations and critical wisdom, will affect luminosity. Such parametric flexibility will be essential in tuning the collider to the highest tune-shift limit and therefore the highest luminosity. One may need to vary the beam emittances, sizes, and shapes (aspect ratios), as well as the damping decrement (damping rate per collision), in order to optimize luminosity.

Numerical simulations suggest that an asymmetric collider should have a parametric reach up to the "asymmetric energy transparency domain," where both beams have identical values for each of the parameters listed below.

1. Linear beam-beam tune shift parameter:

$$\left(\frac{\beta^-}{\beta^+}\right)\cdot\left(\frac{\gamma^+N^+}{\gamma^-N^-}\right) = 1 \qquad (2.2\text{–}1)$$

2. Cross sectional area at the IP:

$$\sigma^+ = \sigma^- \qquad (2.2\text{–}2)$$

(and possibly equal emittance values also).

3. Radiation damping decrement per collision:

$$\lambda^+ = \lambda^- \qquad (2.2\text{–}3)$$

where the damping decrement, $\lambda = \gamma_{SR}\tau_C$, is defined as the product of the absolute radiation damping rate γ_{SR} (s^{-1}) and the time interval τ_C (s) between collisions.

4. Betatron phase modulation due to synchrotron motion:

$$\left(\frac{\sigma_\ell Q_s}{\beta_y^*}\right)^+ = \left(\frac{\sigma_\ell Q_s}{\beta_y^*}\right)^- \qquad (2.2\text{–}4)$$

where σ_ℓ is the rms bunch length and Q_S is the synchrotron tune.

With parameters constrained by these four conditions, the two unequal-energy beams behave identically in our simulations as far as beam-beam effects in the transverse plane are concerned—they evolve dynamically in a similar manner and saturate to the same ξ value. If the conditions above are not satisfied, the two beams settle quickly to a "weak-strong" situation.

To demonstrate the validity of these criteria (by showing that they maintain symmetric behavior in the case of asymmetric beam energies), we apply a modified version of Yokoya's beam-beam simulation program[12] to a situation in which a PEP beam at 12 GeV collides with a 2 GeV beam from a small ring. (This scenario, an early version of the present design, is referred to as APIARY-I.) Yokoya's program tracks particles in a bunch subjected to various localized disturbances, including rf energy kicks; radiation losses; random energy kicks due to photon emission; and a series of motions representing one turn around

the storage ring—a linear rotation of betatron phase in a half-arc, followed by a nonlinear beam-beam kick in the transverse plane (derived from the integrated force of a Gaussian beam), and again a half-arc of linear betatron phase rotation (thus completing the full-turn map).

For the studies reported here, Yokoya's program has been modified to track unequal-energy beams and to include a thick-lens beam-beam force in its simulations. The thick-lens modification was motivated by Siemann's recent finding[9,13] that the betatron phase advance during the collision may give non-negligible effects in beam blowup when the beta function at the interaction point, β^*, becomes comparable to the bunch length. Siemann concluded that it is necessary to treat the beam-beam interaction as a thick element. We incorporate this thick-lens approximation into Yokoya's program by distributing beam-beam kicks into five longitudinally different positions and letting particles drift between them. The rms beam sizes of the incoming beams are assumed to be unchanged during the collision in this approximation.

Simulation Results

The main parameters of the original APIARY-I lattice (used in the simulations described in this section) are shown in Table 2.2–1 below.

Table 2.2–1. Main parameters of the original APIARY-I collider

	Low energy	High energy
Energy, E [GeV]	2	12
Circumference, C [m]	155.3	2200
Number of bunches, k_B	6	81
Emittance, ε_x [nm·rad]	300	100
Bunch length, σ_ℓ [mm]	27.7	16.2
Transverse damping time, $\tau_{x,y}$ [ms]	16.3	15.6
Beta functions at IP		
β_x^* [cm]	25.4	76.2
β_y^* [cm]	2.54	7.62
Bunch current I_b [mA]	89.1	3.3
Nominal beam-beam tune shift		
ξ_{ox}	0.05	0.05
ξ_{oy}	0.05	0.05
Luminosity, $\mathcal{L}$ [$cm^{-2}\,s^{-1}$]	5×10^{32}	

These parameters satisfy the four important criteria discussed earlier. The next few pages discuss how each criterion is satisfied.

Criterion 1: same cross-sectional area at IP:

$$\sigma_{x,-} = \sigma_{x,+}$$
$$\sigma_{y,-} = \sigma_{y,+}$$

Criterion 2: same nominal beam-beam tune shift:

$$\xi_{ox,-} = \xi_{oy,-} = \xi_{ox,+} = \xi_{oy,+} \ ,$$

where the quantities of the low- and the high-energy rings are denoted by the subscripts + and -, respectively.

With these parameters, the beam-beam kicks are equalized in the two rings; any difference in beam dynamics should come from the difference of beam parameters elsewhere in the rings. The computer simulation results for this case are summarized in Figs. 2.2–1 and 2.2–2.

Note that a subscript of zero beneath the tune shifts and beam sizes denotes a *nominal* value determined at the input of the simulation program, in the absence of the beam-beam interaction. The beam-beam simulation modifies these parameters, which settle down to their saturated values. These saturated values, which we refer to as the *dynamic* tune shifts and beam sizes, are written without the subscript zero.

Figure 2.2–1a shows the rms beam sizes as a function of the nominal beam-beam tune shift, ξ_o. One can see that the low-energy beam blows up badly in the vertical plane, while the high-energy beam is practically unperturbed.

Fig. 2.2–1b shows the dynamic beam-beam parameter, ξ, as a function of ξ_o. Reflecting the vertical blowup of the low-energy beam, the tune-shifts ξ_- of the high-energy beam are suppressed to small values, e.g., $\xi_{y,-} < 0.008$. Note that, at low tune shifts, the luminosity goes up in proportion to the square of the beam current; this phenomenon is followed by a linear rise before saturation.

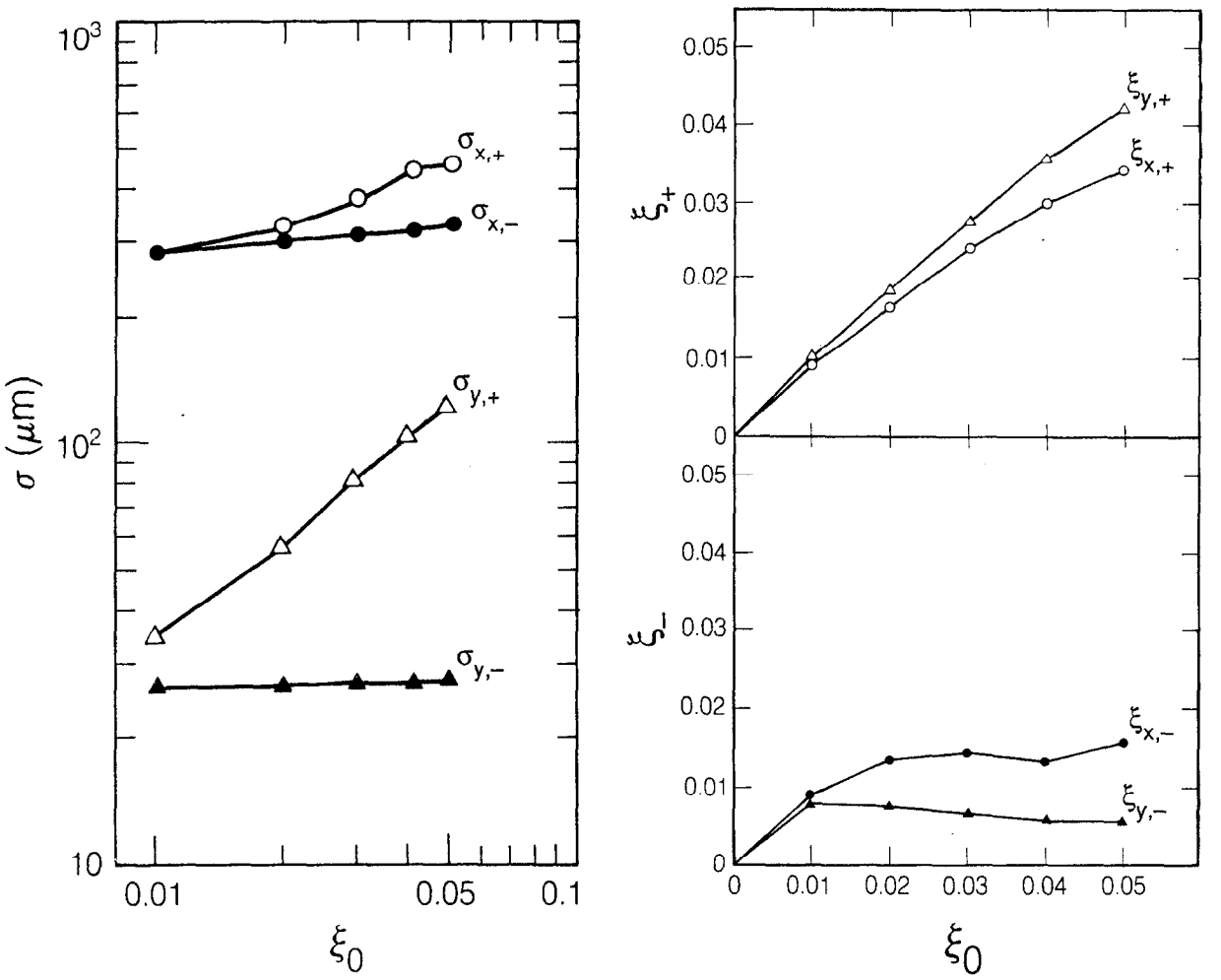

XBL 902-6277

Fig. 2.2-1a (left). RMS beam sizes predicted for nominal APIARY-I parameters.
Fig. 2.2-1b (right). Dynamic beam-beam parameters ξ as a function of ξ_0 for the original APIARY-I lattice parameters.

The actual luminosity at $\xi_0 = 0.05$ drops by a factor of 5 from the design value, as shown in Fig. 2.2–2 below.

In Quest of the Strong-Strong Situation

In the course of numerous simulations we achieved—by trial and error—identical behavior of two beams with unequal energies. Because we do not have enough space to describe all the attempts, we present here only the main results that lead to the asymmetric energy transparency condition.

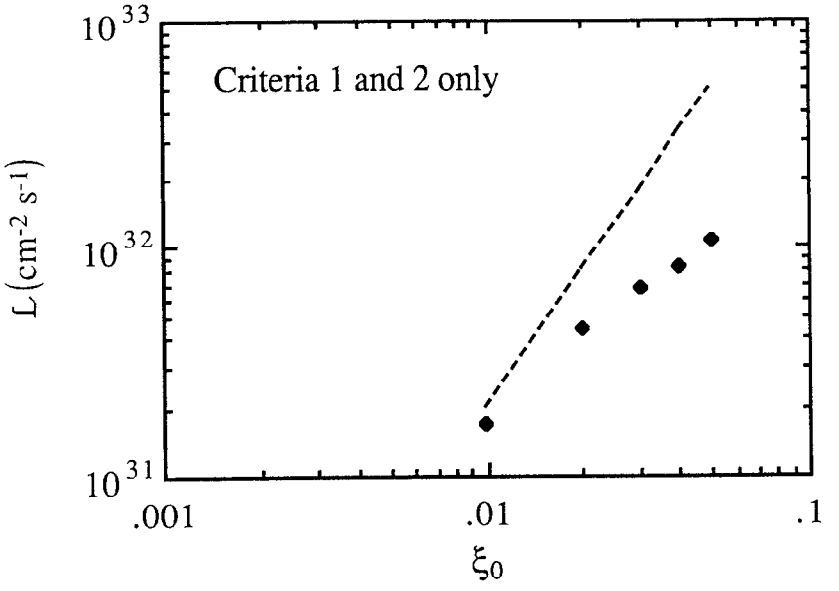

Fig. 2.2–2. Luminosity as a function of ξ_0 for the original APIARY-I lattice parameters.

Criterion 3: same damping decrement.

Synchrotron-radiation damping is an important effect that suppresses external perturbations of beams. There is some evidence[14] that the larger the damping rate, the larger the beam-beam limit will be. Thus, there is a potential benefit to being able to increase the damping rate of the weakly damped low-energy beam. From Criterion 2, the strength of the beam-beam kick per turn is equal in the two rings. However, the number of kicks *per damping time* is different for the nominal APIARY-I parameters: the low-energy beam receives about 14 times more kicks than the high-energy one. Therefore, the low-energy beam is subjected more to the beam-beam interaction, which may partially explain the asymmetric behavior of the two beams shown in Fig. 2.2–1.

Figure 2.2–3a shows the rms beam sizes when the damping decrement of the low-energy beam is increased to the same value as that of the high-energy beam. Now, the vertical blowup of the low energy beam is reduced significantly compared with that in Fig. 2.2–1. The dynamic beam-beam parameters, ξ_+ and ξ_-, are plotted in Fig. 2.2–3b as a function of ξ_0. The horizontal ξ values behave almost identically, and the saturating value of $\xi_{y,-}$ is increased to about 0.017. The luminosity is shown in Fig. 2.2–4 as a function of tune shift; although improved, it still falls short of the design luminosity.

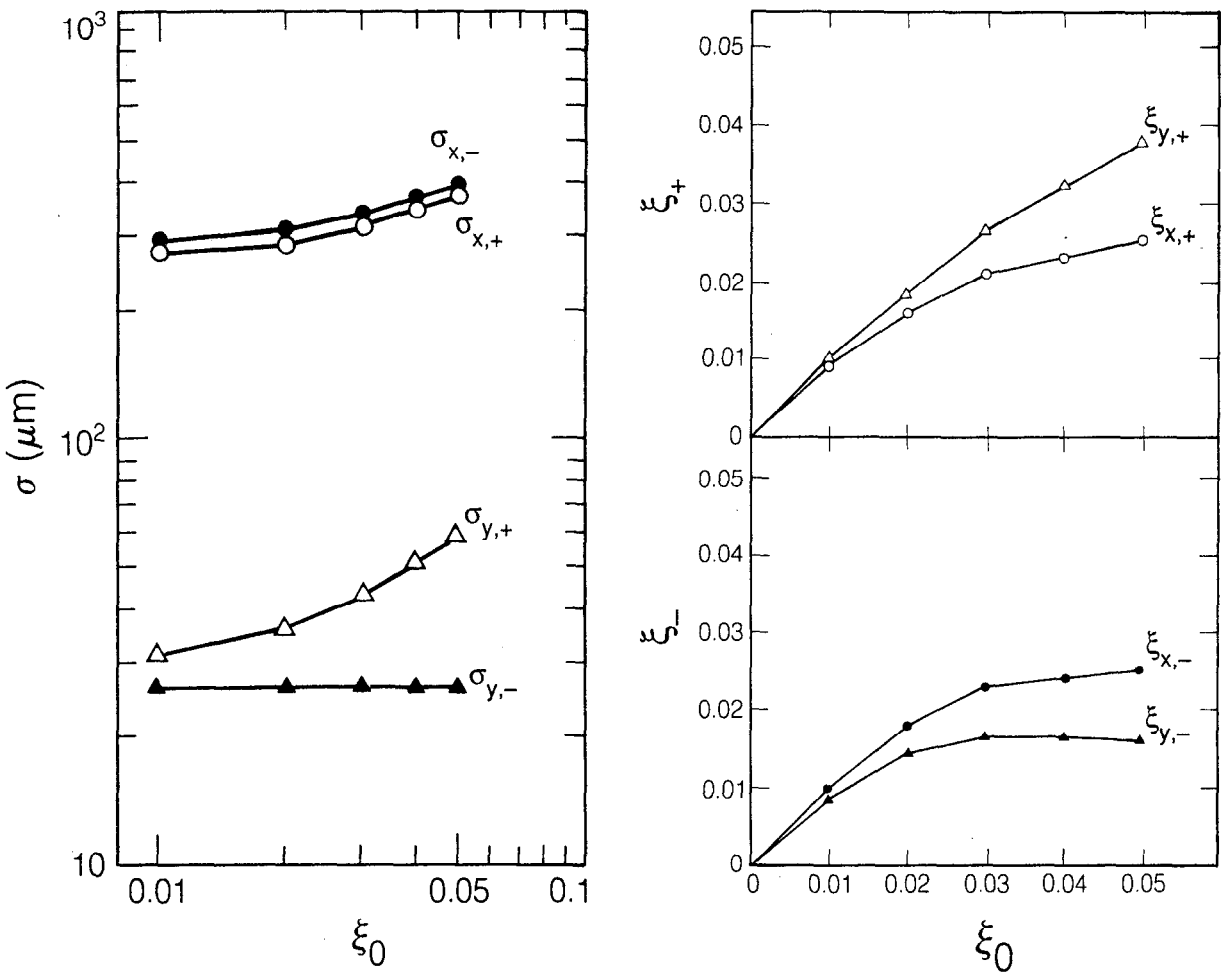

Fig. 2.2-3a (left). RMS beam sizes when the two rings have the same damping decrement.
Fig. 2.2–3b (right). *Dynamic beam-beam parameters ξ as a function of ξ_0. The two rings have the same damping decrement.*

Criterion 4: Same betatron phase modulation due to synchrotron motion (with possibly the same synchrotron tune).

A particle with a longitudinal displacement s from the center of the beam collides with the center of the incoming beam not at the designed IP but at a position longitudinally shifted by s/2. This actual collision point moves, turn by turn, because the particles execute synchrotron oscillations. Thus, the betatron phase advance per turn is also oscillating. This may excite synchrobetatron resonances, which may reduce the beam-beam limit substantially when β^* becomes comparable to the bunch length σ_ℓ. The amplitude of the tune modulation is given[15] by $\sigma_\ell Q_S/\beta^*$, where Q_S is the synchrotron tune. Figure 2.2–5 shows the simulation results when the values of $\sigma_\ell Q_S/\beta^*$ are equalized in the two rings by adjusting σ_ℓ and Q_S. The betatron tunes are also set equal in the two rings. From Fig. 2.2–5b, it

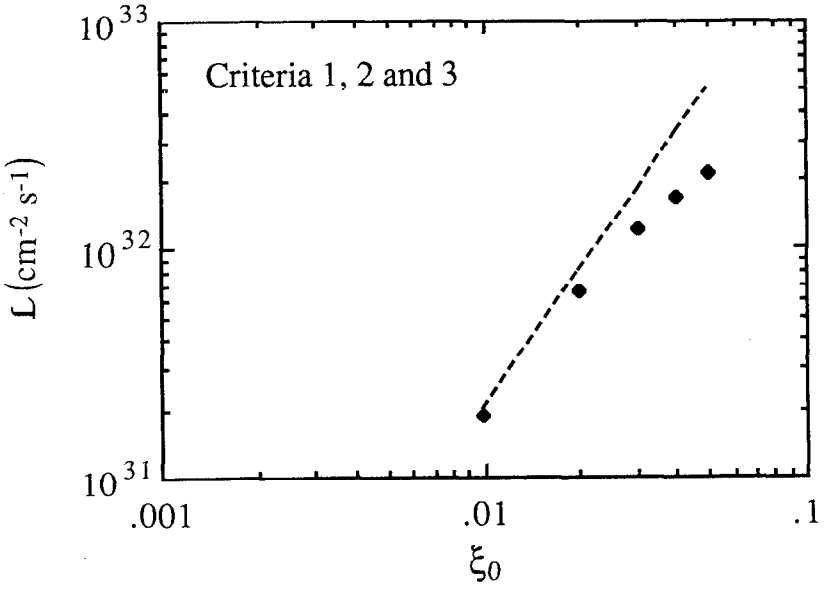

Fig. 2.2–4. Luminosity as a function of tune shift for the original APIARY-I lattice parameters.

can clearly be seen that the beam behavior has been almost equalized. Now, the beam-beam tune shift limit comes horizontally, but no saturation of ξ_x is observed.

Figure 2.2–6 shows the corresponding luminosity trend, which nearly reaches the design luminosity at $\xi = 0.05$.

Coherent Effects

Thus far, we have studied the incoherent effects of the beam-beam interaction upon the colliding beams. However, beam-beam interactions can also excite *coherent* beam oscillations, which may become unstable in some regions of the tune diagram ("stopbands"). The dominant coherent effect is dipole motion of the center-of-mass of the beam;[16] the existence of this phenomenon has been well established experimentally. It leads to instability under any of the following resonance conditions:

$$(k_{B,+}\nu_+ + k_{B,-}\nu_-) = \text{integer},$$

$$2\nu_- = \text{integer},$$

$$2\nu_+ = \text{integer}.$$

Here, k_B is the number of bunches in the ring, ν is the betatron tune, and the subscripts + and - indicate which ring is being

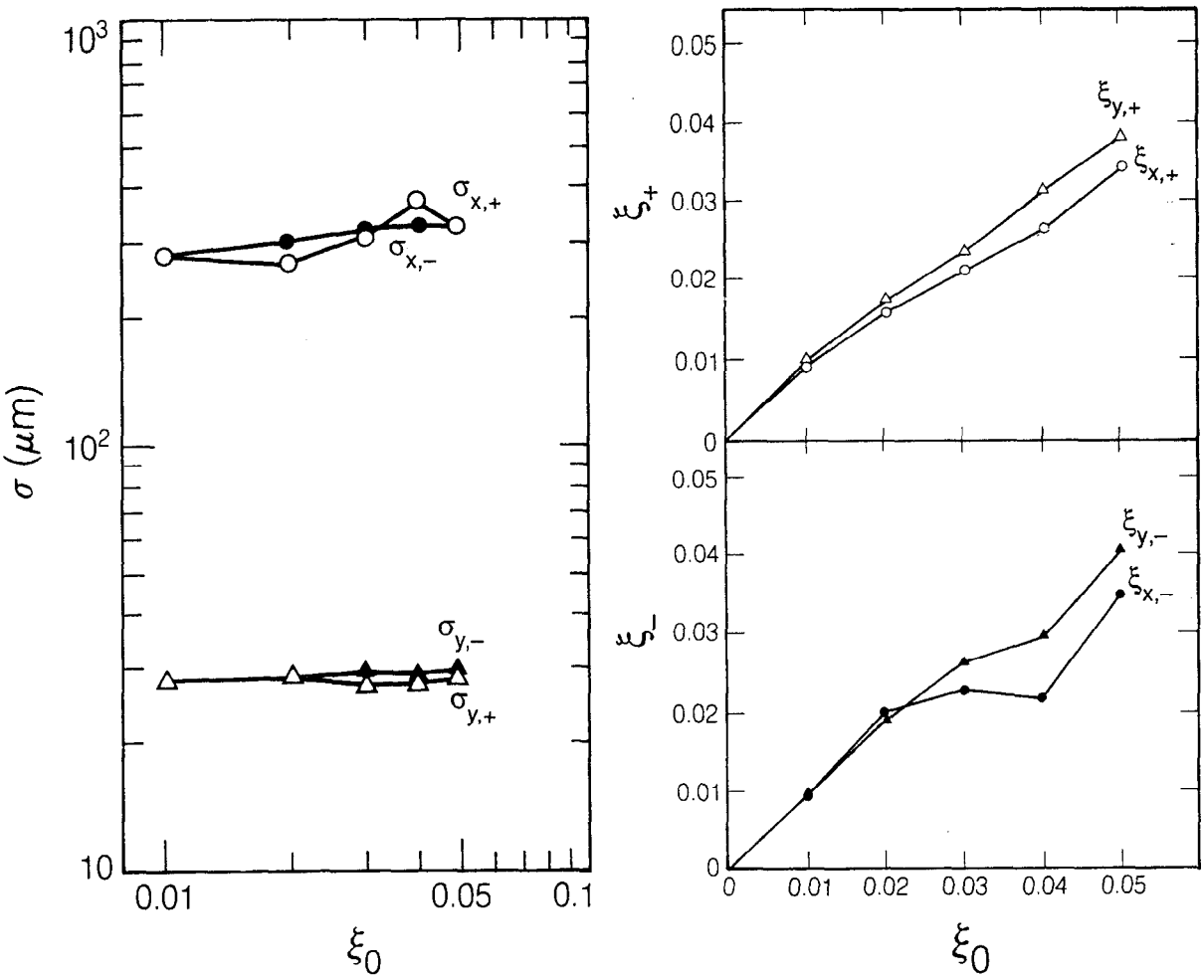

XBL 902-6278

Fig. 2.2-5a (left). *RMS beam sizes when all four criteria have been satisfied.* ***Fig. 2.2–5b (right).*** *Dynamic beam-beam parameters ξ as a function of ξ_0 when all four criteria have been satisfied.*

referred to. (A common factor has been removed from these equations.)

Figure 2.2–7 shows the stopband in (ν_+,ν_-) tune space due to coherent dipole oscillations for the case $(k_{B,+},k_{B,-}) = (1,1)$. The beam-beam tune shift parameter is set equal to 0.03, the value adopted for the present design, to be described in Section 3. Numbers mark the pairs of tunes where the growth rate of the most unstable dipole mode exceeds the radiation damping rate; the blank areas denote stable regions. The case $(k_{B,+},k_{B,-}) = (1,1)$ gives a large stable area (55% of the total tune space). (We note for comparison that a less-favorable case of $(k_{B,+},k_{B,-}) = (1,3)$ still provides stable areas large enough—45% of the total tune space—to allow scanning of the operating point without difficulty.)

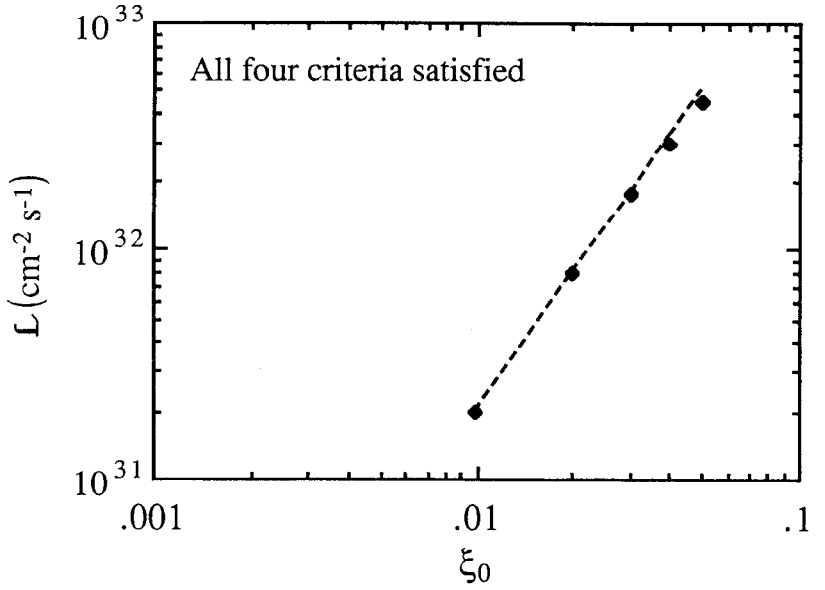

Fig. 2.2–6. Luminosity as a function of ξ_0 when all four criteria have been satisfied.

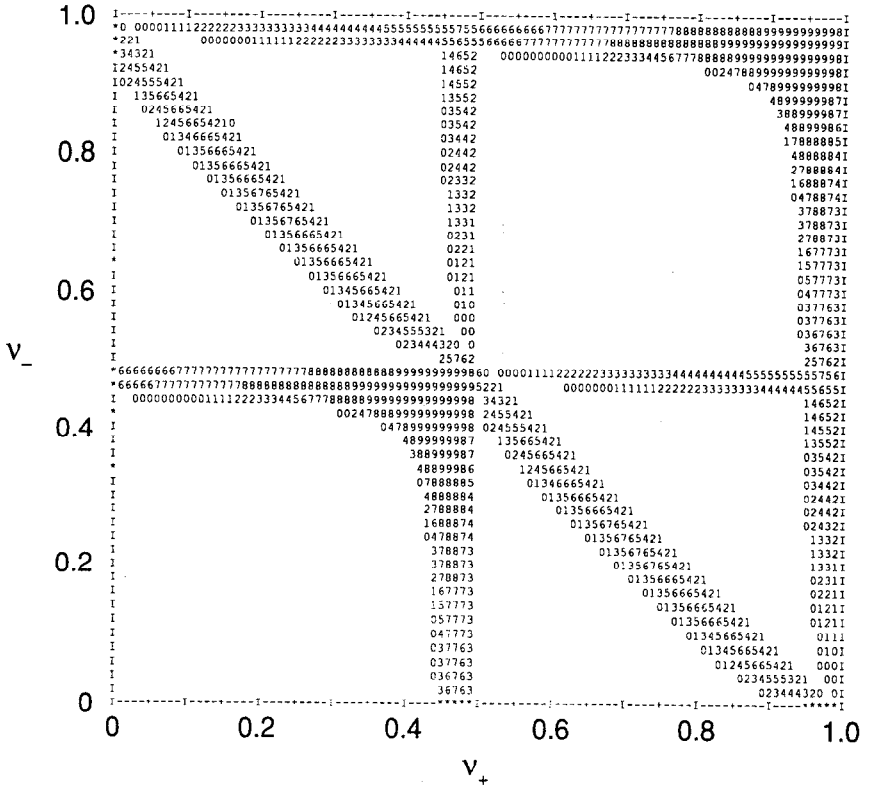

Fig. 2.2-7. The stopbands for coherent dipole beam-beam modes in the tune space of the collider for equal numbers of bunches in both rings.

2.3. Summary of Beam-Beam Studies and Their Implications

We have shown that, if the four criteria given here are all satisfied, two beams of unequal energies should evolve in a similar manner dynamically. It may also be desirable to equalize other parameters, like the emittances and the beta functions at the IP, to ensure full overlap of the bunches in the interaction region. We note that if the synchrotron radiation takes place only in the normal bending magnets of the lattice, the same emittance cannot be compatible with the same damping decrement. A solution to this dichotomy, which is also desirable from the vacuum and beam lifetime points of view, is to use a "wiggler lattice," in which wigglers are distributed along the ring to produce and control the synchrotron radiation.

The simulations described above argue for the idea of symmetrizing both the lattices and the beams of an asymmetric collider, and they show how this regime should be within the parametric reach of the design in order to credibly ensure its performance. At present, when there are no existing asymmetric colliders, it is not known how strictly the four criteria outlined above must be satisfied, or how much they can be relaxed in real machines. For example, the question arises whether one could relax such strong constraints by compensating for one asymmetry with another (e.g., compensating for unequal damping decrements with unequal beam intensities). The answer is not straightforward. While such a scenario might be plausible, we raise several concerns:

- There is evidence[17] that the stability of such a delicately compensated beam-beam mode would be unpredictable. The situation is expected to be "touchy" and could bifurcate easily into a weak-strong situation at high tune shifts.

- Beam intensity is not really a "knob" that can be adjusted freely and easily. The rings must be designed to accept the desired currents. In general, more current would have to be put into the low-energy beam. This is undesirable from a coherent-stability point of view.

For these reasons, we consider the flexibility of symmetrization of both the lattice and the beam to be a safer path towards optimizing the luminosity. Therefore, the wiggler lattice concept, which allows for extra flexibility in adjusting the lattice parameters, has been adopted presently. Elsewhere in this

report we describe such a lattice and justify its selection for the APIARY design.

It is clear that the conclusions from these beam-beam simulations will have major implications for the design of the low-energy ring. It is natural, then, to question the credibility of the simulation. To address this question, we have simulated—without prior knowledge of the actual experimental results—various known luminosity configurations of PEP with various sets of conditions given to us by the PEP machine group.

As an example, we studied the particular PEP configuration summarized in Table 2.3–1. We find that our luminosity

Table 2.3–1. PEP parameters used in simulation comparison.[a)]

Betatron tunes	
Horizontal	21.2962
Vertical	18.2049
Beta functions at IP	
Horizontal [m]	1.342
Vertical [m]	0.053
Dispersion at IP	
Horizontal [m]	0.00049
Emittances	
Horizontal [nm·rad]	99.6
Vertical [nm·rad]	3.96
Synchrotron tune	0.043
Beam current [mA]	18.85
Nominal beam-beam parameter, ξ	
Horizontal	0.04653
Vertical	0.04653
Luminosity	
Nominal [$cm^{-2}\ s^{-1}$]	5.07×10^{31}
Observed [$cm^{-2}\ s^{-1}$]	4.80×10^{31}
Simulation[b)] [$cm^{-2}\ s^{-1}$]	4.34×10^{31}

a) Data from E. Bloom and M. Donald.

b) Using same simulation code used here for estimates for the APIARY collider.

prediction agrees with the measured value to within 10%. In fact, our results are actually pessimistic compared with the observed result, that is, our simulation predicts a value 10% *below* the observed luminosity. We also predict from the simulations that there will be no saturation of the dynamic beam-beam tune-shift parameter, ξ, up to a beam current of 30 mA—again in agreement with experimental observations. Calculations for other PEP configurations yield more or less equivalent agreement with the observed luminosities.

Insofar as the simulation predictions are consistent in trend with the actual PEP observations (and are even slightly pessimistic), we feel that they have withstood at least some test of fidelity.

2.4. Constraints on the Low-Energy Ring Design

A number of constraints are imposed upon the design of the low-energy ring by various beam-dynamics and technological issues. The constraints would be particularly severe if the design were based on bending magnets and focusing elements alone. The damping decrement (damping time per collision), which should be kept as large as possible, varies with E^3/ρ, where ρ is the bending radius. For a 3:1 energy asymmetry, requiring the low-energy ring to have the same damping decrement as the high-energy ring leads to a low-energy ring with a very small bending radius and thus a very high bending field. Although the bending field (up to 1.8 T for a 300-m, 3-GeV ring in a typical PEP-based scenario) is achievable, such a design has some severe drawbacks:

- A pure bending magnet design gives up crucial flexibility with regard to adjusting the damping decrements and the beam emittance, both of which are largely fixed by the lattice. This inflexibility contradicts a basic premise of our design approach.

- If the high-energy ring is quite large and the low-energy ring is small, there is a great disparity in the number of beam bunches in the two rings. According to our understanding of the coherent dipole beam-beam modes, this situation could lead to instabilities and is therefore best avoided.

- The synchrotron radiation power density on the vacuum chamber wall along the path of the beam's synchrotron radiation fan can exceed 10 kW/cm^2 in a small ring—beyond the value generally tolerated by existing vacuum chamber designs. It is important to identify straightforward means of dealing with such a high power density without risking severe damage to the chamber. Degradation of the vacuum under these conditions is also a serious concern.

- The luminosity lifetime in a small ring is lower than in a bigger ring producing the same luminosity, because the number of particles (which are unavoidably lost at a constant rate because of the beam-beam collisions themselves) is reduced.

In order to deal with the issues above, it is very beneficial to equalize the circumferences of the high- and low-energy rings. By doing so, we can load the two rings with equal numbers of bunches, thus avoiding difficulties with coherent beam-beam modes. A large low-energy ring permits a lower bending

magnet field and a larger circumferential length over which the synchrotron radiation power is absorbed by the vacuum chamber, thus reducing the power density to manageable levels. If nothing else were done, however, the price of going to a larger low-energy ring would be a lower radiation damping decrement, which is undesirable.

For these reasons, we have adopted here an alternative that should give the best of both worlds—we utilize a large (2200 m circumference) low-energy ring, and then provide wigglers to permit independent control of the damping decrement and the horizontal and vertical emittances. Indeed, in our concept, the "natural" properties of the low-energy ring lattice (emittance, momentum spread, radiation damping times) are *dominated* by the wiggler parameters. The wigglers provide the flexibility to adjust beam parameters as needed to give the highest possible luminosity. In addition, the majority of the synchrotron radiation power is now concentrated in a few areas that can be suitably engineered to deal with the power density locally.

There are additional advantages to having a low-energy ring identical in circumference to the high-energy ring. These include:

- Luminosity lifetime from beam-beam interactions is improved, since individual bunches from the low-energy ring collide less frequently
- At only a moderate loss in luminosity—by a factor of about $\sqrt{2}$ —there could be two IPs
- If gaps must be imposed in the bunch trains to avoid ion trapping, the gaps could be matched in both rings so that anharmonic beam-beam effects are totally avoided

A potential disadvantage to this approach, of course, is the possible additional cost of a very large low-energy ring. In the case of installing the ring in a preexisting tunnel, however, as could be done with PEP, there are significant offsetting savings (e.g., the availability for reuse of the existing PEP hardware) that make the idea well worthwhile.

3. Design Example

In Section 3, we discuss a specific design example for the APIARY collider. We envision that, after commissioning, the collider would begin operation at a luminosity of 3×10^{33} $cm^{-2}\ s^{-1}$ and then, with suitable improvements, would reach even higher luminosity. What we describe here is not yet a fully optimized design, but rather should be viewed as a "proof of principle." In those areas where a complete solution is not yet in hand, suggested improvements will be indicated.

From the viewpoint of lattice design, the challenging aspects of the APIARY collider involve meeting the following requirements:

- Achieving low beta functions ($\beta^* = 3$ cm for the low-energy ring, $\beta^* = 6$ cm for the high-energy ring) in both planes at the IP
- Separating closely spaced beam bunches to avoid unwanted collisions
- Storing a substantial beam current stably and with a reasonable lifetime
- Having sufficient flexibility to provide, if necessary, a set of "energy transparency" conditions (as discussed in Section 2)
- Making round beams

There are several possible configurations that could be chosen to achieve our luminosity goal. We describe here a rather conventional choice in which the two beams collide head-on. Major parameters for the two rings are summarized in Table 3–1, and a site layout is shown in Fig. 3–1. To indicate the range of possibilities, a second alternative, in which flat beams collide at a nonzero crossing angle (making use of the crab-crossing technique) rather than head-on, is described in Appendix B. An intermediate case, involving head-on collisions with flat beams, will also be examined to permit a comparison among the various available options.

Table 3–1. Main parameters of the APIARY collider.

	Low-energy ring	High-energy ring
Energy, E [GeV]	3.1	9
Circumference, C [m]	2200	2200
Number of bunches, k_B	1296	1296
Particles per bunch, N_b [10^{10}]	7.88	5.44
Total current, I [A]	2.23	1.54
Emittance,[a] ε_x [nm·rad]	66	33
Bunch length, σ_ℓ [mm]	10	10
Momentum spread, σ_p [10^{-4}]	9.5	6.1
Damping time		
$\tau_{x,y}$ [ms]	32.3	37
τ_E [ms]	17.3	18.5
Beta functions at IP		
β_x^* [cm]	3	6
β_y^* [cm]	3	6
Betatron tune		
horizontal, ν_x	37.76	21.28
vertical, ν_y	35.79	18.20
Synchrotron tune, Q_s	0.039	0.053
Momentum compaction, α	0.00115	0.00245
RF parameters		
frequency, f_{rf} [MHz]	353.2	353.2
voltage, V_{rf} [MV]	10	25
Natural chromaticity		
horizontal	-68.5	-57.0
vertical	-80.0	-53.0
Nominal beam-beam tune shift		
ξ_{ox}	0.03	0.03
ξ_{oy}	0.03	0.03
Luminosity, $\mathcal{L}$ [$cm^{-2}\ s^{-1}$]	3×10^{33}	

[a] Equal horizontal and vertical emittances.

Fig. 3–1. Site plan in the vicinity of PEP showing the general location of the APIARY collider

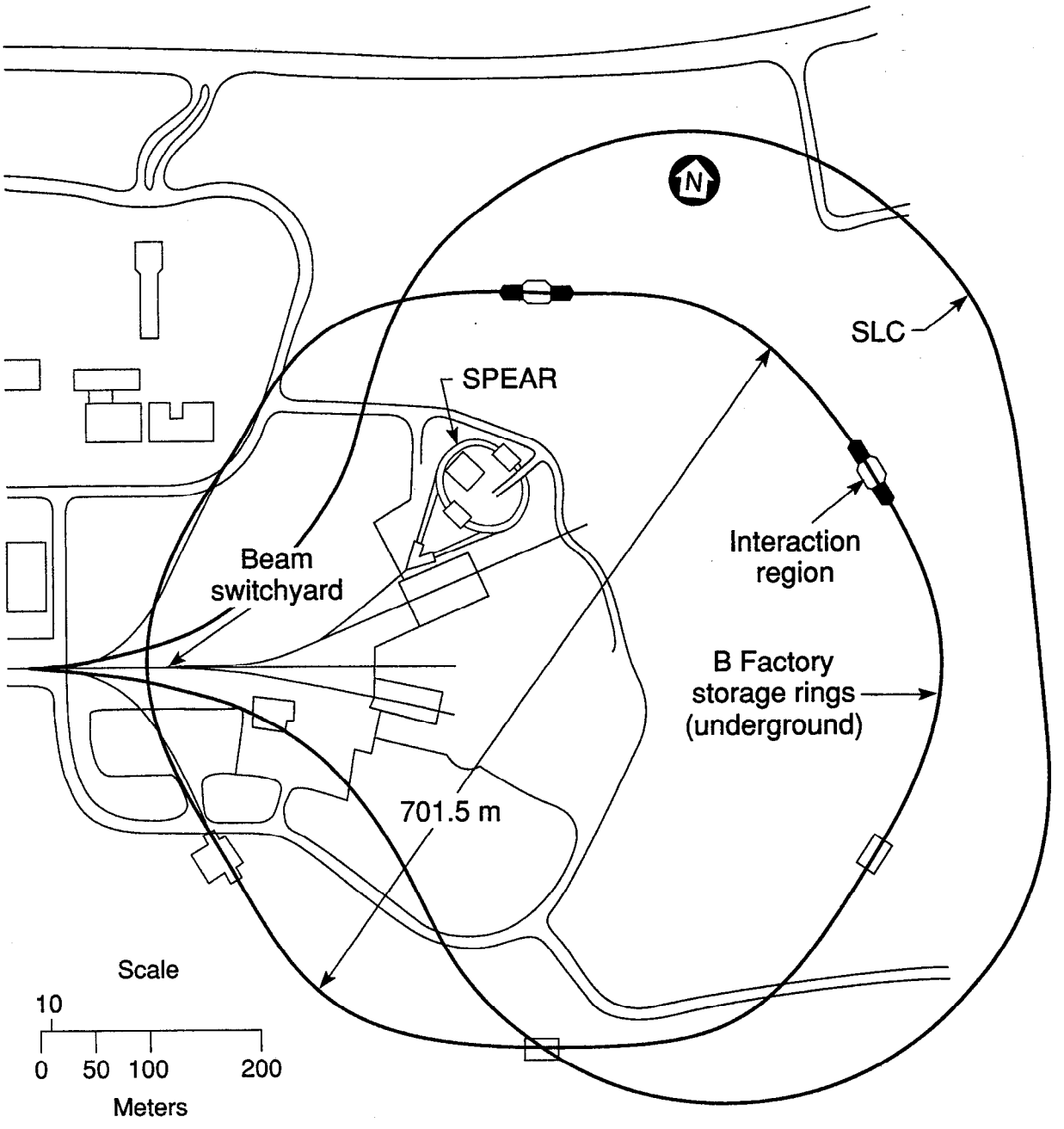

XBL 902-5762
lg/Mac

Specific topics of discussion in the remainder of Section 3 (in order of appearance) are:

- Lattices and Collision Optics
- Beam-Beam Dynamics
- Intensity-Dependent Collective Effects
- RF Systems
- Feedback Systems
- Synchrotron Radiation and Vacuum
- Synchrotron-Radiation Masking and Beam-Pipe Cooling
- Beamstrahlung
- Injection System
- Special-Purpose Hardware

3.1. Lattices and Collision Optics

In this section we describe the two rings that make up the APIARY collider discussed in our example. As mentioned in Section 2, we used the scaling rules outlined in Appendix A to fix the relative parameters of the two rings. For our assumed tune-shift parameter of $\xi = 0.03$, and with the use of round beams in both rings, we can rewrite Eq. (2.1–1) as

$$\mathcal{L} = 1.30 \times 10^{33} \left(\frac{I \cdot E}{\beta_y^*} \right)_{+,-} \quad [\mathrm{cm}^{-2}\,\mathrm{s}^{-1}] \qquad (3.1\text{–}1)$$

where I is in amperes, E is in GeV, β^* is in cm, and numerical values are used for the remaining factors. With our present parameters, the ratio of beta functions in the two rings is 1/2. We require beam currents of $I_+ = 2.23$ A and $I_- = 1.54$ A to reach an initial luminosity of $3 \times 10^{33}\ \mathrm{cm}^{-2}\,\mathrm{s}^{-1}$.

Low-Energy Ring

We consider here a scheme in which the low-energy ring has the same circumference as PEP. As we have shown in Section 2, this choice leaves a large area of tune space available—sufficient space to avoid difficulties with coherent beam-beam modes while easily remaining within parametric range of equal damping decrements, as may be needed to maintain the "energy transparency" condition between the two rings.

Key features of the low-energy ring include:

- Head-on collision optics
- $\beta^* = 3$ cm in both planes, using superconducting quadrupole doublets
- Zero dispersion in both planes at the IP
- Bunch separation of 1.7 m
- Beam separation in the IR first horizontally and then vertically
- Wigglers to permit adjustments of emittances and damping times
- Round beams

Overall ring configuration. The low-energy ring has a circumference of 2200 m and is designed to operate at 3.1 GeV. As illustrated schematically in Fig. 3.1–1, the ring has a hexagonal shape, with six long straight sections and six arcs. One of these long straight sections contains the interaction region (IR) with its low-beta optics; on the opposite side of the ring is a utility straight section (U) for rf, injection, etc. The utility straight section is presently configured as six "empty" FODO cells (i.e., cells without dipoles). Between the IR and U straight sections there are four additional straight sections (W), two on each side of the ring, that contain wiggler magnets.

Arc section and dispersion suppressor. The six arc sections of the ring are of three different types. Each arc is a combination of some number of regular FODO cells, or half-cells, sandwiched between two dispersion suppressors. Figure 3.1–2 shows the layout and lattice functions of half of a superperiod. The lengths of all functional elements are specified in units of the standard half-cell length, $L_{1/2}$ = 7.6389 m, or 1/288 of the total ring circumference.

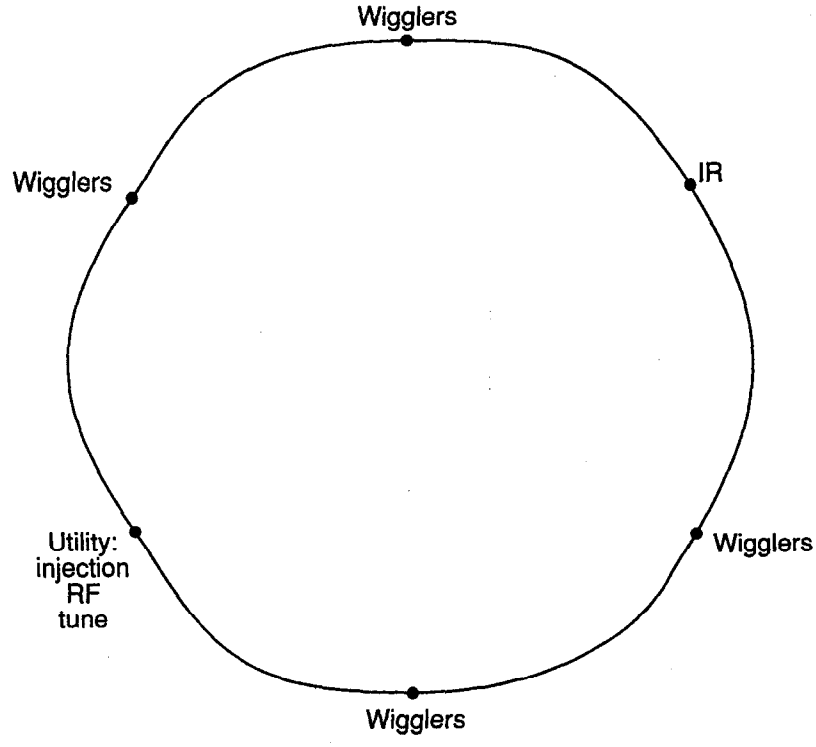

Fig. 3.1–1. Schematic of overall ring configuration (not to scale). The ring has six straight sections, six arcs, and one interaction region.

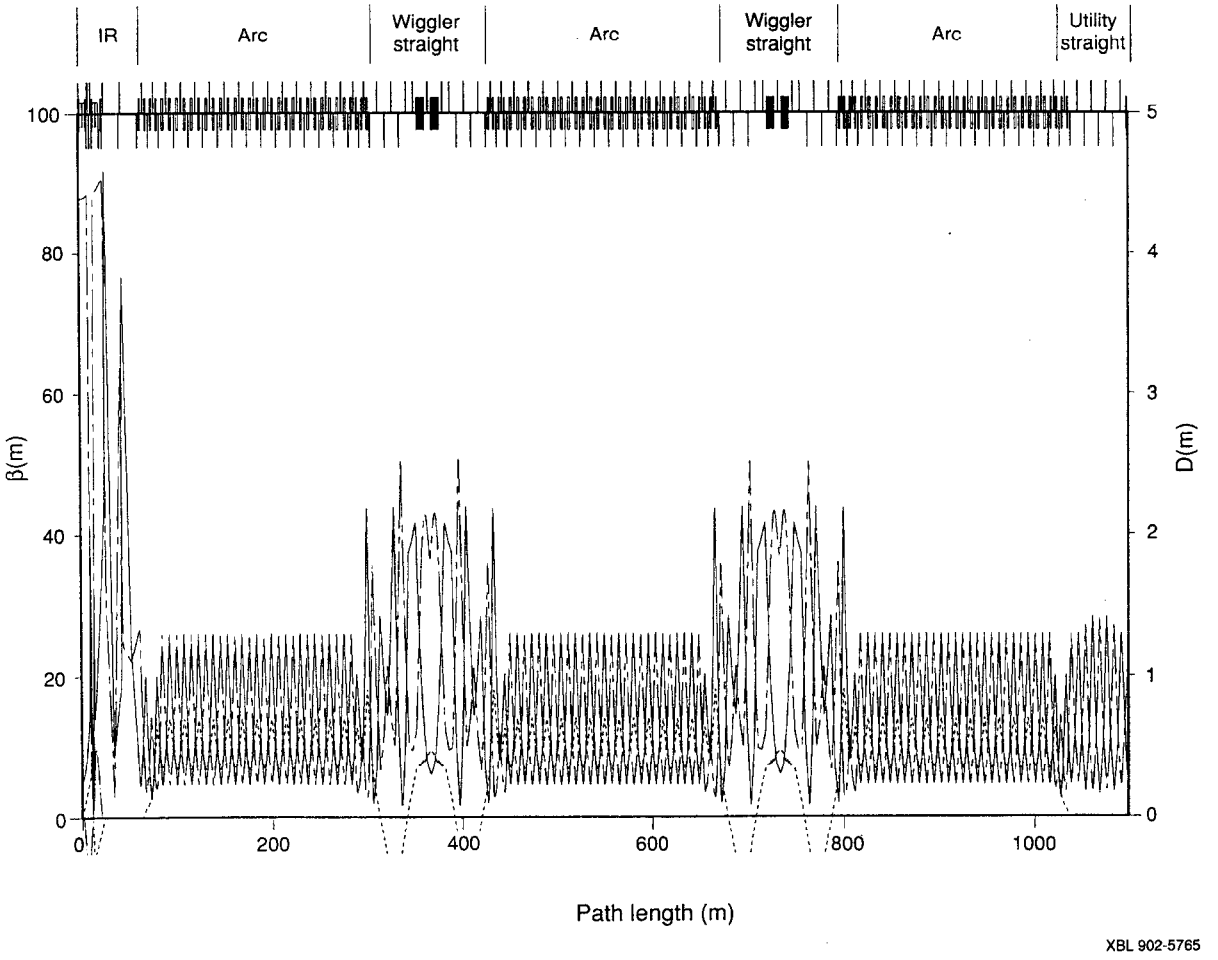

Fig. 3.1–2. Layout and lattice functions of half a reflection-symmetric superperiod in the low-energy ring.

The FODO half-cells contain one 1.95-m dipole and one 0.5-m quadrupole. The optics of a single FODO cell, shown in Fig. 3.1–3, are adjusted to give a phase advance of 90° in each transverse plane. Each arc contains 13 standard cells and a dispersion suppressor at each end. A dispersion suppressor consists of two 90° cells, each having 3/4 the length and 2/3 the bending angle of a standard cell. Thus, a complete arc has the same length as 16 standard cells and the bending of $15\frac{2}{3}$ standard cells. In the dispersion suppressor cells, the dipoles are 1.3 m long and the quadrupoles are 0.6794 m long.

Wiggler section. The straight sections adjacent to the arc cells are designed to accommodate wigglers, as was indicated in Fig. 3.1–2. In the present design, the wigglers have a period length of 2 m and a maximum field of 1.5 T; they are used in units of two periods, i.e., in 4-m sections. The lengths and strengths have not been optimized, but the chosen values are more than sufficient to obtain equal damping decrements for the low- and

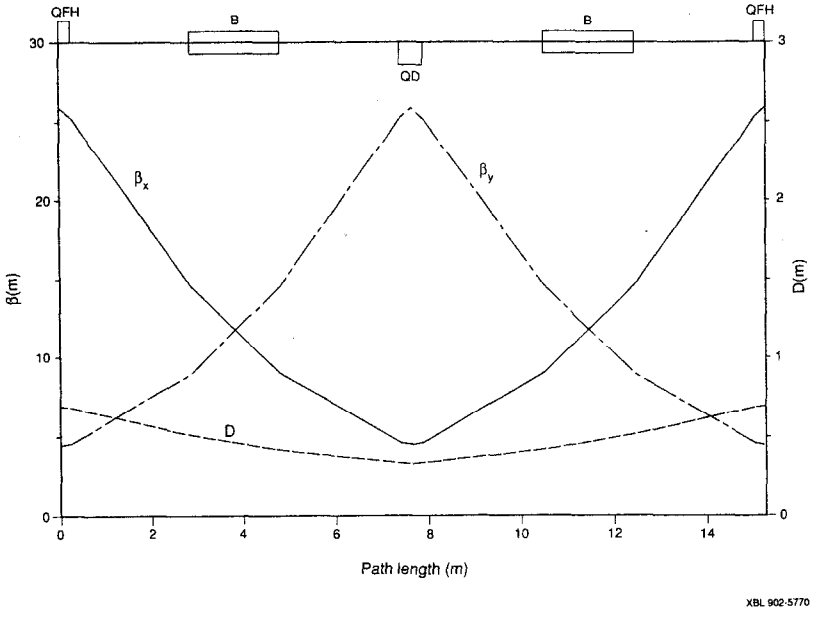

Fig. 3.1–3. Optics of a standard FODO cell.

high-energy rings. On each side of the wigglers, there are four quadrupoles whose function is to match the four lattice parameters (β_x, α_x, β_y, and α_y) into the arc optics. The dispersion suppressors adjacent to the wiggler straight sections have modified focusing to produce dispersion at the wiggler locations; this makes it straightforward to adjust the horizontal emittance of the lattice to its design value.

Interaction region and beam separation. The most difficult aspect of a high-luminosity collider, from the viewpoint of the lattice design, is the interaction region. Because of the energy asymmetry between the two rings, and the need to collide closely spaced bunches, the beam separation must be handled carefully. Figure 3.1–4 shows the separation optics of the IR.

Reaching a luminosity of 3×10^{33} cm^{-2} s^{-1} requires a bunch separation distance of 1.6975 m, corresponding to $2\lambda_{RF}$ at 353.2 MHz. The chosen separation scheme must be capable of separating the two beams rapidly enough to avoid unwanted collisions in places other than the IP. The technique being used, which employs both vertical and horizontal bends, is described below.

Starting at the IP, shown in Fig. 3.1–5, with $\beta_x^* = \beta_y^* = 3$ cm, the low-energy beam is focused by a superconducting quadrupole doublet (QF1, QD2). This doublet produces essentially point-to-parallel optics, preventing substantial beam

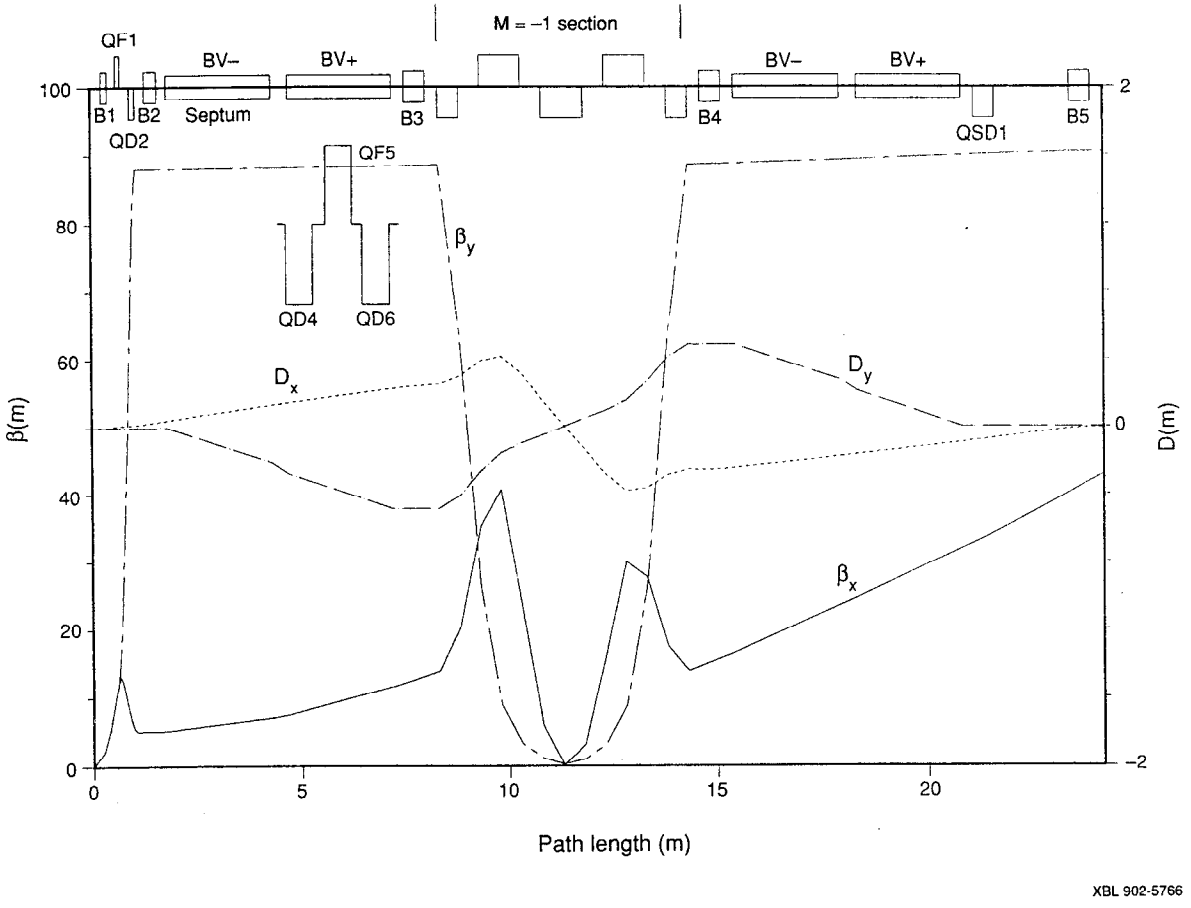

Fig. 3.1–4. Separation optics for the low-energy ring.

blowup over the roughly 25 m until the next focusing quadrupoles. To minimize aperture requirements, the doublet is centered on the low-energy beam orbit.

Because the process of beam separation must begin as soon as possible after leaving the IP, a small horizontal bending magnet, B1 (38 mrad), is located upstream from the superconducting quadrupole doublet, 25.5 cm from the IP itself. Immediately downstream of the doublet, a second horizontal bending magnet, B2 (2.9 mrad), continues the horizontal separation of the two beams sufficiently to permit the low-energy beam to enter the magnetic channel of a Lambertson septum, BV- (9.57°), where it is deflected vertically upwards, away from the high-energy beam.

As shown schematically in the elevation view of Fig. 3.1–6, the low-energy beam is then transported vertically in two steps to a height of about one meter above the high-energy beam by pairs

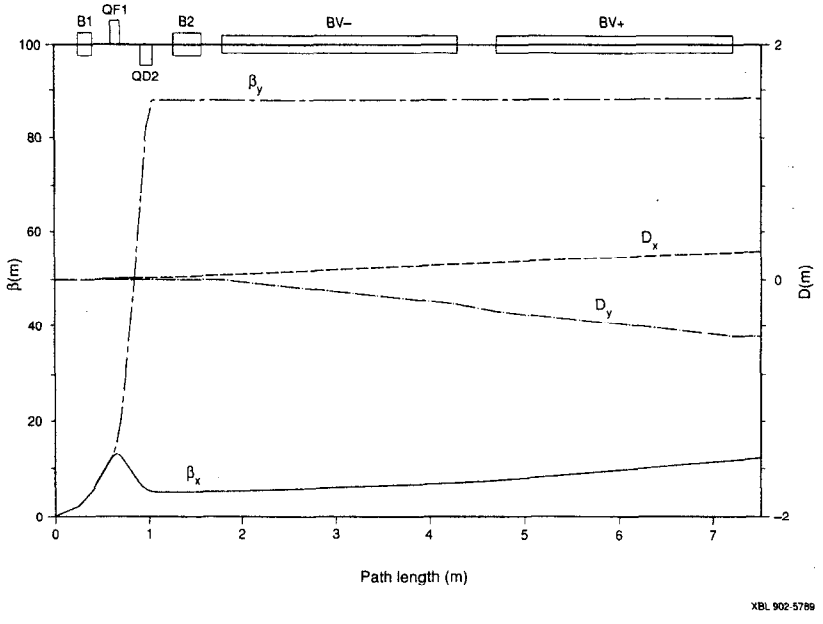

Fig. 3.1-5. IP optics.

of vertical bending magnets: BV-, BV+. The superconducting quadrupole triplet for the high-energy beam fits underneath the first step, as shown in the figure. Between the two steps, five quadrupoles are placed along the low-energy beam. These quadrupoles have a transfer matrix M = -1, which serves to cancel the vertical dispersion caused by the vertical steps (see Fig. 3.1–4).

Fig. 3.1–6. Plan and elevation views of separation scheme.

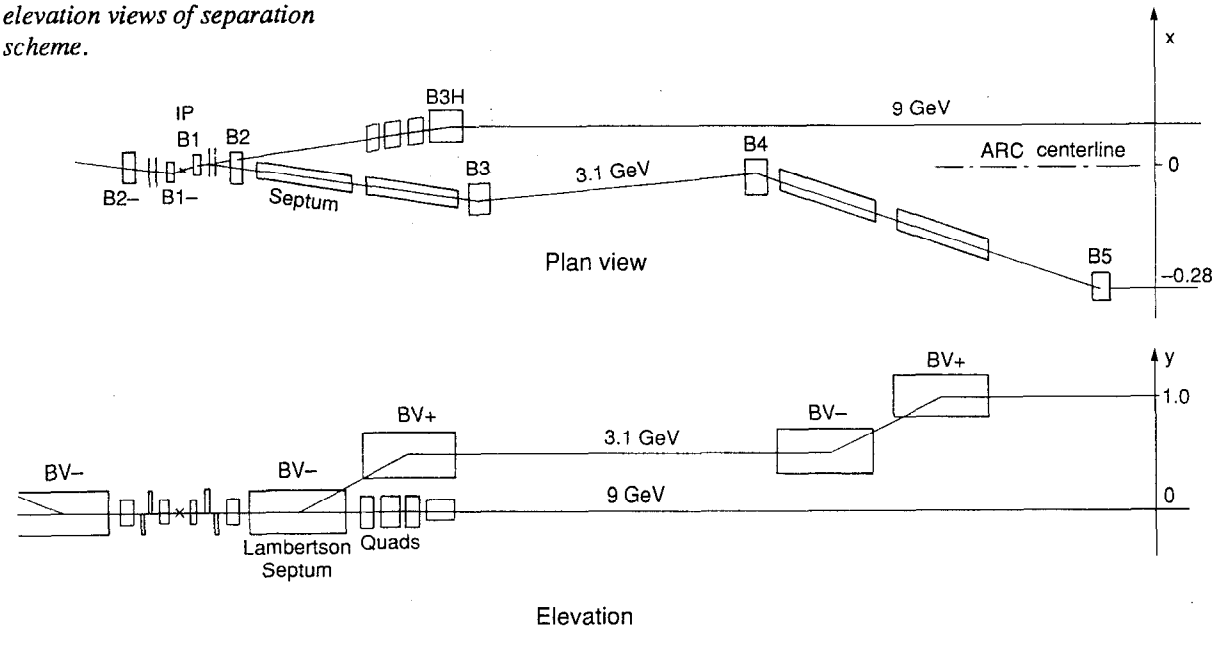

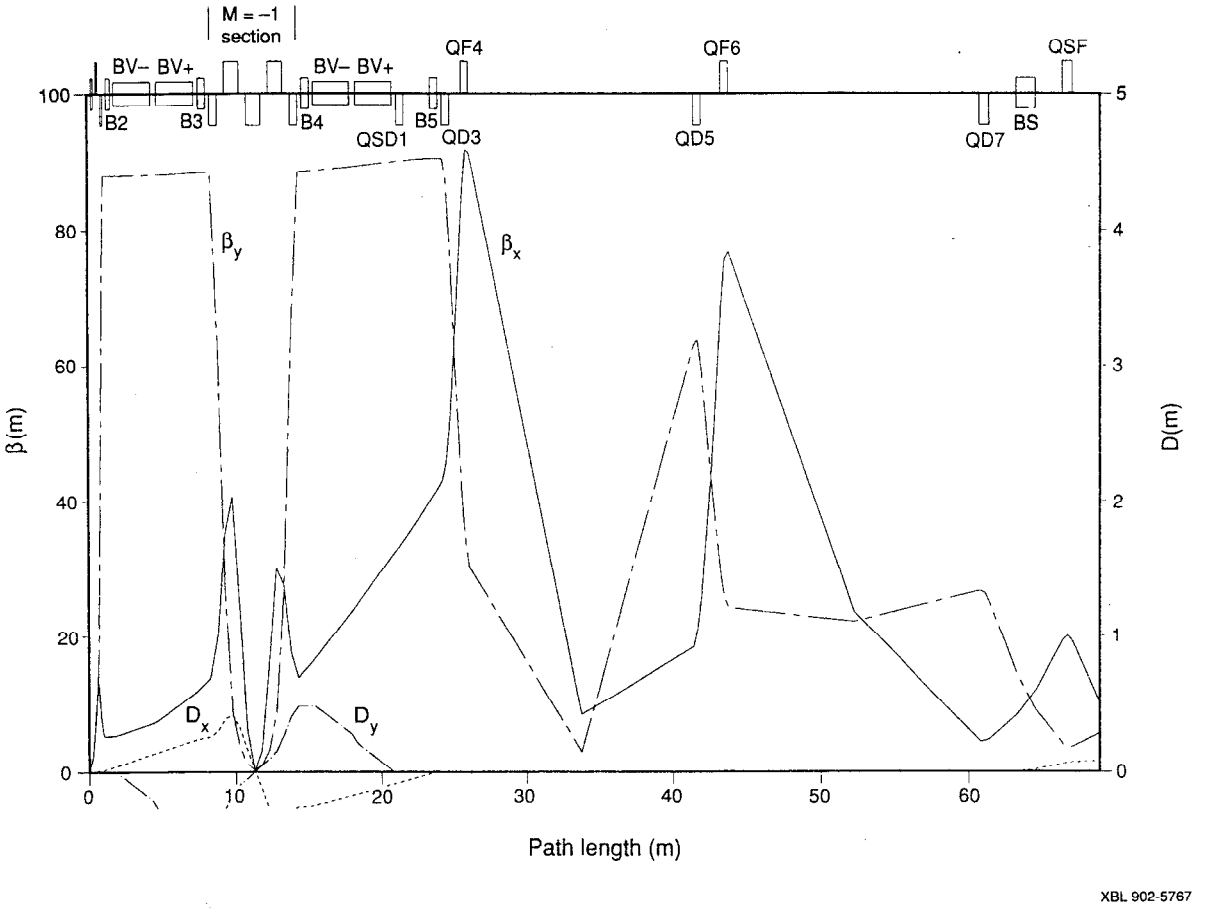

Fig. 3.1–7. Final matching back into FODO optics after IR.

At the ends of this "M = -1" section, there are two horizontal bends, B3 and B4. Together with another bend, B5, and an intervening quadrupole QSD1, they match the horizontal dispersion of the low-energy beam, and make this beam parallel to the high-energy beam in the arcs. Thus, by the end of B5, both horizontal and vertical dispersion are zero and the low-energy beam has been guided geometrically toward its proper path in the arc.

Following the separation and dispersion matching, the remainder of the low-energy beam straight section optics contains five quadrupoles, QD3, QF4, QD5, QF6, and QD7, which match the beta and alpha functions to the values required for the arc cells, as shown in Fig. 3.1–7.

Issues for Further Examination. Although the separation scheme presented here is clearly workable, there are several issues that would benefit from additional study during the optimization phase:

- The strong IR dipole and quadrupole magnets give rise to a difficult synchrotron-radiation masking problem
- The space available in the region near the IP is very tight

To deal with the first issue, centering of some or all of the IR quadrupoles on the high-energy (rather than the low-energy) beam will be investigated. Another approach, currently being studied, is to use flat rather than round beams and to alter the polarities and centering of the quadrupoles. It appears that this approach will indeed ease the masking problem. Whether this is a globally superior solution depends on whether round beams are somehow more resistant to beam-beam effects. When the flat-beam scenario is completed and compared with the round-beam one, a further investigation should be done of possible flexibilities between the round- and flat-beam optics.

The second issue, hopefully, will be amenable to clever engineering solutions. As one example, it will be necessary to use C-magnets for at least some of the IR dipoles, which should permit additional room for pumps and diagnostic equipment.

High-Energy Lattice

The design of the high-energy ring is based upon the existing PEP lattice. PEP has a FODO lattice with six long (117-m) straight sections, and can operate at energies up to 15 GeV. Although the basic lattice hardware is sixfold-symmetric, the addition of a low-beta insertion in one region (Region 2) reduces the actual lattice periodicity to one. Nonetheless, the arc optics retain the symmetry of the hardware rather well, so the periodicity is violated mainly in the single IR straight section.

The basic design requirements for the high-energy ring of the APIARY collider are similar to those for the low-energy ring described above. They include:

- Achieving low beta functions ($\beta^* = 6$ cm) in both planes at the IP
- Separating closely spaced beam bunches to avoid unwanted collisions
- Storing a substantial beam current stably and with a reasonable lifetime
- Making round beams

Given the optics configuration for the interaction region from the low-energy ring, the lattice design for the high-energy ring is already somewhat constrained. In our case, we start from an existing ring, so the technical challenge at hand is to adjust the lattice suitably "without touching anything." The high-energy lattice parameters and optics are based primarily on the standard PEP collider optics. To obtain the appropriate emittance, the standard cells are adjusted to a phase advance of 60°.

Interaction region and beam separation. Figure 3.1–8 shows the IR optics as seen by the high-energy beam. (Note that, because of the large range of beta-function values for the high-energy ring, we will plot $\beta^{1/2}$ rather than β itself.) Common elements with the low-energy ring include the two horizontal dipoles (B1 and B2) and the superconducting quadrupole doublet (QF1 and QD2). Because the high-energy beam has three times the energy, it is relatively unaffected by any of these common magnets, so it passes the Lambertson septum magnet (BV- in Fig. 3.1–4) in the field-free region.

It is clear from Fig. 3.1–8 that the principal challenge for the high-energy optics is to capture the beam from the IP with focusing quadrupoles before it gets too large. The combined horizontal-vertical separation scheme described above is an attempt to get the superconducting triplet needed for the high-energy beam as close as possible to the IP. Despite this approach, the triplet cannot be located much closer to the IP than about 5 m. The beta functions from the IP will grow as

$$\beta_{x,y}(s) = \beta^{*}_{x,y} + \frac{s^2}{\beta_{x,y}} \qquad (3.1\text{–}2)$$

so we expect beta functions on the order of 400 m at 5 m from the IP, in agreement with Fig. 3.1–8.

Arc Cells. As shown in Fig. 3.1–9, once the beam is past the superconducting quadrupole triplet of the high-energy ring, it drifts essentially to the end of the straight section, where it is matched to the FODO optics by means of three quadrupoles, QD6, QSF, and QSD. The dispersion matching requires several bend magnets, as indicated in the figure.

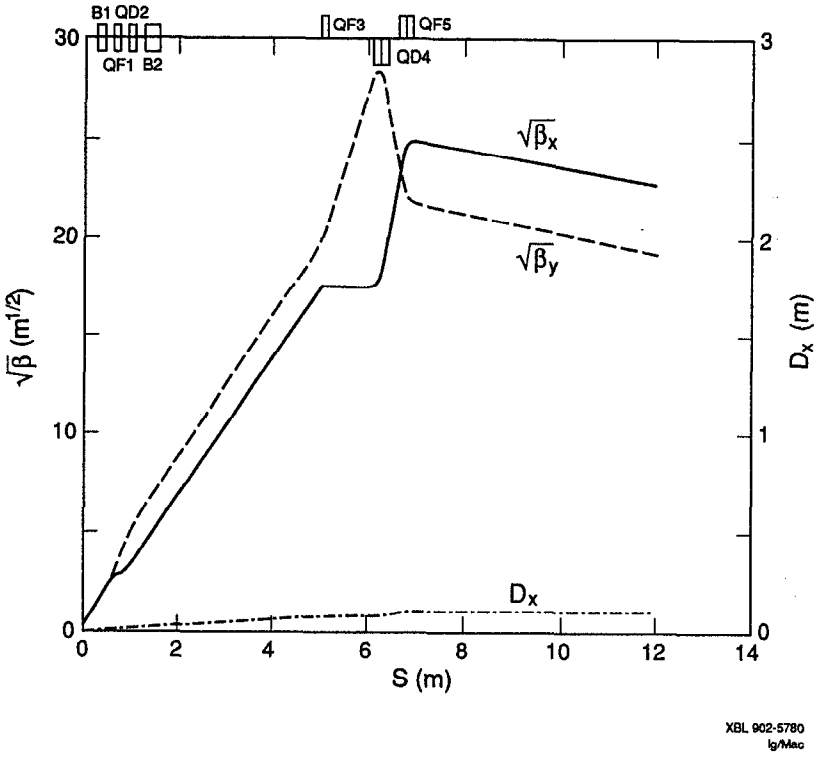

Fig. 3.1–8. IR optics for the high-energy ring.

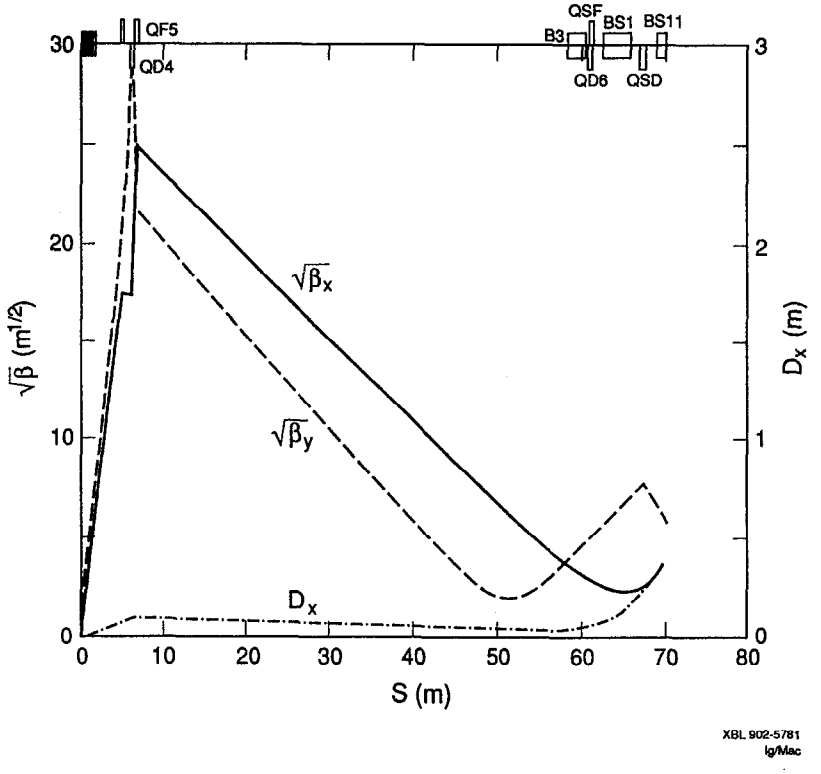

Fig. 3.1–9. Matching of the high-energy beam into the FODO optics after the IR.

In Fig. 3.1–10 we show the optics functions for 1/12 of the PEP ring (including half of the arc section adjacent to the IR). As can be seen, the matching is easily accomplished.

The optics functions in the remaining long straight sections are maintained at the same values as in the arcs by continuing the focusing structure in the straights with "empty" FODO cells, as illustrated in Fig. 3.1–11.

Complete optics functions for the full superperiod are shown in Fig. 3.1–12. Clearly the overall matching is good.

Natural chromaticities for the optics shown here are $\xi_x = -57$ and $\xi_y = -53$; these are comparable to the typical values for the PEP collider optics, and correction does not present any problem. One must take care, however, that the local chromaticity associated with the strong quadrupole triplet in the IR does not get out of hand. It is important to minimize the distance of the triplet from the IP insofar as possible.

The main outstanding issue that will need to be pursued during the optimization phase will be to explore alternative schemes to create round beams in the high-energy ring. This topic is discussed below.

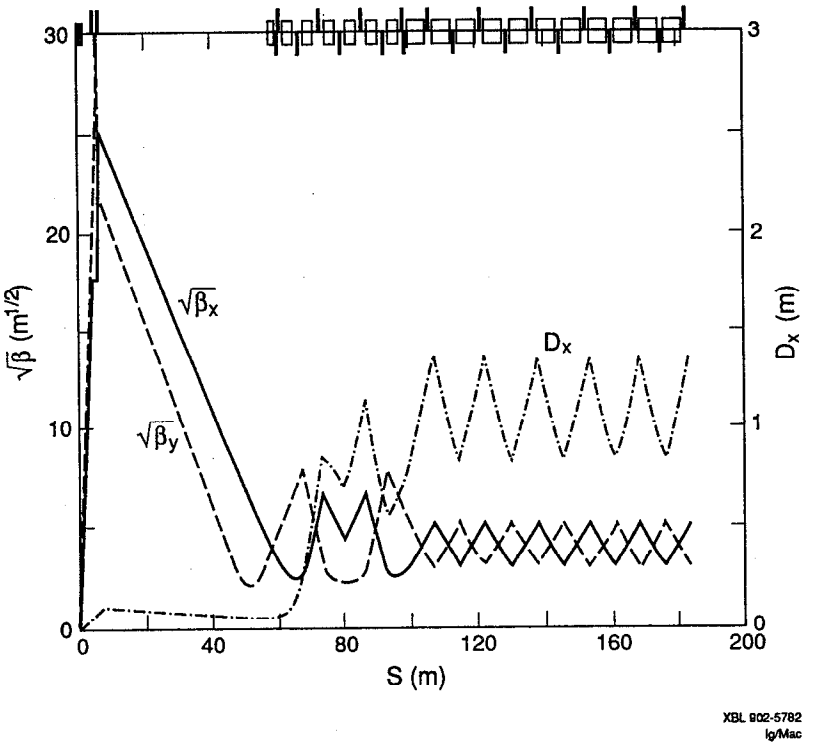

Fig. 3.1–10. Optics functions for one-twelfth of the PEP ring.

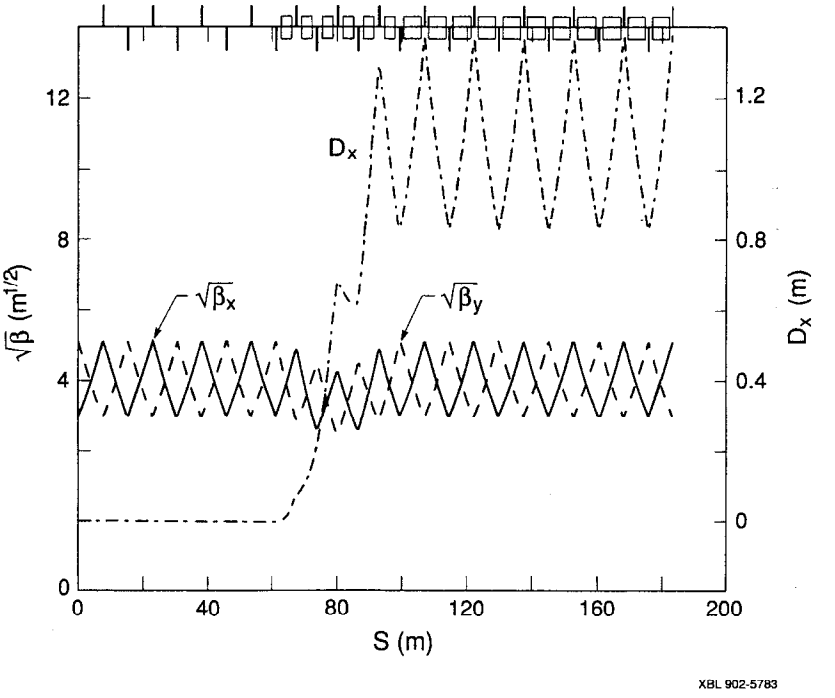

Fig. 3.1–11. The optics for the remaining long straight sections of the high-energy ring.

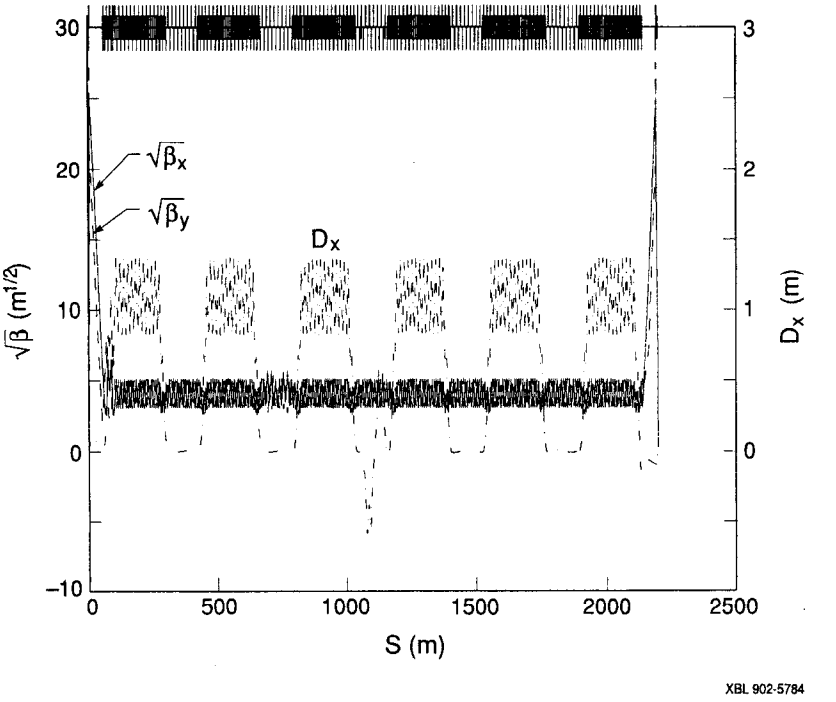

Fig. 3.1–12. Optics functions for one superperiod in the high-energy ring.

Achieving Round Beams

In the low-energy lattice, our calculations predict that the vertical emittance will be dominated by the contribution from the vertical bending magnets that separate the beams. Because these bends are strong and create substantial vertical dispersion, our estimates show that the vertical emittance is comparable to the horizontal emittance, without any significant contribution from the wigglers. In fact, we find that the horizontal emittance of the low-energy ring is also influenced significantly by the contribution from the same region of the lattice—the vertical bending magnets.

To see why this might be so, we refer back to Fig. 3.1–4, which shows that the horizontal dispersion in the vertical bending magnets is only slightly less than the dispersion in the vertical plane. When synchrotron radiation is emitted in this portion of the lattice, there is an increase in both the vertical and the horizontal emittance values. Thus, there seems little doubt that round beams are well within our grasp for the low-energy ring.

Not surprisingly, the situation in the high-energy ring is more difficult. We have estimated that we can produce a more or less round beam by placing wigglers in a region that has about 0.5 m of vertical dispersion. The drawback, however, is that the strength of the wigglers increases the synchrotron radiation emission in the high-energy ring considerably—about a factor of three. This, in turn, would require that the synchrotron radiation in the low-energy ring increase proportionately to maintain the possibility of having equal damping decrements.

Given these difficulties in making a round beam in the high-energy ring, it is worthwhile to explore alternative approaches to the production of round beams. Skew quadrupoles, for example, can be used in several parts of the ring to essentially interchange the two transverse phase planes, that is, to transform $(x,x') \rightarrow (y,y')$ and vice versa. This technique, in effect, means that half of the quantum excitation occurs in each transverse plane, so the emittance is shared between planes via a noiselike excitation. The phase-plane rotator technique is also quite controllable, and the vertical emittance can be reduced to the standard flat beam case if desired. Thus, it will be possible to create a round beam relatively easily with skew quadrupoles. Two further issues—whether this technique causes a loss of dynamic aperture or leads to beam-beam interaction problems—are now under investigation.

3.2. Beam-Beam Simulation Results

The results of our beam-beam simulation studies for the APIARY collider described in Section 3.1 are summarized in Figs. 3.2–1, 3.2–2, and 3.2–3. Compared with the lattice parameters described in Table 3.1, we have chosen slightly different betatron tunes that avoid the excitation of coherent dipole motion, as explained in Section 2.2. The particular values used in the simulations are:

$\nu_{x,+} = 37.78$ $\qquad$ $\nu_{y,+} = 35.78$

$\nu_{x,-} = 21.28$ $\qquad$ $\nu_{y,-} = 18.28$

All the energy transparency criteria established in Section 2.2 except the fourth one are satisfied for these APIARY lattices. That is, we do not have identical values in each ring for the quantity $(\sigma_\ell Q_s/\beta^*)$, which is required in order to have the same betatron phase modulation due to synchrotron motion. However, using the actual lattice parameters, the value of $\sigma_\ell Q_s/\beta^*$ in the low-energy ring is only about 1.5 times that in the high-energy ring. This does not cause any significant degradation of the luminosity.

Fig. 3.2–1 shows the rms beam sizes predicted from the simulations as a function of the nominal beam-beam tune shift parameter, ξ_0. It can be seen that there is essentially no blowup of either beam. The dynamic beam-beam parameters, ξ_+ and ξ_-, are plotted in Fig. 3.2–2 as a function of ξ_0. No evidence is

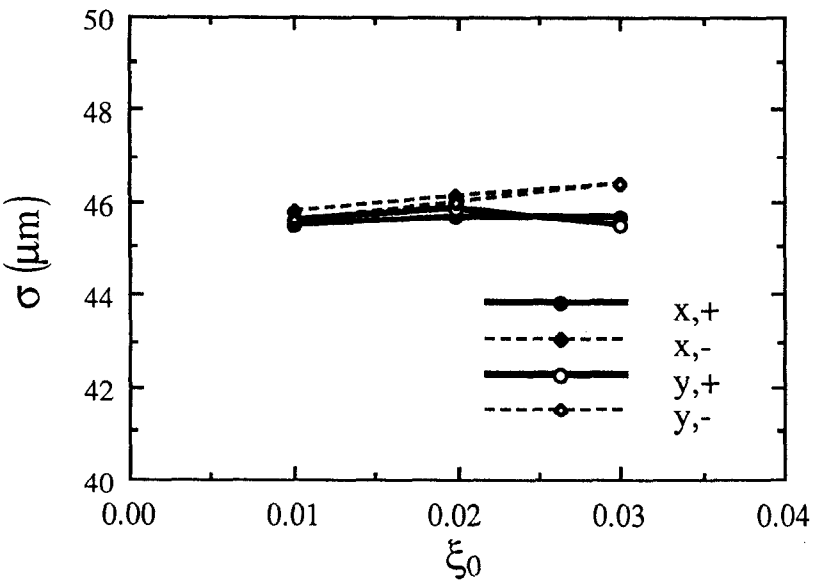

Fig. 3.2–1. RMS beam sizes vs. ξ_0, for the high- and low-energy rings (denoted by - and +, respectively).

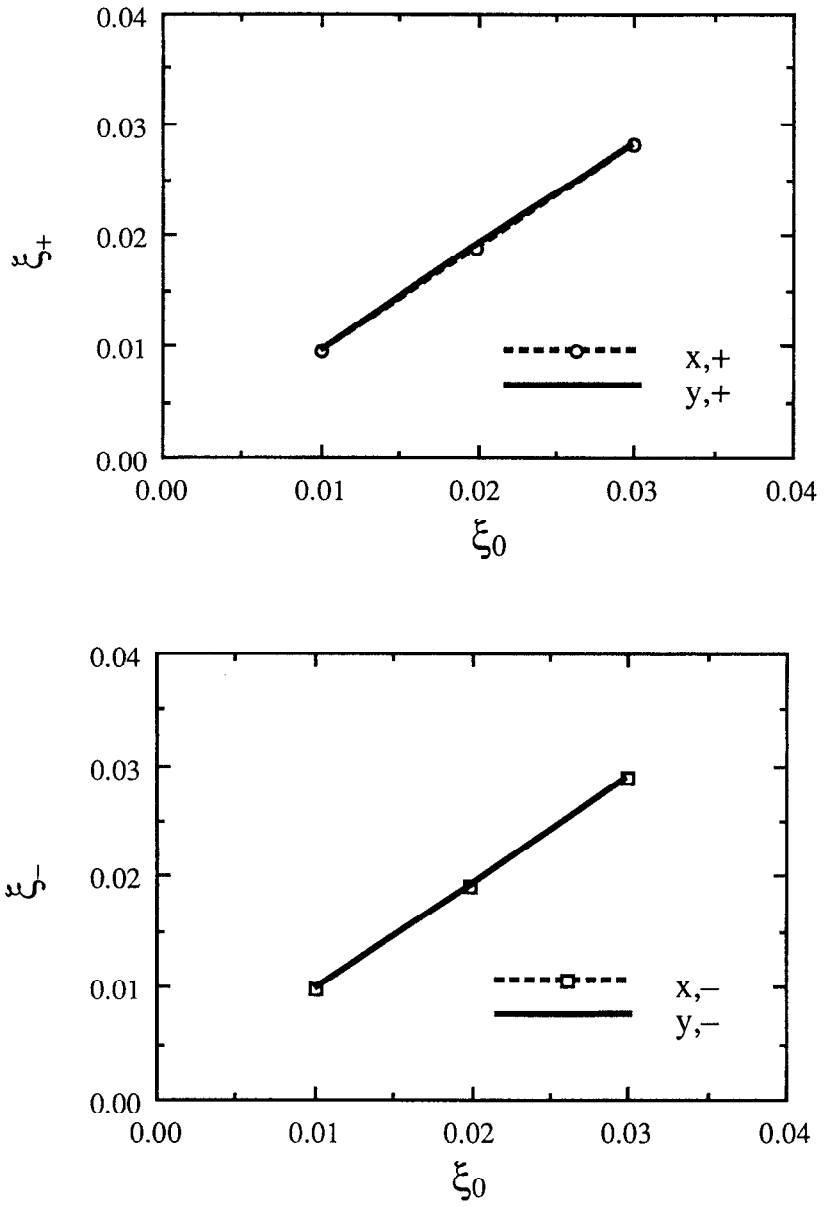

Fig. 3.2–2. ξ_+ and ξ_- vs. ξ_0. The dynamic ξ values differ from the nominal values by less than 5% and no saturation is apparent.

observed for saturation of the tune shift in either transverse plane for either beam. Figure 3.2–3 shows the corresponding luminosity, which reaches 95% of the design value of 3×10^{33} cm^{-2} s^{-1} at $\xi_0 = 0.03$.

If the damping decrements in the two rings were not matched, we would expect some degradation of the luminosity. Although we have not explicitly verified it here, it is expected that this degradation would be less than a factor of two.

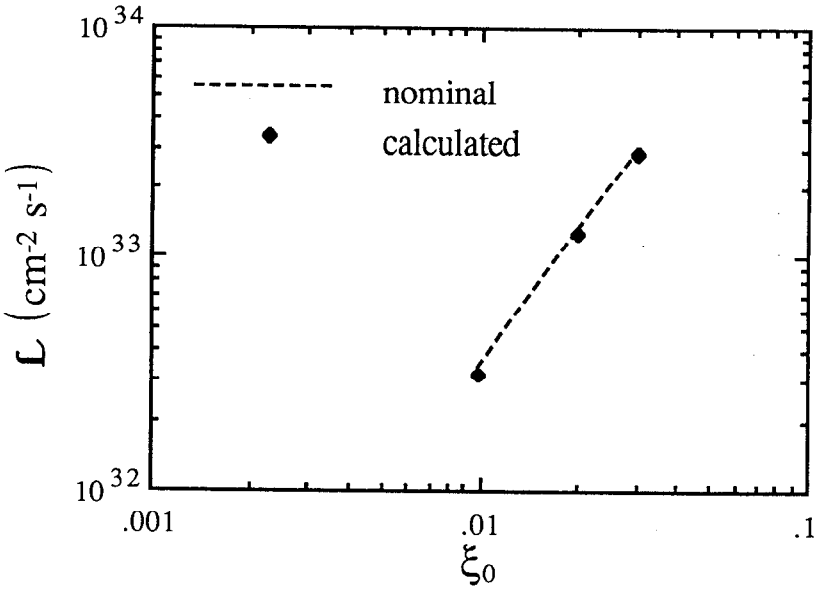

Fig. 3.2–3. Luminosity vs. ξ_0. Actual luminosity is within 5% of the nominal value.

3.3. Intensity-Dependent Collective Effects

In this section, we examine issues related to the large beam currents required to provide a high-luminosity asymmetric collider—that is, the *collective effects* relevant to the APIARY design. The focus here is on single-ring issues, before the beams are brought into collision. The topics considered are:

- Single-bunch thresholds
- Emittance growth from intrabeam scattering (IBS)
- Beam lifetimes (from Touschek scattering, gas scattering, and quantum excitation)
- Multibunch instabilities

The effects of multibunch instabilities are quite severe, and will likely be one of the limitations to the performance of the APIARY collider. In this case, contrary to standard wisdom, it is the high-energy ring that potentially presents the most difficulties, since this ring has more of the rf hardware that drives the multibunch instabilities. The results reported here were all obtained with the LBL accelerator physics code ZAP.[18]

High-Energy Ring

The high-energy-ring calculations are based on the lattice described in Section 3.1. The ring has a circumference of 2200 m and an rf frequency of 353.2 MHz, leading to a harmonic number of h = 2592. The required bunch separation for reaching the design luminosity of 3×10^{33} cm^{-2} s^{-1} corresponds to 1296 equally spaced bunches in the ring; i.e., every second rf bucket is filled.

High-Energy Ring Single-Bunch Thresholds

Longitudinal Microwave Instability. To estimate the growth from the longitudinal microwave instability, we must assume a value for the broadband impedance of the ring. For the APIARY high-energy ring, this value—usually dominated by the rf in a high-energy storage ring—is expected to be lower than the value of $|Z/n| = 3\ \Omega$ obtained from measurements at PEP.[19,20]

The equivalent broadband contribution to the impedance seen by the beam can be estimated, for a given rf system, following the

approach of Reference 18. Basically, we estimate the frequency shift that would be induced in a long beam bunch by the aggregate of the many cavity HOMs, and equate it to the strength of a Q = 1 broadband resonator that would produce the same effect. That is, we take

$$\left|\frac{Z_{\|}}{n}\right|_{BB,rf} = \sum_{HOMs} \left|\frac{Z_{\|}}{n}\right|_j = \sum_j \left(\frac{R_s\,\omega_0}{Q\,\omega_R}\right)_j \qquad (3.3\text{–}1)$$

where R_s, ω_R, and Q are the shunt impedance, resonant angular frequency, and quality factor, respectively, of the j^{th} HOM, and ω_0 is the particle revolution (angular) frequency. With this approach, we find that the present PEP rf system contributes an equivalent broadband component of $|Z/n| \approx 0.026\ \Omega$/cell. Although the design of the smoother room-temperature rf cavity described in Section 3.4 is helpful in minimizing the shunt impedance, the same prescription applied to this case yields an equivalent broadband contribution of $|Z/n| \approx 0.019\ \Omega$, about a 25% improvement.

A more significant gain can be made by producing the required voltage and providing the required power to the beam (to replenish the losses to synchrotron radiation) with many fewer rf cells than the 120 used now at PEP. In the design described in Section 3.4, the voltage is provided by only 20 rf cells. This decrease in the number of cells would by itself reduce, by about a factor of six, the broadband impedance in the ring that stems from the rf system (estimated to be about two-thirds of the total). The decrease in the impedance of individual cells provides another 25% improvement, so we expect to reduce the rf contribution to the broadband impedance by nearly one order of magnitude. If the rf hardware were to totally dominate all contributions to impedance, the overall impedance of the ring might be expected to decrease by this factor. Clearly, however, the broadband impedance from the other components in the beam path (valves, bellows, BPMs, etc.) must contribute to the total seen by the beam, and there will be additional hardware in the APIARY ring (e.g., more powerful feedback kickers) that will have an effect.

With this in mind, we have adopted for now a total broadband impedance of $|Z/n| = 1.5\ \Omega$ for the high-energy ring—a factor of two better than PEP. Even this fairly conservative assumption does not lead to any difficulties in the parameter regime in which the APIARY high-energy ring is designed to operate.

To maintain bunches that are short compared with the smaller β^* value of 3 cm in the low-energy ring, we adopt an rf voltage in the high-energy ring of 25 MV. As shown in Fig. 3.3–1, this voltage gives an rms bunch length of $\sigma_\ell \approx 1$ cm at the required single-bunch current of 1.2 mA. The expected bunch lengthening, and widening, beyond threshold are shown in Fig. 3.3–2, based on the threshold formula given in Eq. (3.3-2):

$$I_b = \frac{\sqrt{2\pi}\,|\eta|\,(E/e)\,\sigma_p^2\,\sigma_\ell}{R\left|\frac{Z}{n}\right|_{eff}} \qquad (3.3\text{–}2)$$

where η is the phase-slip factor, σ_p is the rms relative momentum spread, and R is the machine radius. We remain well below the threshold at the required single-bunch current.

The curves in Fig. 3.3–2 are based on the so-called SPEAR Scaling ansatz,[21] which is a phenomenological representation of the fact that beam bunches that are short compared with the dimensions of typical surrounding structures do not sample the broadband impedance very effectively. The expected reduction in impedance given by this model is

$$\left|\frac{Z}{n}\right|_{eff} = \left|\frac{Z}{n}\right|_0 \left(\frac{\sigma_\ell}{b}\right)^{1.68} \qquad (3.3\text{–}3)$$

where b is the beam pipe radius.

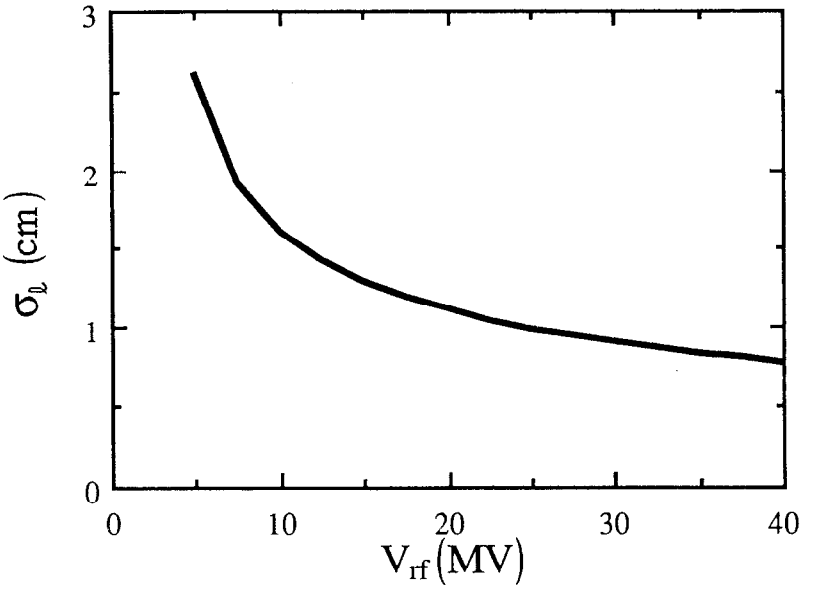

Fig. 3.3-1. Predicted bunch length for the high-energy ring with a single-bunch current of 1.2 mA. A low-frequency broadband impedance of |Z/n| = 1.5 Ω was taken, and an impedance roll-off according to SPEAR Scaling was assumed.

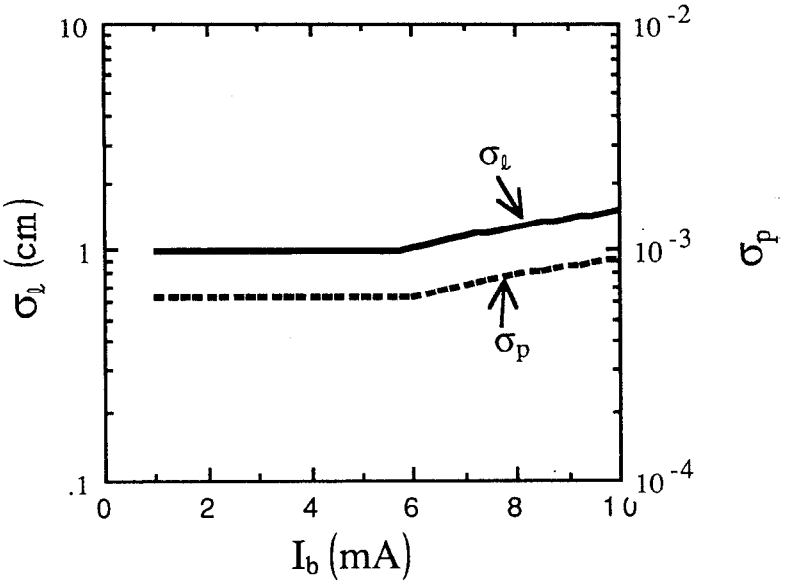

Fig. 3.3-2. Predicted bunch lengthening and widening for the APIARY high-energy ring as a function of single-bunch beam current.

Transverse Mode-Coupling Instability. Because the ring is large, we must also consider the transverse mode-coupling instability, which is known[20] to limit the single-bunch current in PEP. This instability arises when the imaginary part of the transverse impedance $Z_\perp$ couples the frequency of the m = 0 and m = -1 synchrotron sidebands. For long bunches, the threshold is expected to scale as

$$I_b = \frac{4\,(E/e)\,\nu_s}{\langle \mathrm{Im}\,(Z_\perp)\,\beta_\perp \rangle\, R}\,\frac{4\sqrt{\pi}}{3}\,\sigma_\ell \qquad (3.3\text{–}4)$$

where ν_s is the synchrotron tune, $\beta_\perp$ is the beta function at the location of the impedance, and R is the average ring radius. Although the transverse impedance is expected to decrease for very short bunches,[21] we are operating in a regime where the mode-coupling threshold is more or less independent of bunch length. For the impedance presently expected for the high-energy ring, a simple scaling from measured PEP data based on Eq. (3.3–4) suggests that the transverse mode-coupling threshold should be somewhat greater for APIARY than for PEP, even though APIARY will have a lower beam energy. The scaled threshold value, 14 mA/bunch, is well beyond the required single-bunch current of 1.2 mA and should pose no problem.

Since the rf cavities are major contributors to the transverse impedance, it is clear from Eq. (3.3–4) that it is best to "hide"

them in a low-beta region of the ring. This should be more easily accomplished in the APIARY high-energy ring than in PEP, because the total length of rf structure will be considerably shorter. Furthermore, the large aperture rf cavities envisioned for the ring will have an improved transverse impedance compared with the present PEP cavities. Thus, the gain in transverse threshold may be even higher than the assumed reduction in longitudinal impedance would suggest.

High-Energy Ring Intrabeam Scattering

Although we are considering a fairly high energy beam, the requirements for relatively short bunches and relatively high peak currents make emittance growth from intrabeam scattering a possible concern. IBS occurs because, in the bunch rest frame, not all particles are moving in the same direction, so they can collide. In general, the temperatures in the transverse phase planes (x and y) are higher than in the longitudinal plane. This results in small-angle multiple scattering occurring mainly in such a way as to transfer momentum from the transverse to the longitudinal plane. However, in dispersive regions of the lattice (regions where the position of a particle depends on its energy deviation) the resultant momentum change is equivalent to exciting a betatron oscillation, and thus gives rise to an increase in horizontal emittance. Our estimates for the APIARY high-energy ring indicate that no growth is expected in this energy range, so we will not consider this subject further.

High-Energy Ring Beam Lifetime

For a high-energy electron beam, there are three main processes that lead to beam loss: Touschek scattering, gas scattering, and quantum excitation. For the APIARY design, the first of these effects is not important, but the second one is, and the third one has the potential to be so.

Touschek Scattering. The Touschek scattering mechanism is also a single-bunch effect that is related to the IBS mechanism described above. The main difference is that we are concerned now with large-angle, single scattering events that change the scattered particle's momentum sufficiently to make it fall outside the momentum acceptance of the accelerator.

The limit on the tolerable momentum deviation from the design value can come from several sources. There is a longitudinal limit from the potential well ("rf bucket") provided by the rf

system. Particles deviating in momentum from the nominal value by more than this amount do not undergo stable synchrotron oscillations and are lost. There can also be a transverse limit on momentum acceptance, arising from the excitation of a betatron oscillation when the Touschek scattering event takes place in a dispersive region of the lattice. For large momentum deviations ($\delta p/p \approx$ several percent), the resultant betatron oscillation can either hit the vacuum chamber wall elsewhere in the lattice (physical aperture limit) or exceed the dynamic aperture of the machine. (The term "dynamic aperture" refers to the largest betatron amplitudes that can remain stable, after the various nonlinear magnetic fields experienced by a particle as it circulates have been taken into account.) Because the lifetime for Touschek scattering increases approximately as $(\Delta p/p)^3$, where $(\Delta p/p)$ is the limiting momentum acceptance value, there is the potential for a strong degradation if the acceptance is too low.

The rf voltage in the high-energy ring, selected to be 25 MV in order to ensure short beam bunches, actually provides an excessively large acceptance ($\Delta p/p = 1.5\%$) compared with the estimated limitation from the physical aperture ($\Delta p/p = 0.7\%$). This is not beneficial to the lifetime, since it results in a higher bunch density and thus a higher collision probability; this is the price we must pay to obtain short bunches. Fortunately, the Touschek lifetime is not a concern in this parameter regime. At 9 GeV, a Touschek lifetime of about 500 hours is predicted for the high-energy ring.

Gas Scattering. Gas scattering involves collisions with residual gas nuclei present in the vacuum chamber. Such collisions can be either elastic or inelastic (Bremsstrahlung). In the former case, particle loss results from the excitation of a betatron oscillation that exceeds the physical or dynamic aperture of the ring; in the latter case, the loss results from a momentum change that exceeds the momentum acceptance of the ring (see discussion above).

In the case of the APIARY high-energy ring, we must accommodate 1.54 A of circulating beam to reach a luminosity of 3×10^{33} cm^{-2} s^{-1}. This high beam current will give a large amount of desorbed gas load, and substantial pumping speed is needed to maintain a background gas pressure better than 10 nTorr in the ring. Given that most present colliders operate in the pressure range of about 10 nTorr, we will base our lifetime estimates on this value (N_2 equivalent). It is important to note,

however, that achieving such a pressure will require a careful design for the vacuum chamber, as discussed in Section 3.6.

For the high-energy ring, the estimated half-life from gas scattering—dominated by the Bremsstrahlung process—is two hours at a pressure of 10 nTorr. This beam loss process is much more severe in its effects than the Touschek scattering process; therefore we have placed great emphasis on a vacuum system design capable of maintaining a good pressure in the presence of a large gas load from synchrotron-radiation desorption. If the present PEP vacuum system were to be employed unchanged for the APIARY high-energy ring at full current, for example, we would expect a pressure in the ring of several *hundred* nTorr, which would lead to a beam lifetime of only minutes.

Quantum Lifetime. It is worth remembering that one must also keep a watchful eye on the quantum lifetime in a high-energy ring. This loss mechanism results from particles being scraped from the tails of the Gaussian distribution that results from the statistical nature of the synchrotron radiation emission process. The lifetime from this effect goes as:[22]

$$\tau_q = \tau_x \frac{e^{\xi^2/2}}{\xi^2} \qquad (3.3\text{–}5)$$

where ξ is the available aperture in units of the rms beam size, σ_x. For an acceptance of $\xi = 6$, the resultant quantum lifetime is about 15 hours, but for $\xi = 5$ the lifetime would be only about 5 minutes. To account for misalignments that can reduce the available aperture, a typical rule of thumb is to allow for an aperture of at least $\xi = 10$ in both planes.

In a high-luminosity collider the required β^* value is only a few centimeters, which can result in very large beta function values ($\beta \approx 800$ m in our case) in the IR quadrupole triplets, and thus in very large rms beam sizes ($\sigma_x \approx 5$ mm) there. For the high-energy ring, a quadrupole aperture radius of about 5 cm is needed at the superconducting quadrupole triplet.

Presuming that the parameters are suitably chosen to avoid difficulties with quantum lifetime, we can see from the above discussion that the (single-beam) lifetime of the high-energy ring will be dominated by gas scattering, which, as noted, makes the vacuum system a critical issue. To put our predictions in

perspective, we note that the luminosity lifetime in a high-luminosity collider will also be limited by the beam-beam scattering at the interaction point. Porter[23] has estimated the cross section of this process for a typical B-factory collider design and finds a luminosity lifetime of about two hours if the low-energy ring has a small circumference. However, for our parameters the luminosity lifetime due to Bhabha scattering is 260 hours and is not a concern.

High-Energy Ring Coupled-Bunch Instabilities

In a storage ring, wakefields in high-Q resonant structures can cause different beam bunches to interact. In general, such high-Q resonances result from the higher-order modes of the rf cavities. For certain values of relative phase between bunches, the coupled-bunch motion can grow and become unstable, leading to beam loss. In addition to the relative phase between bunches, the instabilities are characterized by their motion in longitudinal (synchrotron) phase space, as illustrated schematically in Fig. 3.3–3. Longitudinally, the a = 0 mode (corresponding to no motion) cannot be unstable, so the lowest longitudinal instabilities are characterized by the a = 1 (dipole) synchrotron motion. In the *transverse* case, the a = 0 motion can also become unstable (referred to as "rigid-dipole" motion).

In the case of a high-luminosity B-factory design, we typically require a large number of rf cells, both to produce the voltage needed to provide the short bunches and to replace the beam power lost to synchrotron radiation each turn. Combined with the required very high average beam currents, the substantial rf system can produce extremely rapid growth of coupled-bunch instabilities. In all the cases studied here, the most severe growth comes from the lowest synchrotron mode, that is, a = 1 longitudinally, and a = 0 transversely. Higher synchrotron modes are predicted either to be Landau-damped or to be growing slowly enough for radiation damping to be effective.

We have estimated the growth rates for both longitudinal and transverse instabilities for typical APIARY parameters, that is, 1296 bunches having a total current of 1.54 A. Given the uncertainties in determining the actual higher-order modes for any particular rf system that we study, it is most sensible to interpret the results shown here "logarithmically." That is, we are interested in seeing whether the fastest growth rates are 1 ms, 0.1 ms, etc., and we should not ascribe too much significance to growth rates that differ by a factor of two.

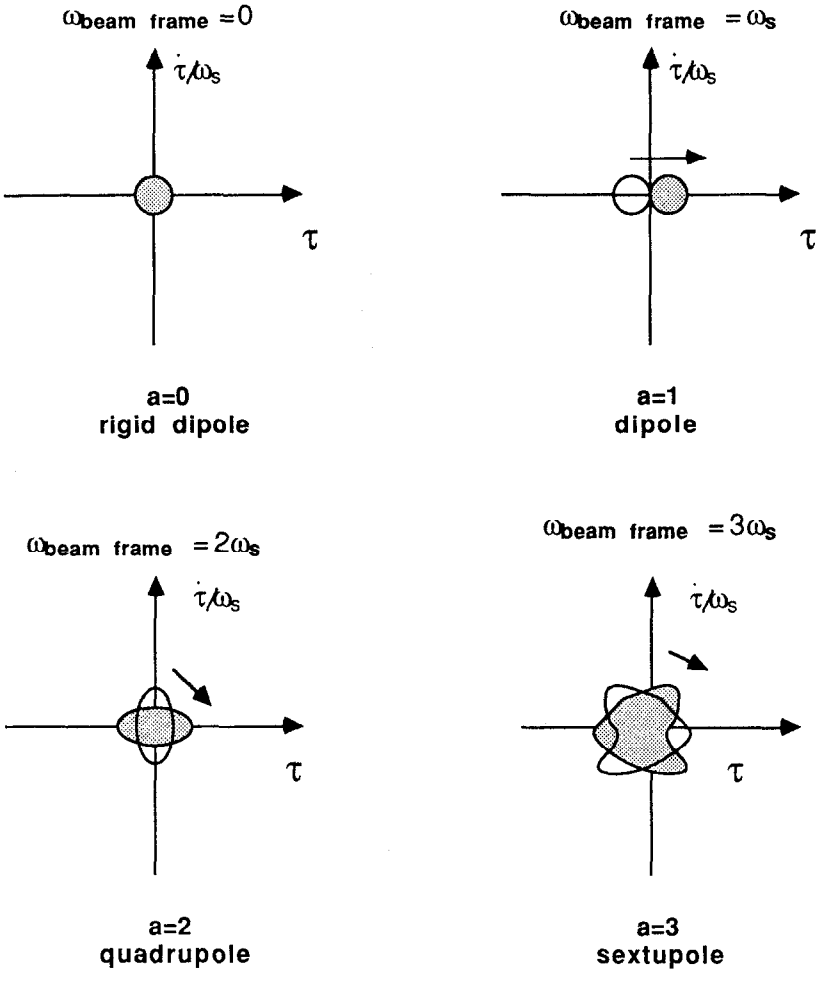

Fig. 3.3-3. Schematic diagram of the lowest few coupled-bunch synchrotron modes. For longitudinal instability, only modes $a \geq 1$ are possible; transversely, the $a = 0$ mode can also be unstable. The most troublesome cases for APIARY are $a = 1$ longitudinally and $a = 0$ transversely.

To give a feeling for the range of possibilities, two different cases were studied:

Case A: Single-cell cavities having a shape consistent with either a room-temperature (RT) or a superconducting (SC) implementation (see Section 3.4); 20 cells

Case B: As in B, but with HOM's de-Qed by a factor of 200; 20 cells

In Case A, we examine the possible benefits of a newly designed rf cavity that has a shape similar to that of a superconducting cavity; that is, the walls have a very smooth contour and there is a large diameter beam port to minimize trapped HOMs. This design provides many fewer HOMs than exist in the present PEP rf cavities.[24] One consequence of this design is that the cavity shunt impedance is rather low, so power

costs will increase somewhat if a room-temperature implementation is chosen. However, in the limit of being in a heavily beam-loaded regime, the lower shunt impedance is not a major issue.

Case B represents what would happen if the higher-order rf modes of the single-cell system were heavily de-Qed by external means, such as HOM couplers. (We note that achieving an equivalent level of Q reduction in the PEP five-cell cavities would not be an easy task, to say the least. However, such a drastic reduction in Q should be practical in the case of specially designed single-cell, room-temperature or superconducting rf cells.)

It is not entirely clear how to compare the room-temperature and superconducting rf system implementations on an equal footing. The gradient achieved in a superconducting cavity should be higher than that in an equivalent room-temperature cavity, so it might be that fewer cells would be needed to provide a given voltage. On the other hand, the use of relatively few superconducting cells to produce the required voltage means that the large beam power that must be supplied has to be delivered through relatively few individual cavity windows. Such high-power cavity windows have not been demonstrated operationally in a superconducting environment.

In a similar vein, the required removal of the HOM power from the superconducting environment may be more difficult than the equivalent task in the room-temperature case. For now, we have taken the window-power constraint to dominate, that is, we assume that the power provided to the superconducting cavity (per window) would only be half that for an equivalent room-temperature cavity. With this assumption, the number of rf cavity cells would be the same in either scenario, so our results can be interpreted as representing either 20 cells of room-temperature or superconducting rf. We have confirmed, by comparison with existing data,[25] that the HOMs used in our calculations are roughly consistent with the kinds of values actually obtained from superconducting rf cells.

Predictions of longitudinal growth times (for the fastest growing mode) for both of the rf scenarios considered are summarized in Table 3.3–1. The optimized cavity shape, with only minor de-Qing (Case A), gives a = 1 growth times of about 0.1 ms (for I = 1.54 A). Substantial de-Qing (Case B) does help slow down the growth considerably, to times longer than 1 ms. Note

that the feedback system power required to counteract these instabilities will scale as the square of the growth rate, so a change of a factor of ten is extremely significant.

(A) RT/SC; Q/2	
$\tau_{a=1}$	0.4 ms
$\tau_{a=2}$	22 ms
(B) RT/SC; Q/200	
$\tau_{a=1}$	4 ms
$\tau_{a=2}$	390 ms

Table 3.3-1. Longitudinal coupled-bunch growth times for the APIARY high-energy ring (9 GeV; τ_E = 18.5 ms).

Transverse results, summarized in Table 3.3–2, are similar to those for the longitudinal case. Here too, we find that the lowest two synchrotron modes, a = 0 and a = 1, grow faster than the radiation damping rate. We again note the benefits of substantial de-Qing (Case B) in slowing down the growth rates to more manageable levels.

(A) RT/SC; Q/2	
$\tau_{a=0}$	1.2 ms
$\tau_{a=1}$	38 ms
(B) RT/SC; Q/200	
$\tau_{a=0}$	2 ms
$\tau_{a=1}$	66 ms

Table 3.3-2. Transverse coupled-bunch growth times for the APIARY high-energy ring (9 GeV; τ_x = 36.8 ms).

Investigations done previously have indicated that the behavior shown in Tables 3.3–1 and 3.3–2 is insensitive to energy in this regime, so increasing the energy asymmetry by raising the energy of the high-energy ring to 12 or 14 GeV would not be especially helpful. It is also found that the coupled-bunch growth rates for the case of a high-luminosity collider scale mainly with total current, and do not change significantly if the bunch pattern changes (e.g., choosing half as many bunches, with twice the single-bunch current). This latter study—carried out using a time-domain multibunch instability code written by K. Thompson at SLAC—qualitatively confirms the growth time predictions made here with ZAP, and shows that, for example, leaving a gap in the bunch train (to clear ions) does not affect the growth rates significantly.

Low-Energy Ring

Major parameters of the low-energy ring considered here (see Section 3.1) were summarized in Table 3.1–1. The ring is assumed to operate at the same rf frequency (353.2 MHz) as PEP, which leads to a harmonic number of 2592. Reaching the desired beam current requires 1296 bunches with 1.7 mA/bunch. To maintain short beam bunches in this ring (see Fig. 3.3–4), the rf system must provide at least 10 MV. This requires 10 cells of the new rf system described in Section 3.4.

Low-Energy Ring Thresholds

Taking into account the expected[21] impedance roll-off for short beam bunches, the longitudinal microwave instability threshold for the low-energy ring is shown in Fig. 3.3–5. For this ring, the broadband impedance used in the calculations shown here was again 1.5 Ω, despite the reduced number of rf cells. As is clear from Fig. 3.3–5, this impedance value does not lead to any problems.

It is also worth noting here that we have estimated the natural momentum spread of the low-energy beam to be 1×10^{-3}. This relatively large value is associated with the significant amounts of "extra" synchrotron radiation (generated in the wigglers and vertical separation magnets) needed to achieve the equal damping decrement and round beam conditions discussed in Section 2.2.

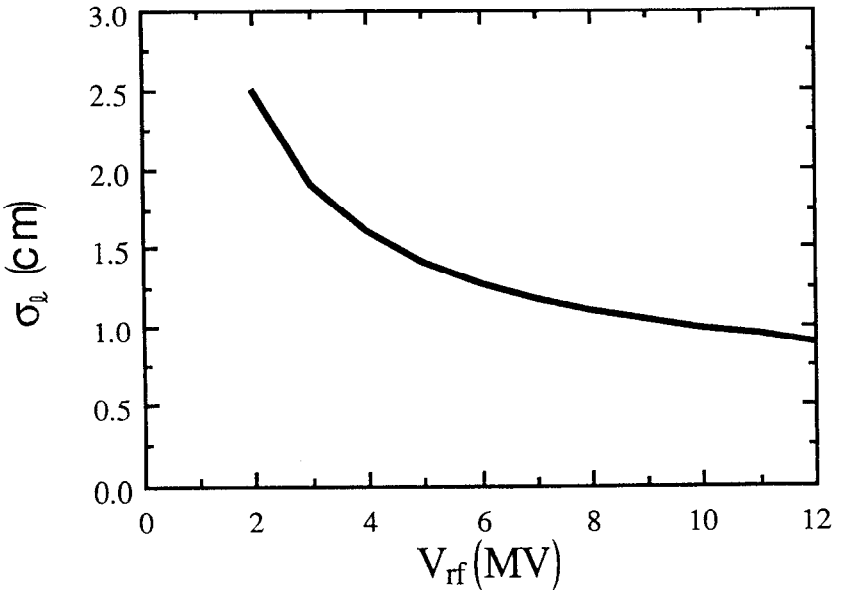

Fig. 3.3-4. Predicted natural bunch length for the APIARY low-energy ring as a function of rf voltage.

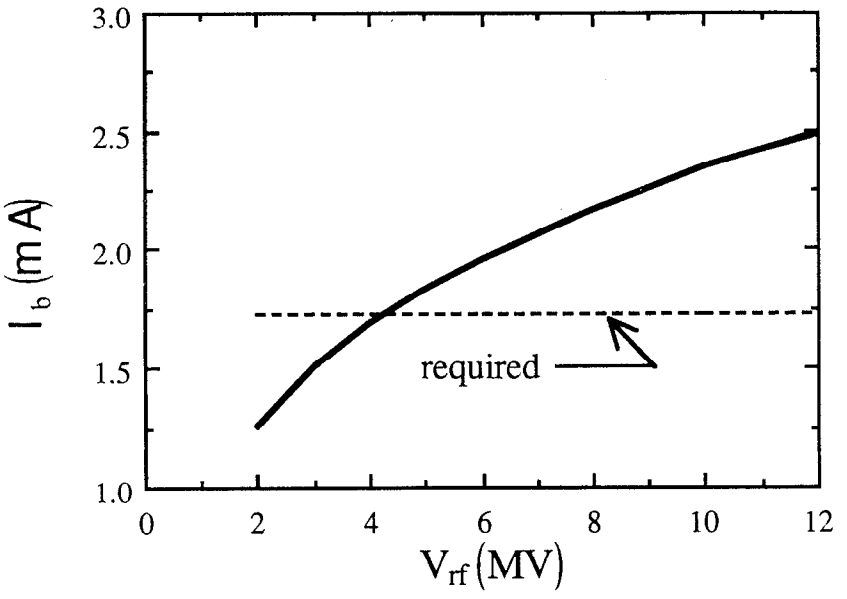

Fig. 3.3-5. Predicted threshold for longitudinal microwave instability for the APIARY low-energy ring. The threshold is above the required single-bunch current of 1.7 mA throughout most of this voltage range.

On the one hand, the increase in momentum spread has the undesirable effect of increasing the natural bunch length, so that $\sigma_\ell \approx 1$ cm requies $V_{rf} = 10$ MV but, on the other hand, it has the beneficial effect of stabilizing the bunches against growth from the longitudinal microwave instability, as can be seen from inspection of Eq. (3.3–4).

Transverse thresholds were predicted to be beyond the range of interest, and so are of no concern.

Low-Energy Ring Intrabeam Scattering

In this case, the lower beam energy enhances the IBS growth rates, and the single-bunch current is much higher than for the high-energy beam, but these aspects are compensated by the larger transverse emittance values. Thus, we again predict no emittance growth from intrabeam scattering.

Low-Energy Ring Beam Lifetime

Touschek Scattering. In contrast to the high-energy ring, the physical momentum acceptance limit, $\Delta p/p \approx 2.5\%$, is above that of the rf bucket ($\Delta p/p \approx 2.3\%$). Although the energy is lower than in the other ring, the large acceptance makes the Touschek lifetime about 900 hours, and thus not of concern.

Gas Scattering. At a gas pressure of 10 nTorr (N_2 equivalent), the lifetime is predicted to be dominated by the inelastic

scattering process. Similar to what was found for the high-energy ring, the overall beam half-life is about 3 hours. Because the lifetime depends mainly on the background gas pressure in the low-energy ring, special care must be taken in the design of the vacuum chamber; this topic is discussed in Section 3.6.

Quantum Lifetime. The beta functions in the low-energy ring are generally rather small, but there is nonetheless one area where quantum lifetime could be an issue—in the IR superconducting quadrupole doublet. These magnets require a high gradient and, both because the beta functions are increasing rapidly with distance from the IP and because azimuthal space is restricted, they cannot simply be lengthened. The design specifications for both quadrupoles call for an available beam aperture of $\xi = 15$. This is sufficient, and leaves some margin for beam misalignments. In practice, it is already necessary for other reasons to have good control of the orbit in this region, so this aspect does not imply a new constraint, but it should be noted that care will be required in the alignment of these quadrupoles to avoid beam loss.

Low-Energy Ring Coupled-Bunch Instabilities

For the low-energy ring we studied the same two rf scenarios described earlier, with the number of rf cells reduced compared with the high-energy case to account for the lower voltage requirement. The general caveat mentioned earlier about not overinterpreting the results applies equally here.

Longitudinal growth times, summarized in Table 3.3–3, are more or less comparable to those for the high-energy ring. The results of Cases A or B are not unlike those predicted for the Advanced Light Source, now under construction at LBL. Feedback is needed, but the requirements should be manageable.

Table 3.3-3. Longitudinal coupled-bunch growth times for the APIARY low-energy ring (3.1 GeV; τ_E = 17.3 ms) at a beam current of 2.23 A.

(A) RT/SC, Q/2	
$\tau_{a=1}$	0.3 ms
$\tau_{a=2}$	20 ms
(B) RT/SC, Q/200	
$\tau_{a=1}$	3 ms
$\tau_{a=2}$	290 ms

Similar statements apply to the transverse growth times, which are summarized in Table 3.3–4. As for the high-energy ring,

growth of the higher synchrotron modes ($a \geq 2$) is not a problem.

(A) RT/SC, Q/2	
$\tau_{a=0}$	1 ms
$\tau_{a=1}$	57 ms
(B) RT/SC, Q/200	
$\tau_{a=0}$	5 ms
$\tau_{a=1}$	110 ms

Table 3.3-4. Transverse coupled-bunch growth times for the APIARY low-energy ring (3.1 GeV; τ_E = 32.3 ms) at a beam current of 2.23 A.

Summary of Findings

We have seen here that the performance of both the high- and low-energy rings is likely to be limited mainly by coupled-bunch instabilities. Our choice of specially designed single-cell rf cavities helps to reduce the longitudinal impedance by permitting the voltage to be produced with many fewer cells and by permitting the cavity to be more "monochromatic." Furthermore, such a cavity design serves to lower the transverse impedance by having a relatively large bore size and by permitting the siting of the rf cells in a low-beta region of the ring.

Taken together, these features lead to a strong reduction in coupled-bunch instabilities and a strong increase in the transverse single-bunch threshold. Even after all of this, the ability of APIARY to achieve its luminosity goal will depend largely on the capability of the feedback system (described in Section 3.5).

Total beam current limitations in both rings will depend upon the ability of the vacuum system to maintain an acceptable pressure, below 10 nTorr, in the presence about 2 A of circulating beam. Single-bunch limitations appear to arise only from the allowable beam-beam tune shift, that is, neither bunch lengthening and widening due to the longitudinal microwave instability (which places a limit on the allowable broadband impedance), nor current limitations arising from the transverse mode-coupling instability are predicted to be constraints in the multibunch scenario considered here.

3.4. RF Systems

The rf systems for the APIARY collider rings must be capable of stably storing about 1000 bunches of electrons or positrons, each with a current of 1–2 mA. As discussed earlier, the most severe limitation on stable performance arises from coupled multibunch instabilities, which are driven by narrow, resonant higher-order modes (HOMs) of the rf cavities. For the usual room-temperature reentrant cavities, growth times under these beam conditions are predicted to be fractions of a millisecond; counteracting such growth would require extraordinarily powerful feedback systems.

Despite this difficulty, it seems clear that the multibunch mode of operation is essential for a high-luminosity B factory—there is no reason at present to imagine that tenfold to hundredfold improvements in luminosity will result from increases in the beam-beam tune-shift limit. In fact, it appears preferable to have many bunches with less current per bunch, as discussed earlier. There are three reasons for this view:

1. Single-bunch instabilities are decreased.

2. Beam power losses to higher-order modes are reduced considerably, due to the lessened harmonic content of more closely spaced bunches.

3. Multibunch coupled motion is driven predominantly by average current, and is predicted to be so strong in B-factory colliders that it would be relatively insensitive to the temporal pattern of the bunches.

It is clear that the present PEP rf system is inappropriate for a B-factory collider. PEP has 24 five-cell reentrant rf cavities, for a total of 120 cells. The rf cavities occupy about 100 m in the ring and, on the average, they sample a rather high beta-function value—about 30 m. The bore size of these room-temperature cavities is typically small, which gives a high transverse impedance. The combination of high beta functions at the cavity locations and high transverse impedance is already known to limit the beam current.[19,20] (Note that, as discussed earlier, more than two-thirds of the impedance in PEP presently stems from the substantial rf system.)

For the APIARY collider, these factors argue strongly for replacing the PEP rf system with compact, lower-impedance rf cavities. The new rf system must have the following features:

- Lowest possible number of cavities that can achieve the desired voltage (i.e., many fewer cells than PEP now has)
- Minimal higher-order impedance
- Large bore size to reduce transverse impedance
- Compact length so the rf can be localized in low-beta regions of the rings
- High gradients (up to 3–5 MV/m)

Fortunately, these requirements can be met with either of two approaches: superconducting rf cavities or specially designed, low-impedance conventional cavities.

In either approach, *single-cell rf cavities with a shape similar to the superconducting cavities of LEP should be used;* this choice reduces HOM impedance and lends itself to taking full advantage of the HOM loading and coupling techniques already developed[25,26] at CERN for LEP and at DESY for HERA. The frequency used for the LEP rf system, 352 MHz, is essentially the same as that already used in PEP, so a cavity shape appropriate for the APIARY rings has already been developed and tested at CERN.

RF Scenarios

The room-temperature approach would use copper cavities, each driven by a single, commercially available 1-MW klystron. Using a high input power minimizes the number of cavities needed, but would require development of a cavity input window capable of transmitting about 600 kW of rf power without breakdown. Such windows are now used for output coupling in klystrons; with some R&D they can be made to work for input power coupling in cavities as well. It is also possible to split the power in two and transmit it through two separate input windows, if that were needed. We do not anticipate problems with meeting the cooling requirements of the copper cavities, since the cavity shape is ellipsoidal (in fact, almost spherical) and is therefore relatively easy to cool. However, this aspect must be confirmed by detailed engineering calculations.

In the superconducting approach, each klystron would drive two cavities, so the power per window would be reduced to 300 kW. This reduction in input power compared with the room-temperature scenario is possible because superconducting rf cavities have far lower wall losses than room-temperature cavities. Thus, we expect that—at any given level of power coupled through a window—the superconducting approach will have the advantage of requiring fewer cavities.

On the other hand, a superconducting rf system requires refrigeration and makes use of generally more complex technology, so it would probably be the more costly approach. Obviously, if R&D efforts lead to a high-power window design capable of handling 0.5–1 MW in a cryogenic environment, the use of superconducting rf becomes even more attractive.

With either rf scenario, the proposed cavities have an active length of 0.33 m. However, their overall geometry is complicated because each cavity requires input and loading couplers; we assume that at least 1 m of azimuthal space in the ring will be required per cavity.

Parameters of conventional and superconducting rf cavities for the 9- and 3.1-GeV APIARY rings are compared in Table 3.4–1 on the next page.

Cavity Shape and Parameters

The shape for one quadrant of the rf cavity we are considering is shown in Fig. 3.4–1. This shape was used for computing the properties of the cavity fundamental mode (TM_{010}) with the frequency-domain electromagnetic code URMEL. The exact frequency used in the computations was 352.0525 MHz, corresponding to a wavelength of 0.852 m; this differs slightly from the nominal PEP frequency of 353.2 MHz. Predicted parameters of the cavity are summarized in Table 3.4–2.

Figs. 3.4–2 through 3.4–4 below show the electric-field patterns (direction and relative strength) of the fundamental and of two higher-order longitudinal modes, including that at the pipe cutoff frequency, i.e., $f/f_c = 1$.

Table 3.4–1. Comparison of room-temperature and superconducting rf-system parameters for the APIARY storage rings.

High-Energy Ring	Room Temp.	Supercon.
Accelerating voltage [MV]	25	25
Cavity shunt impedance* [MΩ]	2.77	277 000
Number of cavities	20	20
Gap voltage per cavity [MV]	1.25	1.25
Field gradient [MV/m]	3.75	3.75
Wall loss per cavity* [kW]	280	0.003
Wall loss, total for ring* [kW]	5640	0.056
Number of 1-MW klystrons*	20	10
Total klystron power* [MW]	20	10
Available power for beam and waveguide losses* [MW]	14.36	10

Low-Energy Ring	Room Temp.	Supercon.
Accelerating voltage [MV]	10	10
Cavity shunt impedance* [MΩ]	2.77	277 000
Number of cavities	10	10
Gap voltage per cavity [MV]	1	1
Field gradient [MV/m]	3.0	3.0
Wall loss per cavity* [kW]	180	0.002
Wall loss, total for ring* [kW]	1810	0.018
Number of 1-MW klystrons*	10	5
Total klystron power* [MW]	10	5
Available power for beam and waveguide losses* [MW]	8.2	5.0

*) Denotes significant differences between room-temperature and superconducting scenarios.

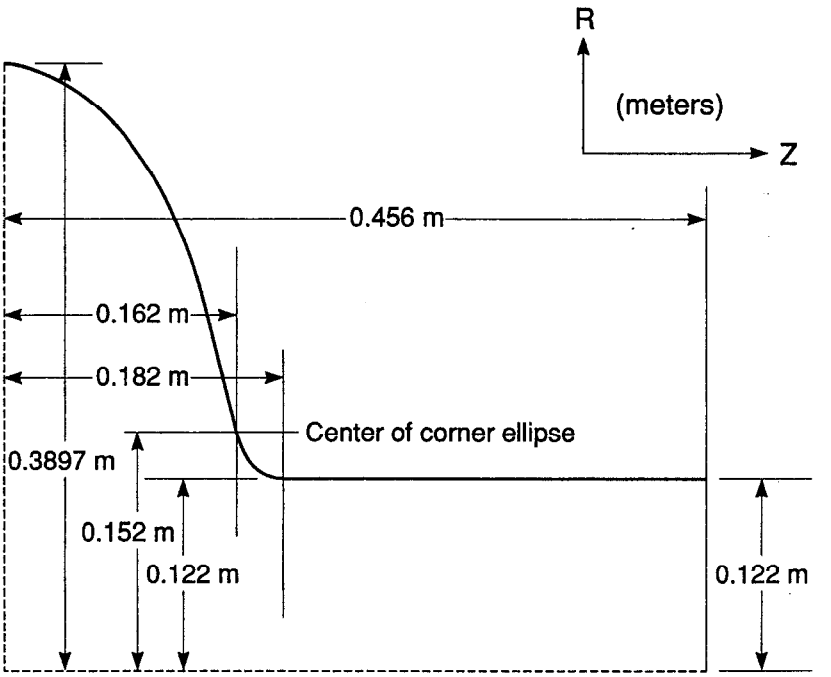

XBL 8910-6321

Fig. 3.4–1. Shape of a single quadrant of the rf cavity used at LEP which we have selected for APIARY.

Table 3.4–2. Predicted properties of APIARY rf cavity.

Parameter	Value
TM-mode beam-tube cutoff frequency, f_c [MHz]	940.5134
Ratio of fundamental to cutoff frequency, f/f_c	0.374
Unloaded Q at fundamental	45 218
(R/Q) at fundamental [Ω]	61.41
Single-particle loss parameter for the fundamental mode,[a] k_l (= $V^2/4U$) [V/pC]	0.0628

[a] V is the peak voltage and U is the stored energy.

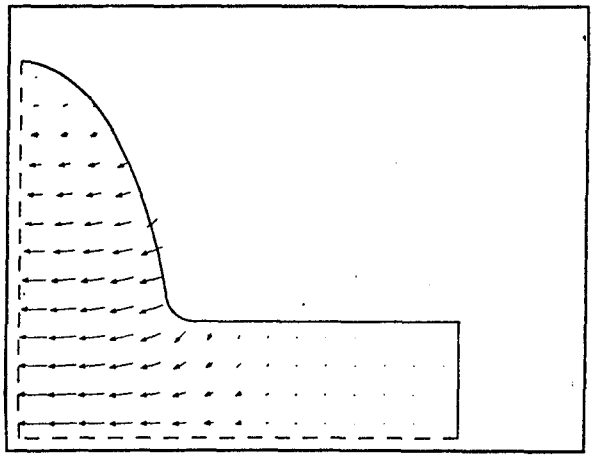

Fig. 3.4–2. Electric-field pattern at 352.11 MHz.

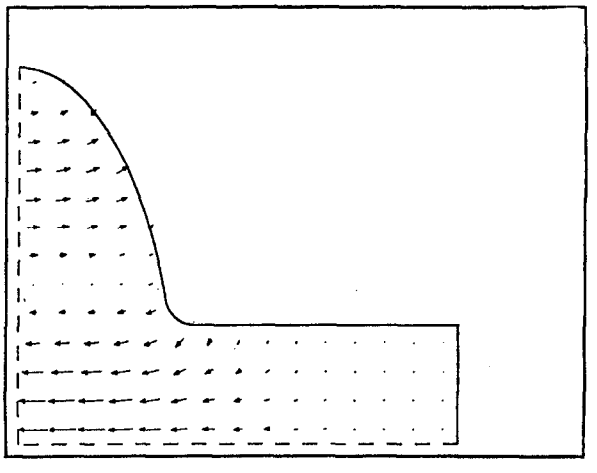

Fig. 3.4–3. Electric-field pattern at 726.33 MHz.

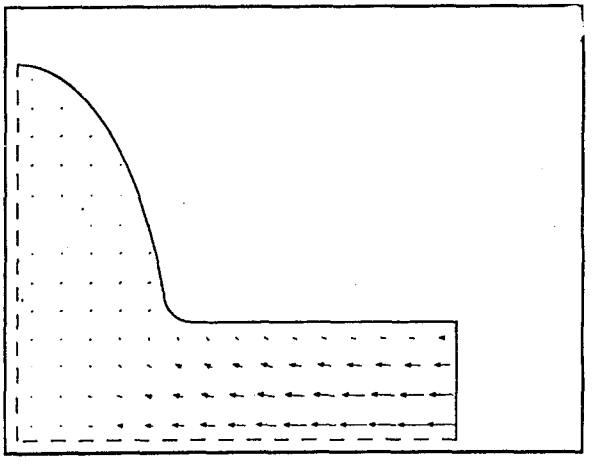

Fig. 3.4–4. Electric-field pattern at 963.37 MHz, the pipe cutoff frequency.

General Remarks on the Superconducting RF System

It is clear from the previous discussion that the number of cells goes down as the power per window goes up. At the Blois Workshop[27] it was concluded that superconducting rf would become attractive only if it is possible to transmit more than 400 kW through a window. (Other requirements identified at the workshop include a fundamental Q of 2×10^9, a loaded $Q \approx 50$–100 for the higher-order modes, and a gradient of 5–9 MV/m.) Otherwise, room-temperature cavities that are shaped like superconducting ones (to allow efficient HOM loading) would be equally attractive.

The prospect of achieving these performance levels in superconducting rf cavities holds great promise. The required gradient and fundamental Q have already been achieved. At DESY, broadband de-Qing of HOMs has been advanced to the level of $Q_L \approx 200$–500 with specially designed HOM couplers.[25]

Considerable progress has also been made in high power transmission through windows. In the TRISTAN ring at KEK, levels of 85-100 kW per window have been reached during low-current beam tests in the accelerator. The 500-MHz superconducting cavities in Petra at DESY have achieved 350 kW per window for 18 ms and 250 kW per window for 3 hours, both in laboratory tests at room temperature. The 352-MHz CERN cavities for the superconducting LEP upgrade, whose design we would use, are rated at 120 kW per window and have been tested in the SPS ring under actual beam conditions; furthermore, they have achieved 380 kW in room-temperature laboratory tests at DESY. Finally, at Cornell, power levels in excess of 500 kW have been reached in laboratory tests under ideal conditions.

There do not seem to be any fundamental limits that would prevent us from achieving the goal of producing high-power, high-quality, single-cell superconducting rf cavities of the type needed for B-factories, although considerable R&D and detailed technical design remain to be done. In particular, special attention must be paid to three issues:

- Thermal isolation of the power window from the cryogenics
- Coupling the power into the cavities

- Coupling out high levels of HOM power loss through the cryogenic, superconducting environment into room-temperature loads

Perhaps the most important barrier to the use of superconducting rf systems is psychological. At present, there is no operational experience with using such systems to support beam currents on the order of amperes in a stable fashion. (We note, however, that the LEP-style cavities installed in the SPS ring survived a test involving circulation of proton-beam currents as high as 300 mA without damage.) Questions of quenching, thermal decoupling, and high beam loading weigh heavily. Fortunately, significant R&D is in progress at various laboratories. For the present, however, it is comforting to know that a specially designed room-temperature rf system will meet the B-factory requirements, given some improvements in rf-window capabilities.

The effects on the beam of higher-order modes of both the room-temperature and superconducting cavities were discussed in Section 3.3. To briefly summarize, we find that even with these well-designed cavities, growth of coupled multibunch motion—albeit at a reduced rate with growth times of 1 ms—can be expected. A feedback system will be essential, so it will be necessary to design one at the outset. The salient issues for the feedback system are the level of power required and the hardware complications introduced. In addition, one must consider whether the feedback hardware (detectors and kickers) defeats its own purpose by adding too much impedance to the ring.

3.5. Feedback Systems

If no improvements were made in rf system design, the APIARY storage rings would presumably employ standard, room-temperature, reentrant rf cavities. Because of the relatively high shunt impedances and high quality factors (Q) of the higher-order modes of such cavities, this choice would lead to significant growth rates for coupled-bunch instabilities—both longitudinal and transverse—and the feedback system would have to face the task of controlling coupled-bunch motion on a time scale of 0.1 ms or less. However, with the improved rf system (either superconducting or modified room-temperature) proposed here, the feedback system need control longitudinal coupled-bunch motion with an e-folding growth time of only about 4.5 ms. (It is worth noting, however, that the power requirements for the feedback system are dominated by the need to compensate for injection errors.)

In this section we will focus on the feedback system needs for the APIARY high-energy ring, as these are the more demanding. Although the growth rate in the low-energy ring is comparably high, energy deviations from injection errors will be smaller, making the feedback demands comparable or less.

Modes of higher order than the dipole synchrotron mode longitudinally, or the monopole synchrotron mode transversely, should be effectively suppressed by synchrotron-radiation damping. Thus, we need only consider dipole (a = 1) synchrotron motions for longitudinal feedback, and only monopole (a = 0) synchrotron motion for transverse feedback.

The feedback-system bandwidth W required to affect the coupled-bunch motion of B symmetrically spaced bunches in the ring is

$$W = \frac{1}{2} B f_0 \quad , \qquad (3.5\text{–}1)$$

where f_0 is the bunch revolution frequency. To achieve a luminosity of 3×10^{33} cm^{-2} s^{-1}, every second rf bucket in PEP must be filled, for a total of 1296 bunches. From Eq. (3.5–1), the bandwidth required would be about 90 MHz, about 10% of the feedback frequency, which we take to be near 1 GHz.

The strongest higher-order mode of the rf cavities produces a growth time (the inverse of growth rate, g) for the most unstable mode of 4.5 ms. About 20 neighboring modes will also have strong growth from this source.

The greatest voltage kick required of the feedback system is that needed to stabilize the beam that is injected with errors in energy and phase. Each injection pulse will provide 1/5 of a full bunch, or 1/6480 of an entire fill at the rate of 60 Hz. Energy error will be about 2×10^{-3} of 9 GeV, and timing jitter about 100 ps. These combine in quadrature to produce an initial synchrotron amplitude of 28 MeV. The greater part of this local excursion, representing stable modes of oscillation, will be damped by radiation, but it includes perhaps 100 unstable modes each with initial amplitude of

$$\frac{\Delta E}{e} = \frac{2}{6480}\,(28\ \text{MeV}) = 8.64\ \text{kV per mode} \qquad (3.5\text{–}2)$$

The feedback system must suppress the growth of these modes in bunches that are coupled to the injected bunch through narrow-band impedances. Not all of these grow at the maximum rate $1000/4.5 = 224\ s^{-1}$, but for good control, it is prudent to design for a damping rate of $500\ s^{-1}$. Also, to allow for the coincidental addition in some bunches of amplitudes from the 100 modes, we provide (as explained in Appendix C) for a maximum kick per turn of

$$V_k = 2\left(\frac{g}{f_o}\right)\frac{\Delta E}{e} \times 100 = 6.35\ \text{kV per turn.} \qquad (3.5\text{–}3)$$

This voltage will suppress growth and add to the radiation damping to reduce by a factor of three the injection oscillation before the next injection pulse.

The output power to the kicker is given by[28]

$$P_k = \frac{1}{2}\frac{(V_k^2)}{R_{\|}T^2} \qquad (3.5\text{–}4)$$

where $R_{\|}T^2$ is the kicker shunt impedance modified by the transit-time factor, T. For economy, a large $R_{\|}T^2$ is desired but this and spurious responses of the kicker appear as added contributions to the storage-ring beam impedance.

A feasible feedback scenario employing a specific type of kicker that meets these requirements of bandwidth, power, and shunt impedance is described below.

Design Scenario

We have considered various types of kickers[28] and pickups, e.g., capacitive plates, resonant cavities, the stripline family of devices, and traveling-wave structures. Stripline quarter-wavelength ("λ/4") series loops appear to be the most attractive. A resonant cavity could provide very high shunt impedance, which minimizes power requirements, but at the cost of bandwidth. Even at a high frequency like 1 GHz, the Q of a cavity would have to be lowered significantly in order to achieve the necessary bandwidth. To obtain a bandwidth of Δf = 90 MHz, the Q (given by $f/\Delta f$) would have to be about 11, which would be rather difficult to obtain. Moreover, resonant cavities would add relatively more impedance in the beam's path. However, it is feasible, as discussed at the end of this section, to employ a number of separately-powered tuned cavities, each with a bandwidth of about 10 MHz and together spanning 90 MHz.

Stripline electrodes are directional couplers and have terminals at both ends. Their signals may therefore be added by simple series connection; such an array is shown in Fig. 3.5-1, taken from Ref. 28. The sinusoidal signals, progressing upstream, add in phase if the closely spaced loops are λ/4 long at midband and if the connecting transmission lines (each of impedance $Z_L \approx$ 100 Ω) are λ/2 long. Assuming no mismatch in signal and particle velocities, the response of N such loops is N times enhanced over that of a single loop, and the bandwidth narrows linearly as the transit time becomes longer. The frequency bandwidth $\Delta\omega$ within the half-power range is,[28] for $N \geq 2$,

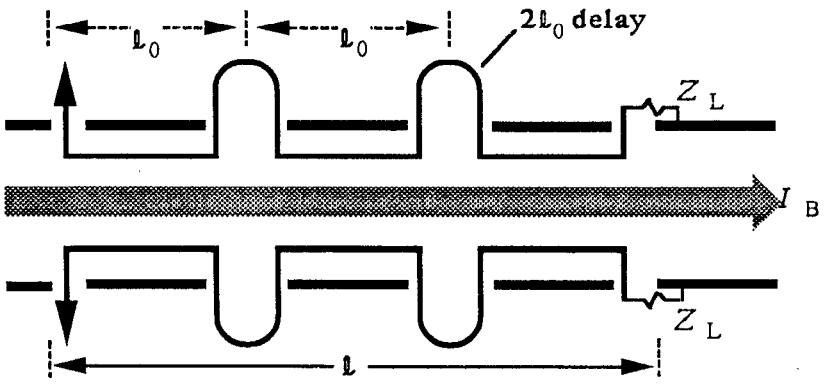

Fig. 3.5–1. Array of series-connected stripline electrodes.

approximately $0.9(\omega/N)$. By using the series array of striplines described here, it is easy to exercise flexibility in exchanging bandwidth for gain and, through proper matching, to avoid wasting power on unused bandwidth.

The product of bandwidth and peak power gain (i.e., shunt impedance) is proportional to the pickup length ℓ and is given by[28]

$$R_{\|}T^2\Delta\omega \approx \frac{3.6}{\pi} Z_L c\,(k_0 g_{\|})^2 \ell \quad , \qquad (3.5\text{–}5)$$

where $g_{\|} = 1/2$ is a reasonably attainable geometric factor; Z_L is the line impedance (taken to be 50 Ω) and $k_0 = \omega_0/c$, with ω_0 being the central angular frequency of the kicker.

We envision a series of loop stripline pairs at a central frequency of 1 GHz. (Although higher frequencies give higher shunt impedance, practical problems with assembling the device in the vacuum chamber are encountered for central frequencies beyond about 1 GHz; we take this as a practical upper limit for the design frequency of the feedback system.) The 1-GHz, $\lambda/4$ striplines are 7.5 cm long. For the required bandwidth of 90 MHz, we would need 10 such loops connected in series. Some allowance must be made for reflections in such an array. If 0.2 dB per loop is allowed, an average power loss of 21% results. The properties of one array would be:

Bandwidth	90 MHz
Length	75 cm
$R_{\|}T^2$	2.5 kΩ
Ave. Loss	21%

Four of these would be used to deliver the 6.35 kV per turn, requiring 640 watts each for a total power of 2.6 kW. At this level, the power amplifiers can be traveling-wave or solid-state devices, as used in stochastic cooling systems, but with smaller bandwidth required for this application.

The kickers and pickups will also respond to the driving beam current, and will generate wakefields that will act back on the beam. The broadband impedance from these devices is peaked at the central frequency (1 GHz here) with a bandwidth determined by the device length (e.g., 90 MHz for the ten-loop array); there are also higher harmonics (2 GHz, 3 GHz, etc.)

present, but with ever-decreasing strength. The peak value of the longitudinal impedance $R_{||}T^2$ at the fundamental frequency is a quarter of the shunt impedance.[29] The central frequency of 1 GHz corresponds to a revolution-frequency harmonic of $n \approx 7338$ for a ring circumference of 2200 m.

The total longitudinal resistive broadband impedance at the peak of the kicker fundamental is then

$$\frac{Z_{||}}{n} = \frac{1}{4}\frac{R_{||}T^2}{n} \approx 0.4\ \Omega \qquad (3.5\text{–}6)$$

for $R_{||}T^2 = 10\ k\Omega$. Considering the contribution from the pickups to be about 25% of this (because there will be fewer pickups than kickers), the total resistive longitudinal impedance is $(Z_{||}/n)_T \approx 0.5\ \Omega$. The low-frequency reactive impedance will be reduced from this figure by the Q value of the structure ($Q \approx 11$) to about 0.05 Ω. Contributions from the higher harmonics will fall off rapidly with frequency.

The bandwidth of the impedance generated by the feedback structure described here is broad enough to avoid inducing instability in the coupled-bunch motion it is supposed to cure, that is, its wakefields have sufficient time to damp between successive bunch passages. On the other hand, the impedance bandwidth is not large enough to affect single-bunch (internal) motion significantly.

For the purpose of estimating the effects on a single bunch, such as bunch lengthening, we must calculate an "effective broadband impedance." This involves a convolution of the frequency-dependent impedance with the power spectrum of the bunch, $h_a(\omega)$, as described in Ref. 18:

$$\left[\frac{Z_{||}}{n}\right]^a_{eff} = \sum_{n=-\infty}^{\infty} \left[\frac{Z_{||}(\omega_{n,a})}{(\omega_{n,a}/\omega_0)}\right] h_a(\omega_{n,a}) \qquad (3.5\text{–}7)$$

where $\omega_{n,a} = n\omega_0 + a\omega_s$, with a being the synchrotron mode number. Explicit computation of this sum yields a rather low value of this effective impedance (on the order of 0.003 Ω). Thus, the feedback system is not expected to exacerbate any beam instabilities.

Wideband multibunch feedback can be implemented in many ways:

- Fast bunch-by-bunch feedback that influences single bunches directly; this requires only simple filtering and can be visualized simply in the time domain
- Damping of selected modes; this is accomplished by performing careful modal analysis in the frequency domain and selecting and affecting specific modes
- All-mode damping; this may be necessary when dealing with large numbers of bunches, but it requires many electronic channels with complicated notch filtering and special frequency-dependent gain and phase characteristics

For our situation, which involves very many multibunch azimuthal modes but only a few synchrotron modes (dipole and perhaps quadrupole), the fast and direct method of bunch-by-bunch feedback is preferred, being conceptually and electronically straightforward. The following steps must be carried out:

- Beam signals are detected over a suitably large bandwidth ($\geq$ 90 MHz)
- Detected phase and slope of the zero-crossing are processed with fast phase-shifters, delays, and voltage modulators
- The modified signals are fed through a power amplifier and applied directly to the kicker.

With today's high-frequency digital signal processing, this method is entirely feasible. A block diagram of the feedback loop is shown in Fig. 3.5–2.

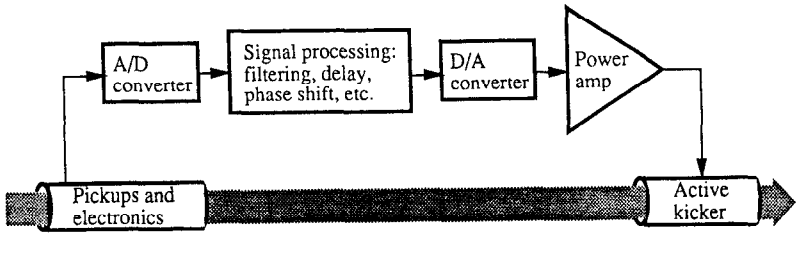

Fig. 3.5–2. Diagram of feedback loop.

An alternative hardware solution for an amplifier-kicker combination of moderate bandwidth is the use of multiple rf cavities. These would be stagger-tuned to cover the 90 MHz bandwidth in the region of 800 MHz. For a power source, each would be driven by a UHF TV klystron with a bandwidth of about 10 MHz and a power of 11 kW. The cavities would be constructed with internal losses to provide a loaded Q of about 90 and ten in parallel would constitute a kicker of about 60 kΩ shunt impedance. Clearly, such a system could provide more than ten times the feedback correction we have specified above, if that were desired. Otherwise, the specified single-band system is to be preferred.

3.6. Synchrotron Radiation and Vacuum

When an electron beam circulates in a storage ring, the vacuum-chamber walls are subjected to synchrotron radiation. This radiation incident on the walls produces very high thermal flux densities due to the narrowness of its spatial distribution, which means that the chamber wall must be cooled. Normally, this is accomplished by water cooling the external surface of the chamber. An additional benefit associated with the cooling is that it maintains the chamber wall at a relatively low temperature, thus decreasing the gas load resulting from thermal desorption.

There are two design issues related to the copious production of synchrotron radiation in a high-intensity storage ring:

- Heating of the vacuum chamber walls due to the high thermal flux density
- Radiation-induced gas desorption (both photodesorption and thermal desorption)

In this section we will estimate these effects and see what impact they have upon collider performance. As we shall see, the difficulties associated with the high beam currents in the APIARY storage rings are amenable to standard engineering solutions. Note that we use "electrons" in this section in the generic sense of referring either to electrons or to positrons.

Wall Heating

In the APIARY design (at its full luminosity), we are dealing with a beam current in each ring more than a factor of 10 higher than is typical for a high-energy storage ring, so the heat load is quite high. As will be obvious from the discussion below, the difficult parameter to deal with is not the power *per se*, but rather the linear thermal flux density. For this reason, it turns out that—contrary to intuition—a small-circumference ring is a more difficult problem to deal with. In fact, if a very small low-energy ring design were selected, the heating problem would be considerably more severe than in the high-energy ring, despite the fact that the beam energy, and thus the synchrotron radiation power itself, is lower than in the high-energy ring. The option we consider here—a low-energy ring having a circumference identical to that of the high-energy ring, i.e., 2200 m—avoids any concerns in this regard.

To estimate the heat load, we start from the well-known expression for the synchrotron radiation power (in watts), given by:

$$P_{SR} = \frac{88.5\, E^4\, I}{\rho} \qquad (3.6\text{–}1)$$

where E is the total energy (in GeV), I is the total beam current (in mA), and ρ is the bend radius of the dipoles (in m). For the high-energy ring, we take a typical value of ρ = 165 m. Then, the linear power density (in W/cm) along the radiated circumferential path length is given by

$$P_L = \frac{0.01 \cdot P_{SR}}{2\pi\rho} = \frac{0.885\, E^4\, I}{2\pi\rho^2} \quad . \qquad (3.6\text{–}2)$$

For a 9-GeV, 3000-mA beam, which corresponds to the design maximum current for the high-energy ring, we obtain P_L = 102 W/cm.

The vertical angular spread (in radians) of the synchrotron radiation fan is given approximately by

$$\theta \approx \frac{m_0 c^2}{E} = \frac{1}{\gamma} \quad , \qquad (3.6\text{–}3)$$

which, for a 9-GeV electron beam, is θ = 0.06 mrad. Although not strictly true, we will assume here that the power is uniformly distributed over this angular extent, in which case we calculate the height of the vertical band illuminated by the synchrotron radiation fan to be

$$h = 2\left[\sigma_y^2 + d^2 \cdot \left(\sigma_{y'}^2 + \theta^2\right)\right]^{1/2} \qquad (3.6\text{–}4)$$

where σ_y is the rms beam height, $\sigma_{y'}$ is the rms angular spread, and d is the tangential distance from the beam orbit to the chamber wall, as shown in Fig. 3.6-1.

The value for d can be easily calculated from the geometry shown in Fig. 3.6–1, where w/2 is the transverse distance from the beam orbit to the outer wall of the vacuum chamber:

$$d = \sqrt{\left(\rho + \frac{w}{2}\right)^2 - \rho^2} \qquad (3.6\text{-}5)$$

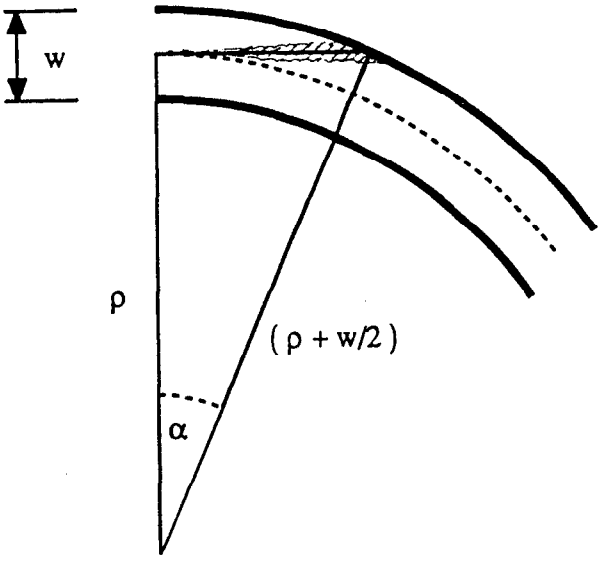

Fig. 3.6–1. Geometry of the synchrotron-radiation fan hitting the vacuum-chamber wall (not to scale).

For a standard vacuum chamber half-width of 5 cm and a 165 m bending radius, we would obtain d = 4.06 m, with an angle of incidence given by $\alpha = d/\rho = 25$ mrad.

To be conservative, we estimate the radiation power density ignoring the contribution from the finite beam emittance, that is, we take $\sigma_y = \sigma_{y'} = 0$ in Eq. (3.6–4). With this approach, we find the height of the illuminated strip to be $h = 2\theta d = 0.5$ mm, and the thermal flux density becomes $P_A = P_L/h = 2$ kW/cm^2. This value could be decreased by a factor of two by inclining the wall at 30°.

It is important to note that our flux density estimate applies to the case of a photon beam incident on the vacuum chamber wall at a shallow angle ($\alpha = 25$ mrad in the example above). In the worst-case of an object *normal* to the incident flux, such as a flange or radiation mask, the density would increase in the ratio $\sin(\pi/2)/\sin(\alpha) = 1/0.025 \approx 40$, giving $P_A = 80$ kW/cm^2. This value is quite high, but within the standard operating range for properly engineered masks.

Having calculated the thermal flux, we can now estimate the temperature drop ΔT across the vacuum chamber wall using a thermal relaxation program. Typical results for a copper and an aluminum chamber, with cooling water at 30°C, are shown in Fig. 3.6–2. With this approach, it is possible to model the influence of wall thickness, fins, and cooling tubes in order to obtain an optimized design.

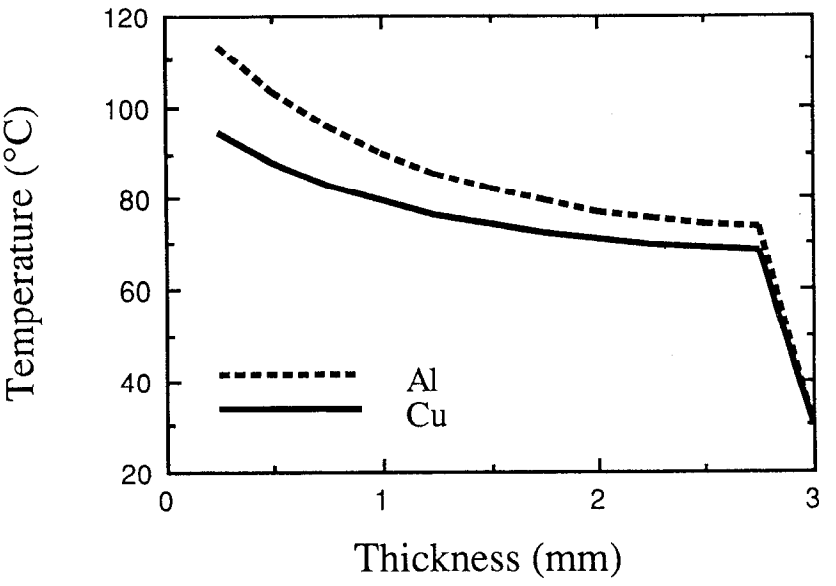

Fig. 3.6–2. Temperature distribution of example vacuum chamber wall from thermal relaxation code. Results for aluminum and copper are quite similar.

Table 3.6–1 summarizes both the nominal current and maximum current cases for the low- and high-energy rings, compared with values from PEP. We see that the wall temperature is below the original design specification for the PEP chamber.

Gas Desorption

Gas desorption in an electron storage ring arises from two causes:

- Thermal outgassing
- Synchrotron-radiation-induced photodesorption

The first mechanism is common to all vacuum systems, and occurs in the absence of synchrotron radiation. In essentially all electron storage rings, the thermal outgassing component of the pressure is negligible compared with that from the photodesorption, and contributes mainly to the base pressure of the ring in the absence of a circulating beam. The gas load from synchrotron radiation, on the other hand, determines the actual running pressure of the ring.

In the case of the APIARY design, the high- and low-energy rings will have circulating beam currents of approximately 1.5 A and 2.2 A, respectively, to reach the design luminosity of 3×10^{33} $cm^{-2}s^{-1}$. For design purposes, however, we specify a maximum current in each ring of 3 A. This beam current is at

Table 3.6–1a. *Comparison of radiation loads and heat fluxes in PEP and the APIARY low-energy ring. For PEP an aluminum chamber is used; the APIARY estimate assumes a copper chamber.*

PARAMETER	PEP	APIARY Low Energy Nominal current	APIARY Low Energy Maximum current
Magnetic radius [m]	165	58.3	58.3
Bend magnet field [T]	0.3033	0.1774	0.1774
Energy [GeV]	15.00	3.10	3.10
Current [mA]	200	2230	3000
Power [kW]	5,436	313	421
Chamber wall linear flux [W cm^{-1}]	52.43	8.54	11.49
Beam divergence 2θ [mrad]	0.07	0.33	0.33
Tangential distance d (m)	4.06	2.42	2.42
Angle of incidence α [mrad]	24.62	41.42	41.42
Beam height [mm]	0.554	1.592	1.592
Linear flux on masks at 90° [W cm^{-1}]	2130	206	277
Wall heat load [kW cm^{-2}]	0.95	0.05	0.07
Wall thickness [cm]	0.60	0.22	0.22
ΔT across wall [°C]	32.09	2.22	2.99
ΔT, chamber to water [°C]	15.91	2.64	3.55
ΔT, total, inner wall to water [°C]	48.00	4.86	6.54
Inlet water temperature [°C]	22.00	22.00	22.00
Water temperature rise [°C]	9.06	1.48	1.98
Average wall temperature [°C]	74.5	27.6	29.5

Table 3.6–1b. Comparison of radiation loads and heat fluxes in PEP and the APIARY high-energy ring. For PEP an aluminum chamber is used; the APIARY estimate assumes a copper chamber.

PARAMETER	PEP	APIARY High Energy Nominal current	APIARY High Energy Maximum current
Magnetic radius [m]	165	165	165
Bend magnet field [T]	0.3033	0.1820	0.1820
Energy [GeV]	15.00	9.00	9.00
Current [mA]	200	1540	3000
Power [kW]	5,436	5,424	10,567
Chamber wall linear flux [W cm^{-1}]	52.43	52.32	101.92
Beam divergence 2θ [mrad]	0.07	0.11	0.11
Tangential distance d (m)	4.06	4.06	4.06
Angle of incidence α [mrad]	24.62	24.62	24.62
Beam height [mm]	0.277	0.461	0.461
Linear flux on masks at 90° [W cm^{-1}]	2130	2125	4140
Wall heat load [kW cm^{-2}]	1.89	1.13	2.21
Wall thickness [cm]	0.60	0.22	0.22
ΔT across wall [°C]	79.83	24.16	47.07
ΔT, chamber to water [°C]	54.31	16.17	31.50
ΔT, total, inner wall to water [°C]	134.14	40.33	78.57
Inlet water temperature [°C]	22.00	22.00	22.00
Water temperature rise [°C]	9.06	9.04	17.61
Average wall temperature [°C]	160.67	66.85	109.37

least an order of magnitude beyond the typical value for today's colliders, and as such presents an appreciable challenge to the vacuum system designer.

To estimate the desorption rate, we follow the approach of Gröbner et al.[30] After taking the spectrum of the synchrotron radiation photons into account, we can express the photon flux in the spectral interval (0,x) in the form

$$\dot{N}(x) = \frac{\sqrt{3}\, r_e}{e\hbar c} F(x)\, E\, I \qquad (3.6\text{–}10)$$

where

$$x = \frac{\varepsilon}{\varepsilon_{crit}} = \frac{\varepsilon}{\left(\frac{3\hbar c}{2}\right)\left(\frac{\gamma^3}{\rho}\right)} \qquad (3.6\text{–}11)$$

with ε the photon energy, ε_{crit} the critical energy in the dipoles, and F(x) the integral over the modified Bessel function

$$F(x) = \int_0^x \int_u^\infty K_{5/3}(y)\, dy\, du \quad . \qquad (3.6\text{–}12)$$

For large values of x, $F(x) \rightarrow 5.53$. After rearranging and inserting appropriate values for the constants, we obtain for the total flux

$$\dot{N} = 8.08 \times 10^{17}\, E{\cdot}I \ \ [\text{photons/s}] \qquad (3.6\text{–}13)$$

where E is in GeV and I is in mA. Desorbed gas molecules are produced in proportion to the photon flux, with the proportionality constant, η_F, giving the number of molecules produced per incident photon, that is,

$$\dot{N}_{Mol} = 8.08 \times 10^{17}\, E{\cdot}I{\cdot}\eta_F \ \ [\text{molecules/s}] \qquad (3.6\text{–}14)$$

There has been a great deal of discussion in the literature about the appropriate value for η_F; typical values range from about 2×10^{-7} to 5×10^{-6}. For this document, we take a conservative choice of $\eta_F = 1.5 \times 10^{-5}$, which was used in the PEP design. Using the Ideal Gas Law, we can relate the number of molecules to a gas load with a conversion factor of 3×10^{-20} Torr-liters/molecule. This gives the effective gas load from the photodesorption as

$$Q_{gas} = 2.42 \times 10^{-2}\, E \cdot I \cdot \eta_F \ \text{[Torr·liters/s]} \quad (3.6\text{–}15)$$

or, for our assumed desorption coefficient of $\eta_F = 1.5 \times 10^{-5}$,

$$Q_{gas} = 3.64 \times 10^{-8}\, E \cdot I \ \text{[Torr·liters/s]} \ . \quad (3.6\text{–}16)$$

In Table 3.6–2, we use Eq. (3.6–16) to estimate the gas loads produced in the low- and high-energy storage rings. Maintaining a pressure of 10 nTorr in the low-energy ring requires a total pumping speed of about 350 000 l/s at the maximum design current. To put this into perspective, it is about 1/3 the pumping capacity, per meter of ring circumference being installed on the ALS ring at LBL.[31] If it turns out that a lower η_F value can be justified, the pumping requirements can be reduced accordingly. The high-energy ring requires about three times the pumping speed of the low-energy ring, that is, about the same as the ALS specifications.

Installation of the Low-Energy Ring in the PEP Tunnel

During its initial design phase, room was made available in the PEP tunnel to accommodate an additional (proton) ring that was to have been located on top of the electron ring. Fig. 3.6–3 shows a cross section of the PEP tunnel as this was envisioned. Thus, we have the possibility of adding the APIARY low-energy ring in this location. If the new ring were prepared in advance, such that it could be installed during the same shutdown needed for upgrading the PEP vacuum system, the incremental installation time would be minor. We estimate the required length of the shutdown to be about two years; the additional penalty for installation of a second ring simultaneously is thought to be only about six months.

Table 3.6–2a. *Comparison of vacuum loads and pumping speed requirements in PEP and the APIARY low-energy ring.*

PARAMETER	PEP	APIARY Low Energy Nominal current	APIARY Low Energy Maximum current
Magnetic radius [m]	165	58.3	58.3
Bend magnet field [T]	0.3033	0.1774	0.1774
Energy [GeV]	15	3.1	3.1
Current [mA]	200	2230	3000
Power [kW]	5,436	313	421
Gas load [Torr-l s^{-1} mA^{-1}]	3.63×10^{-7}	7.50×10^{-8}	7.50×10^{-8}
Total photon gas load [Torr-l s^{-1}]	1.09×10^{-3}	2.51×10^{-3}	3.38×10^{-3}
Assumed desorption coefficient (η_F)	1.50×10^{-5}	1.50×10^{-5}	1.50×10^{-5}
Photon gas load [Torr-l s^{-1} m^{-1}]	1.05×10^{-6}	6.85×10^{-6}	9.22×10^{-6}
Base pressure required [nTorr]	10	10	10
Distributed pumping [l m^{-1} s^{-1}]	105	685	922
Total distributed pumping [l s^{-1}]	108,900	250,942	337,590
Thermal desorption coef. [Torr-l cm^{-2}]	1.50×10^{-11}	1.00×10^{-11}	1.00×10^{-11}
Calculated wall temperature [°C]	74.52	27.60	29.53
Thermal desorption [Torr-l $°C^{-1}$ cm^{-2}]	7.45×10^{-11}	1.84×10^{-11}	6.35×10^{-12}
Total perimeter of ring [m]	2200	2200	2200
Calculated thermal load [Torr-l m^{-1}]	2.24×10^{-7}	5.52×10^{-8}	1.91×10^{-8}
Total calculated thermal load [Torr-l]	4.92×10^{-4}	1.21×10^{-4}	4.19×10^{-5}
Total gas load [Torr-l]	1.50×10^{-3}	2.63×10^{-3}	3.42×10^{-3}
Total pumping [l s^{-1}]	158,086	263,085	341,784

Table 3.6–2b. Comparison of vacuum loads and pumping speed requirements in PEP and the APIARY high-energy ring.

PARAMETER	PEP	APIARY High Energy Nominal current	APIARY High Energy Maximum current
Magnetic Radius [m]	165	165	165
Bend Magnet Field [T]	0.3033	0.1820	0.1820
Energy [GeV]	15	9	9
Current [mA]	200	1540	3000
Power [kW]	5,436	5,424	10,567
Gas load [Torr-l s^{-1} mA^{-1}]	$3.63E \times 10^{-7}$	2.18×10^{-7}	2.18×10^{-7}
Total photon gas load [Torr-l s^{-1}]	1.09×10^{-3}	5.03×10^{-3}	9.80×10^{-3}
Assumed desorption coefficient (η_F)	1.50×10^{-5}	1.50×10^{-5}	1.50×10^{-5}
Photon gas load [Torr-l s^{-1} m^{-1}]	1.05×10^{-6}	4.85×10^{-6}	9.15×10^{-6}
Base pressure required [nTorr]	10	10	10
Distributed pumping [l m^{-1} s^{-1}]	105	485	945
Total distributed pumping [l s^{-1}]	108,900	503,118	980,100
Thermal desorption coef. [Torr-l cm^{-2}]	1.50×10^{-11}	1.00×10^{-11}	1.00×10^{-11}
Calculated wall temperature [°C]	160.67	66.85	109.37
Thermal desorption [Torr-l $°C^{-1}$ cm^{-2}]	1.61×10^{-10}	4.46×10^{-11}	5.96×10^{-11}
Total perimeter of ring [m]	2200	2200	2200
Calculated thermal load [Torr-l m^{-1}]	4.82×10^{-7}	1.34×10^{-7}	1.79×10^{-7}
Total calculated thermal load [Torr-l]	1.06×10^{-3}	2.94×10^{-4}	3.93×10^{-4}
Total gas load [Torr-l]	2.15×10^{-3}	5.33×10^{-3}	1.02×10^{-2}
Total Pumping [l s^{-1}]	214,939	532,533	1,019,424

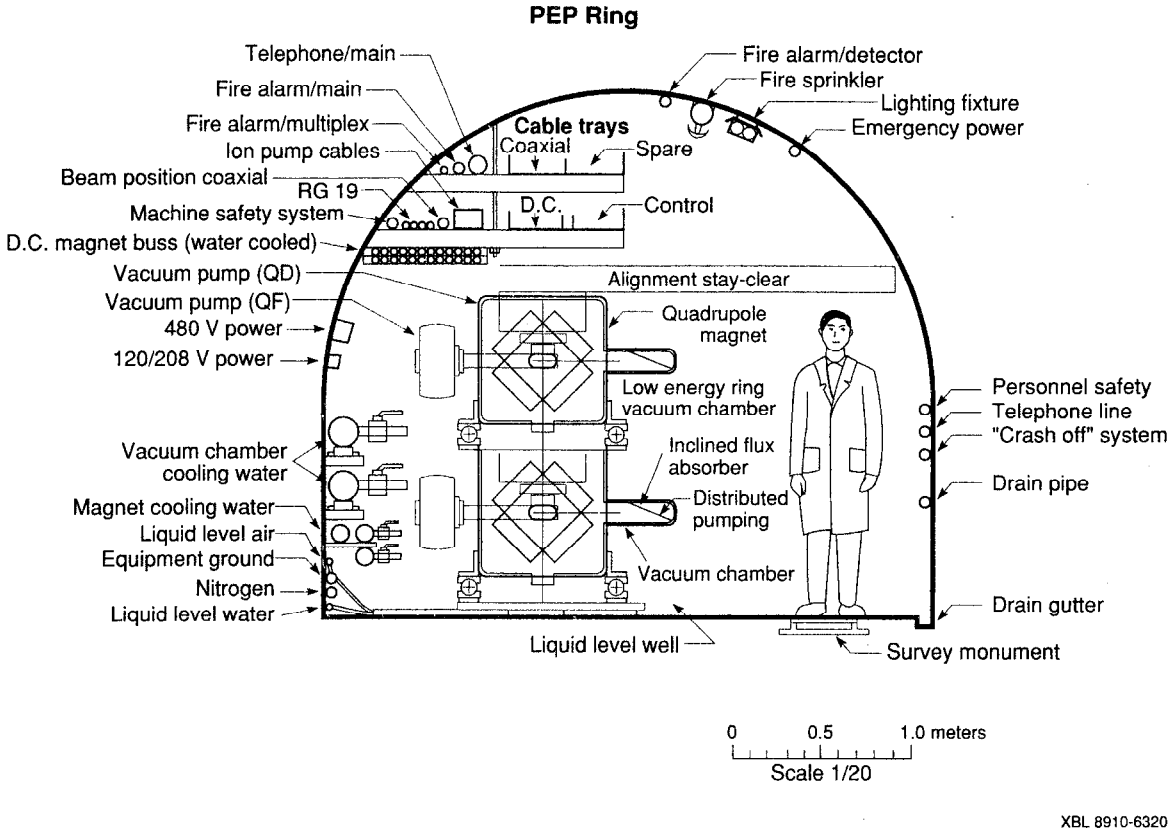

Fig. 3.6–3. Cross section of the PEP tunnel with a second ring installed atop the existing PEP ring.

We have already described here a lattice design for such a ring. However, it is not clear that the damping time at 3.1 GeV for such a large ring would be sufficient to avoid difficulties with the beam-beam interaction, so a lattice with wigglers to adjust the emittance and damping times is envisioned. To provide round beams, we believe that such a wiggler-dominated low-energy ring will be required in any case, so this is not a disadvantage. For such a large ring, the required dipole field is rather low, which should permit the magnet designers a great deal of flexibility to optimize the ring design. In addition, the potential savings in conventional facilities are attractive.

Radiation from Wigglers

We showed in Section 2.2 the desirability of maintaining equal damping decrements in the high- and low-energy rings to minimize the effects of the energy asymmetry on the beam-beam interaction. To accomplish this, we envision the use of wigglers to create additional energy loss. The damping decrement for a storage ring can be written as

$$\lambda = \frac{T_0}{\tau_x} = \frac{U_0}{2E} \qquad (3.6\text{–}17)$$

from which it is clear that, for equal damping decrements, the required synchrotron radiation energy loss per turn for the high- and low-energy APIARY rings must simply scale proportionately to the beam energy in the ring. In the high-energy lattice (ρ = 165 m; E = 9 GeV), the energy loss is dominated by the normal bends, so we can obtain the energy loss from

$$U_0 = 0.0885 \frac{E^4}{\rho} \qquad (3.6\text{–}18)$$

which gives U_0 = 3.52 MeV/turn. For equal damping decrements then, we need an energy loss in the low-energy ring of

$$U_{0,+} = U_{0,-} \frac{E_+}{E_-} = 3.52 \left(\frac{3.1}{9.0}\right) = 1.21 \text{ MeV/turn} \qquad (3.6\text{–}19)$$

In the low-energy ring, we have a bend radius of ρ = 58.3 m, so, from Eq. (3.6–18), we have U_0 = 0.14 MeV/turn, i.e., only about one-tenth of the requisite amount. (To create the matched damping decrement from the bending magnets alone would require a bend radius of 6.75 m, which is impractical in terms of thermal power density.) In addition to this contribution, we must consider the synchrotron radiation emission in the very strong vertical bends used to separate the two beams beyond the IP. For a total vertical bending length of L_V = 20 m, the energy loss from the two sets of vertical separation magnets in the IR can be estimated by scaling Eq. (3.6–18):

$$U_{0,V} = 0.0885 \frac{E^4}{\rho} \frac{L_V}{2\pi\rho} = 0.12 \text{ MeV/turn} \qquad (3.6\text{–}20)$$

(Note that, at the maximum design current, this loss corresponds to about 180 kW in each set of dipoles, so special vacuum chambers will be needed here as well as for the

horizontal dipoles.) Thus, the lattice itself is contributing a total energy loss of 0.26 MeV/turn from the bending and separation magnets. To reach equal damping decrements, then, we must produce an additional energy loss of 0.95 MeV/turn from elsewhere. In the present lattice, we accommodate this need by including wiggler magnets in some of the straight sections.

At present, we envision four wigglers with two periods of λ_W = 2 m, in each of four utility straight sections located symmetrically around the ring. The total length of wigglers is thus 64 m. For a wiggler field that varies sinusoidally along the beam path, the total radiated power in MeV/turn is given by:

$$U_{0,W} = 6.33 \times 10^{-4} E^2 B_0^2 L_W \qquad (3.6\text{–}21)$$

where E is in GeV, B_0 is the wiggler peak field in T, and L_W is the total wiggler length in m. With the requirements above, a wiggler field of B_0 = 1.6 T would be needed to provide the additional 0.95 MeV/turn to equalize the damping decrements.

As mentioned above, the wigglers will be located in four straight sections around the ring. At the maximum current of 3 A, each will produce about 700 kW of synchrotron radiation power. This power must be dealt with externally to the ring vacuum chamber in specially designed photon beam dumps.

To see what the power density will be, we estimate the angular spread in the wiggler bend plane to be given by:

$$\delta_w = \frac{K}{\gamma} = 93.4 \frac{B_0 \lambda_W}{\gamma} = 48 \text{ mrad} \qquad (3.6\text{–}22)$$

and in the non-bend plane (for $\beta_y \approx 40$ m and $\varepsilon_y = 66$ nm ·rad) to be

$$\psi = \left(\frac{\varepsilon_y}{\beta_y} + \frac{1}{\gamma^2}\right)^{1/2} = 0.17 \text{ mrad} \qquad (3.6\text{–}23)$$

At a distance 40 m downstream from the source point, the illuminated area is

$$A = D^2 \delta_W \psi = 130\ \text{cm}^2 \qquad (3.6\text{–}24)$$

and we have a thermal power density of $P_A = 700/130 = 5.4$ kW/cm^2. This is somewhat higher than would be comfortable to handle, but if the absorber is inclined at 20° to the incident photon beam the power density drops to 1.8 kW/cm^2, which we feel is acceptable.

3.7. Synchrotron Radiation Masking and Beam-Pipe Cooling

Radiation Masking

Synchrotron radiation from the beam going through bending magnets and quadrupoles near the IP can be a possible source of background in the detector. To estimate this for the APIARY design, variants of the program QSRAD were used to trace beam-particle trajectories through the magnetic optics near the IP and tally the number of photons hitting various surfaces near the detector. The program EGS was then used to estimate the probability of scattering, or backscattering, into the detector region. For these simulations, nominal beam bunches of 5.44×10^{10} particles were assumed for the high-energy beam and 7.88×10^{10} particles for the low-energy beam. The beam spatial distribution was taken to consist of a Gaussian profile with the nominal rms size, along with a tail having 7.2% of the primary beam intensity (3.9×10^9 and 5.7×10^9 particles for the high- and low-energy rings, respectively) in a Gaussian of 2.7 times the nominal rms value. Both components of the distribution were truncated at the 10σ level. (This model for the beam profile is based on experimental data from PEP.) The studies were done for two sources of synchrotron radiation: the IR quadrupoles and the IR bending magnets.

The geometry of the magnetic elements and masks located near the IP is shown in Fig. 3.7-1. All masks and magnet apertures shown in the figure honor a beam-stay-clear of 12 times the nominal rms beam size.

The basic geometry of the IP differs from that considered in our earlier studies. We now envision that the initial separation dipoles, B1, on either side of the IP will have opposite polarities (a so-called "S-bend" configuration). Each beam thus leaves the IP region with an angle to the collision axis that matches the incoming beam angle. With this new configuration, dipole radiation from the beams passing through the relatively strong B1 magnets essentially misses all surfaces near the collision point (± 1.5 m) and is not a background issue.

The strong B1 magnets do introduce a complication in this design, because one of the beams will always be offset when traveling through the Q1 and Q2 magnets. The offset beam produces extra "dipole" radiation and the photons from this source could cause serious background problems by hitting

various surfaces near the IP. This problem can be alleviated by setting the quadrupole on the incoming-beam axis.

Even though the dipole radiation (both from B1 and from the offset beam in Q1 and Q2) does not strike any surfaces near the IP, the intensity of these fans of photons will certainly necessitate a close look at where they are being absorbed and whether or not backscattered photons could cause further increases in detector background. Even the power from the dipole radiation in these magnets is becoming uncomfortably high. Consequently, we intend to pursue new design directions corresponding to lattices that have reduced magnetic field strengths in these elements.

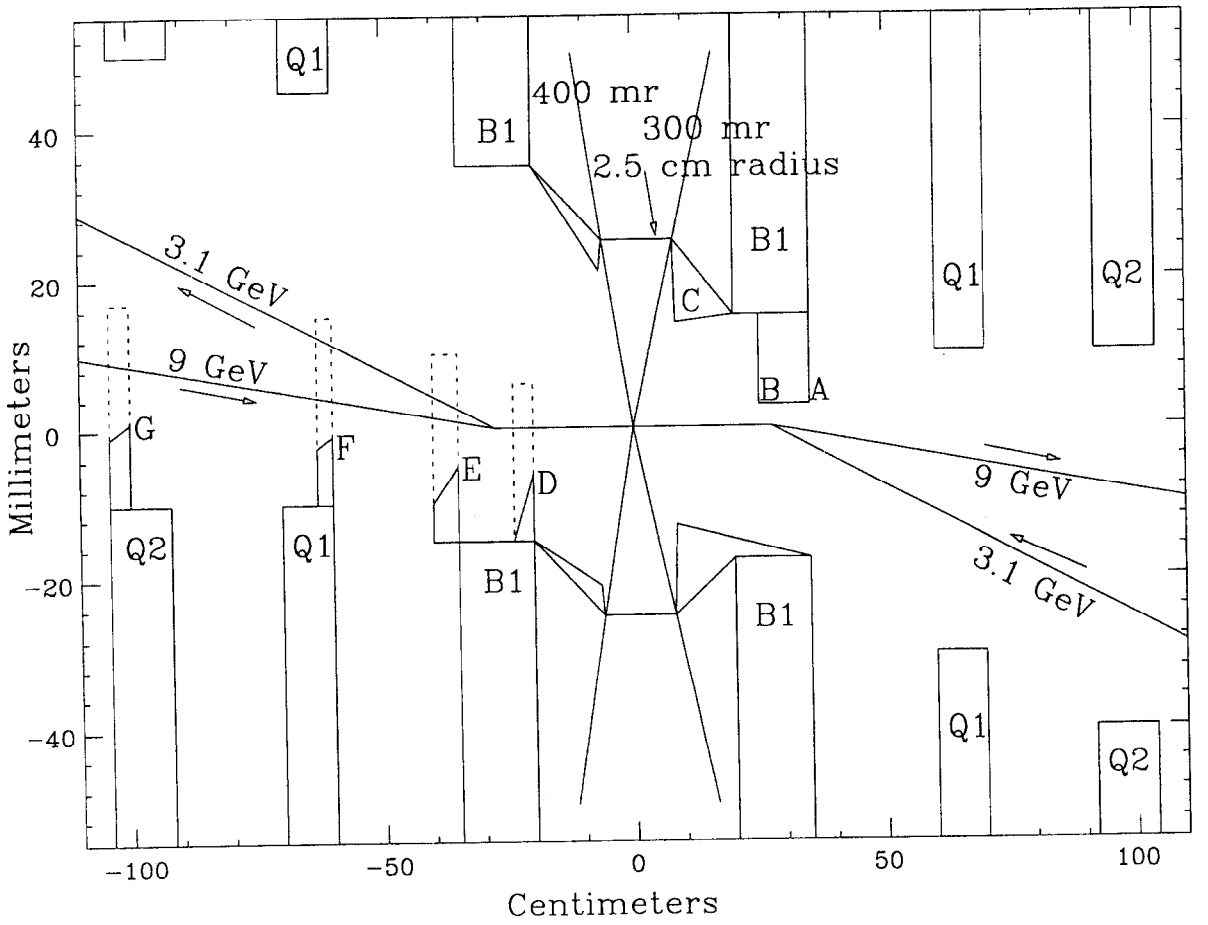

Fig. 3.7–1. Geometry of the magnetic optics near the interaction point. Tentative locations of masks are indicated.

Synchrotron radiation from the 3.1-GeV beam in the IR doublet does pose some difficulties, since direct radiation could hit the detector beam pipe. To protect the detector beam pipe (2.5-cm radius, spanning ±7 cm from the IP) from this source of radiation, a mask having a 4-mm aperture in the +x direction is positioned on one side of the IR, 25-35 cm from the IP (surfaces A and B in Fig. 3.7–1). The vertical aperture of this mask is ±6 mm. The mask aperture in the opposite (-x) direction is kept as large as possible to minimize the amount of quadrupole radiation from the 9-GeV beam that can strike it and then backscatter onto the detector beam pipe.

If it were left unmasked, the synchrotron radiation generated when the 9-GeV beam goes through Q4, Q5, and Q6 would produce too many photons incident on surface B and on the secondary mask labeled C in Fig. 3.7–1. To reduce the photon rate on these surfaces, four masks (labeled D, E, F, and G) are introduced. These masks are all of a similar "C-shaped" design, i.e., each has an open slot on one side. The slots allow the dipole radiation from the 3.1-GeV beam in the B1 magnets to escape without striking these masks. However, photons from the 9-GeV quadrupole radiation do strike the inside edges of these four masks, and can then forward scatter onto the detector beam pipe.

Synchrotron radiation from the 9-GeV beam in the low-energy quadrupole doublet (Q1, Q2) does not contribute to detector background, because it is confined to a narrow cylinder throughout the detector region.

Table 3.7–1 summarizes our results for the photon flux hitting the detector beam pipe. It is assumed that this pipe is composed of 500 μm of beryllium coated inside with 25 μm of gold; only 10% of the incident flux will be transmitted through such a pipe. To put the values in Table 3.7-1 in perspective, we note that 1 photon/cm^2 per crossing corresponds to roughly 1 Mrad/yr in silicon. This amount of exposure in a radiation-hardened device is considered to be tolerable. Thus, with the geometry presently envisioned, an acceptable rate would be about 2500 photons per crossing incident on the inside of the beam pipe, which is well beyond what we expect. More refined numbers require consideration of the details of the photon energy spectrum and a more thorough study of the various materials to be used for masking surfaces. The present design assumes a high-Z material (Au) for all masking surfaces and edges. Of course, the results quoted here are not yet based on an optimized IR design (from the viewpoint of radiation masking), so it is expected that

significant improvements will result from iterations between the IR optics and masking designs.

Compared with our earlier design, the masking solution described here is considerably improved. The new IR geometry is better from a masking perspective, and has permitted the detector beam pipe radius to be reduced from 3 cm to 2.5 cm. We are eventually aiming for a solution that will accommodate a 2-cm beam pipe radius. The photon rate incident on the beam pipe is slightly higher in this new design than was the case earlier. However, all local sources of synchrotron radiation have now been included in this new estimate and we still find acceptable results. It should be recognized, of course, that the results quoted here are very preliminary. Clearly, much work remains to be done to reduce the photon rate in the detector, and to provide adequate cooling for the masks.

Beam-Pipe Cooling

In a high-luminosity collider, the finite resistivity of the beam pipe wall will result in power on the order of 1 kW being dumped in the region of the detector, where the beam pipe must be of small diameter to allow precise vertex detection. The change in diameter of the vacuum chamber to reach a beam-pipe radius of 2–3 cm in the interaction region will also result in higher-order-mode losses of comparable size. These losses are absorbed as heat by the beam pipe, and, at these power levels, it is necessary to provide active cooling of the pipe in the interaction region. The cooling system must not introduce a large amount of material in the path of the final-state particles, as multiple Coulomb scattering in the beam pipe would then compromise the precision of vertex detection.

The Jet Propulsion Laboratory of Caltech has provided us with a study[32] of a variety of applicable cooling techniques. The concept common to all techniques investigated was that a coolant would flow through an annular region surrounding the beam pipe. A heat pipe was also considered, but it was determined that a device of this complexity was not required to meet the cooling and material-thickness requirements of our application.

Of the various techniques considered, the two best were found to be cooling with water, and cooling with helium gas at a pressure of 5–10 atmospheres. A variety of examples have been considered, with heat loads as large as 4 kW, and with radii of 10 and 20 mm. Satisfactory configurations have been found for

Table 3.7-1. Preliminary estimates of synchroton radiation background (photons per crossing). Parenthetical values correspond to reduction of the assumed beam tails by a factor of 100, to provide an estimate of the background contribution from the core alone.

Scattering surface[a]	Photons (> 4 keV) hitting surface		Solid angle to detector beam pipe (msr)	Second-surface reflection fraction	Photons incident on beam pipe	
	9-GeV beam in Q4, Q5, Q6					
F	3.8×10^{8}	(3.7×10^{8})	~0.25	8.4×10^{-4}	10	(10)
E	1.7×10^{8}	(1.5×10^{8})	0.13	8.4×10^{-4}	3	(2.6)
D	3.1×10^{6}	(2.3×10^{5})	75.4	8.4×10^{-4}	31	(2.3)
C	3.1×10^{4}	(3.4×10^{2})	1833	3.0×10^{-3}	27	(0.3)
B	5.1×10^{7}	(1.7×10^{7})	13.7	3.0×10^{-3}	12	(4.0)
					83	(19)
	3.1-GeV beam in Q1, Q2					
B	7.0×10^{7}	(2.9×10^{7})	0.94	8.4×10^{-4}	0.1	(0.05)
C	2.0×10^{3}	(2.2×10^{1})	1833	8.4×10^{-4}	0.5	(0.01)
E	1.7×10^{6}	(1.8×10^{4})	24.5	3.0×10^{-3}	9.7	(0.10)
					10	(0.16)
	3.1-GeV beam in BV1					
B	4.8×10^{8}		0.013	8.7×10^{-6}	0.01	
	3.1-GeV beam in B1					
B	1.0×10^{7}		0.013	1.5×10^{-5}	0.0003	
	9-GeV beam in B1					
	--- no hits between Q2 magnets ---					
	9-GeV beam in Q1, Q2					
	--- no hits between Q2 magnets ---					
Grand Total					93	(19)

a) See Fig. 3.7-1.

all these cases, using either water or helium-gas cooling. As water cooling is the simpler of the two techniques, we will restrict the discussion below to this case.

We will consider an example case consisting of a 500 mm long tube with two concentric cylinders of 0.5 mm wall extruded beryllium, the inner cylinder having a radius of 20 mm. The annular gap between the cylinders is 0.25 mm. If this gap is filled with water, the total number of radiation lengths presented by the two beryllium cylinders and the water to a particle incident at 90° is 4.2×10^{-3}.

If 2 kW is deposited uniformly on the inner wall, the heat flux is 32 kW/m^2. The heat can be removed through forced convection to the water, with a temperature rise of less than 5°C, at a flow rate of 0.76 gpm. This can be achieved with a pressure differential of 1 atm, at a flow velocity of 1.5 m/s. (Flow-induced vibrational instabilities under these conditions have been calculated assuming clamped boundary conditions and found to be of no consequence.) Thus, there is a practical solution in terms of the thermal requirements that has a sufficiently small multiple-scattering contribution and that represents a reasonable regime of water flow rate and pressure.

Realization of this concept requires attention to a number of practical engineering considerations. Important issues are listed below:

- To avoid corrosion, it is necessary to plate the beryllium with gold or nickel. As such plating is needed in any case to absorb synchrotron radiation photons in the x-ray region, this presents no additional complexity. Even with the plating, deionized water should be employed as the coolant.

- The wall thickness must be sufficient to avoid buckling under the external pressure. The specified case represents a substantial safety margin in this regard. (If considered as simply-supported, the gravitational sag of the tube structure is substantially less than 1 micron, and is not a concern.).

- If an adequate safety margin is to be maintained against thermally induced stresses, it is necessary to provide a bellows mount for the inner cylinder of the beryllium beam pipe structure. This is standard in most storage ring designs.

- Extruded beryllium tubing with 0.5-mm wall thickness is commercially available. (If required, a wall thickness of less than 0.375 mm can be produced.) The mechanical properties of extruded beryllium are somewhat different from those of beryllium sheet (which is formed into a cylinder through lap-brazing), the extruded material being somewhat less ductile. Further investigation of the mechanical properties of the various types of beryllium is under way.

Although the effort to produce an engineered design is not finalized, it is clear that adequate cooling of the beam pipe in a high-luminosity storage ring is a quite tractable problem.

3.8. Beamstrahlung

The radiation loss due to "beamstrahlung" (Bremsstrahlung caused by the mutual electrical and magnetic effects of two beams) can be characterized by the beamstrahlung parameter d, which gives the fractional energy radiated by a single particle in the beam. For the APIARY collider, this energy is entirely in the classical regime,[33] since the upsilon parameter Υ, even for the 9-GeV beam, is much less than unity:

$$\Upsilon \equiv \frac{2\hbar\omega_c}{3\gamma m_0 c^2} = \frac{5}{6}\,\frac{\gamma r_e^2 N_B}{\alpha\sigma_\ell(\sigma_y+\sigma_x)} = 1\times 10^{-6} << 1 \qquad (3.8\text{–}1)$$

where α is the fine-structure constant and r is the aspect ratio. The beamstrahlung will be in the range of 10–100 keV, with a critical photon energy E_{crit} of 35 keV. The beamstrahlung parameter in this classical regime is given by[33]

$$\delta \rightarrow F_1\,\frac{r_e^3 N_B^2 \gamma_0}{\sigma_x\sigma_y\sigma_\ell}\,\frac{4r}{(1+r)^2} \qquad (3.8\text{–}2)$$

where

F_1 = 0.22 is a form factor independent (to within a few percent) of the aspect ratio r,
γ_0 is the relativistic gamma factor of the radiating particle,
N_B is the number of particles in the opposing bunch, and
σ_x, σ_y, and σ_ℓ are the dimensions of the opposing bunch.

The value for the beamstrahlung parameter δ of the 9-GeV beam would then be about 2.7×10^{-8}, leading to a total beamstrahlung power of

$$P_{beamstr.} = \delta I\left(\frac{E}{e}\right) \approx 370\ \text{kW}$$

for round beams.

Beamstrahlung is much less severe in the low-energy ring. The low-energy beam would have about one-third the δ of the high-

energy beam and about one-ninth as much beamstrahlung power loss, regardless of the circumference.

The beam-disruption parameter D is given by[33]

$$D = \frac{r_e N_B \sigma_\ell}{\gamma \sigma_x \sigma_y}\left[\frac{2r}{1+r}\right] \quad . \qquad (3.8\text{–}3)$$

Its value is about 0.06; in other words, beam disruption is modest and most of the beamstrahlung would be emitted ahead of the beams, fanning out only a few milliradians. A fraction of this radiation may hit the apertures of the superconducting quadrupoles, so their design would have to allow for this source of heating.

3.9. Injection System

APIARY will require high-energy, low-emittance sources of positrons and electrons suitable for filling the storage rings rapidly. Ideally, the filling time should be much shorter than the luminosity lifetime of the rings. For the purpose of estimating the characteristics of the injection system, the maximum time for a complete fill of both rings is taken to be about 3 minutes. Because of the expected short luminosity lifetime, it is clear that a dedicated and powerful injection system is required. This linac could, subject to other demands, be the existing linac and damping ring complex used for the SLC, or it could be a totally new system. Here we describe the use of the SLC linac and damping rings as an injector for APIARY. This choice is dictated by the following facts:

- When the B-factory is completed, the SLC will be nearing the end of its usefulness for particle-physics research. Thus, it will be possible to use portions of it as a dedicated injector for the B-factory.

- The SLC is capable of producing low-emittance beams with 5×10^{10} positrons or electrons in a single bunch—appropriate characteristics for our needs.

- Some relatively inexpensive modifications to the existing complex will make it straightforward to produce positrons in the 3–6 GeV range and electrons in the 6–9 GeV range. In order to conserve electrical power, the linac will run at a maximum repetition rate of 60 Hz. Since the frequency of the storage ring rf system, 353.2 MHz, does not have a simple harmonic relationship with the linac frequency (2856 MHz), it is not convenient to fill a train of buckets on a single linac pulse. However, since the SLC was designed to accelerate electrons and positrons on the *same* linac pulse, it will be possible to put a bunch of electrons in one bucket of the 9-GeV ring and positrons in one bucket of the 3.1-GeV ring with the same linac pulse.

The SLC system, modified for injecting into the B-factory, is shown in Fig. 3.9–1. The modifications consist of the following:

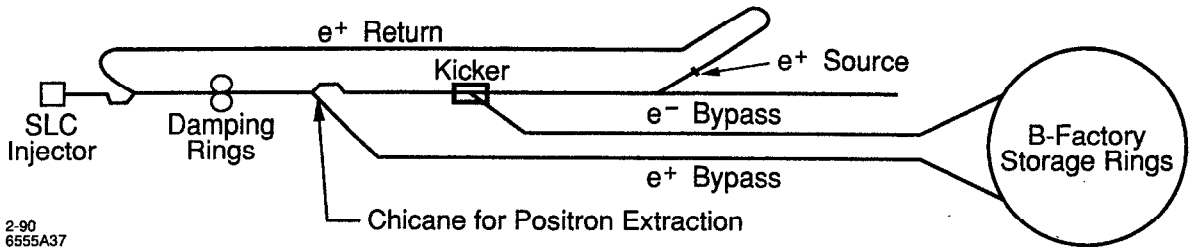

Fig. 3.9–1. SLC injection system modified for B-factory injection.

- A DC magnet system for extracting the e^+ beam from the linac when the beam reaches 3.1 GeV;
- A positron bypass transport line;
- A kicker to extract the 9-GeV e^- beam from the linac while letting another bunch continue to be accelerated down to the positron source;
- An e^- bypass line.

The bypass lines are considerably simpler and cheaper than the present SLC positron return lines, since the beams have a factor of 100 lower emittance, and they are more than an order of magnitude higher energy than in the SLC case. Thus, a FODO lattice with a quadrupole every 50 meters would suffice. The two bypass lines would have a total of about 100 small quadrupoles, about two-thirds the number in the present SLC positron return line.

Filling Times and Sequences

Table 3.9–1 gives the parameters of each of the rings which are related to the injection process.

In understanding the strategy of filling, it is important to note that it takes 22 seconds to hit each of 1296 buckets once with the linac pulsing at 60 Hz. Furthermore, the two rings can be filled concurrently since the SLC linac can accelerate both electrons and positrons on the same machine pulse. Based on present experience, it is reasonable to accelerate 5×10^{10} particles, i.e., 8 nC, in each bunch. A filling efficiency of 50% is assumed, so a maximum injected charge per pulse is 4 nC. Finally, for an accelerated charge per bunch less than 1.5 nC (captured charge

less than 0.75 nC), it is possible to vary the charge continuously in a predictable manner, since in this regime the beam loading and wakefield effects are small.

Table 3.9–1. Collider parameters related to the injection process.

	e^- Ring	e^+ Ring
Energy [GeV]	9	3.1
T_0 [μs]	7.3	7.3
Current [A]	1.54	2.23
Total charge [μC]	11.3	16.4
Number of bunches	1296	1296
Charge per bunch [nC]	8.7	12.6
Charge injected per linac pulse [nC]		
fill from 0 to 80%	1.6	2.5
topping-off	0.4	0.6
Time required [s]		
fill from 0 to 80%	88	88
topping-off	88	88

When filling the rings from zero, the injector is run in a high-current mode until each bucket in each ring is approximately 80% full. In this mode, it is not straightforward to independently vary the e^+ and e^- intensities on a pulse-to-pulse basis because of beam loading and wakefield effects. Because the SLC linac will be running at 60 Hz, but the horizontal damping time τ_x, is approximately 38 ms, it is not possible to put successive pulses into the same rf bucket. Rather, successive injector pulses will go into buckets that are perhaps 90^o or 180^o apart in azimuth. Since the revolution time of the PEP storage ring is 7.3 μs, it is easy to do this with injection kickers that do not disturb the last filled bucket.

When all buckets in both rings have reached about 80% (or perhaps 90%) of their desired charge, the injector linac will be switched to its low-current or topping-off mode. In this mode, it should be possible to independently program the intensity of the e^+ and e^- bunches on a pulse-to-pulse basis. The injected charge per pulse is less than 5% of the total charge in a bucket. At this rate it will take about 88 seconds to fill both rings from 80% to 100% of full current. The 5% granularity may be fine enough to avoid the need for subsequent adjusting of the charge per pulse.

Automatic Injection

It is clear that, to achieve uniform filling of 1296 buckets in each ring in a time less than 3 minutes, the whole process of measuring the charge in each bucket, and sequencing the filling of the buckets must be automated. Presumably the filling from zero will be done only rarely, while the routine filling will be topping-off from about 80%; in this case, the injection time will be less than 100 seconds.

3.10. Special-Purpose Hardware

To implement the APIARY collider outlined in this report, it will be necessary to design and fabricate some special-purpose, state-of-the-art devices. Foremost among these will be the feedback system, discussed in Section 3.5, and the superconducting quadrupoles, which we will discuss here. Although we have not yet invested a major design effort into these magnets, we have investigated the magnet parameter specifications to get a feeling for their degree of difficulty to achieve. As we will see below, the triplet required for the high-energy ring is expected to be relatively straightforward, whereas the doublet required for the low-energy ring is more of a challenge.

High-Energy Ring

As described in Section 3.1, the IR of the high-energy lattice contains a pair of superconducting quadrupole triplets, located about 5 m on either side of the IP. Because of the relatively long distance of the quadrupoles from the IP, the beam size is increasing rapidly there, and the required focusing strength is therefore substantial. In the present optics, the following parameters have been taken for these magnets.

- Maximum gradient: 72 T/m
  (corresponding to 5 T at r = 69.4 mm)
- Magnetic lengths:

  85.9 mm (QF3)
  317.9 mm (QD4)
  244.4 mm (QF5)

- Separation between magnets: $\geq$ 250 mm

The gradient requirement was originally obtained by constraining the field at the edge of the aperture to be 5 T, along with a second constraint that the quadrupole aperture remain at least 12 times the rms beam size at its location (to avoid beam loss associated with quantum lifetime, as discussed in Section 3.3). Although these parameters are not trivial, we note that they are quite similar to parameters of the low-beta quadrupoles now being constructed[34] for the Amy detector at TRISTAN. The Amy quadrupoles will have a gradient of 70 T/m, a "good field" aperture radius of 40 mm, a coil inner radius of 70 mm, and a magnetic length of 1.17 m.

In the APIARY high-energy-ring quadrupoles, the coil radius corresponding to the 69.4 mm aperture radius would be about 75 mm. Thus, the gradient and coil spacing that are required for our purposes are clearly compatible with existing technology. Indeed, the quadrupoles can be designed to meet the specifications listed above at a temperature of 4.5 K. Then, if necessary or desirable, the achievable gradient could be increased by reducing the operating temperature to 2 K. Alternatively, the capability of operating at lower temperatures could be considered as a performance safety margin at this stage.

One of the difficult aspects of the design of the triplet for the high-energy ring concerns the separation between magnets. At the present time, the available separation between the magnetic elements to accommodate the coil geometry is 25 cm. While this is probably sufficient, it would greatly simplify the engineering design of the magnets if a larger separation were permissible. If it were necessary to somewhat increase the spacing between magnets, the operating gradients could probably be increased accordingly to maintain the same integrated focusing strengths; this change should be relatively invisible to the lattice optics.

Low-Energy Ring

In the low-energy ring, the optics require a superconducting dipole (B1) and a superconducting quadrupole doublet (QF1, QD2). The dipole begins 25.5 cm from the IP, and the nearest quadrupole (QF1) begins 60 cm from the IP. The required parameters for the magnets, based on the optics described in Section 3.1, are summarized in Table 3.10–1.

Table 3.10–1. Preliminary specifications for the APIARY low-energy ring IR magnets.

	B1	QF1	QD2
Field [T]	2.65	—	—
Gradient [T/m]	—	295	152
Magnetic length [mm]	150	100	128
Aperture radius [mm]	20	14.3	27.2
Distance from the IP [mm]	255	600	830

The three superconducting magnets are contained in the same cryostat. Due to the required short distances from the IP, the cryostat is cantilevered through the endcap of the detector into the central field volume, which has a solenoidal field of about 1.5 T. The volume available to the magnets within the detector region is a cone centered on the IP, with its axis on the beam line and a vertex angle of 0.3 radians on one side and 0.4 radians on the other side. This stay-clear region is indicated in Fig. 3.7–1.

To avoid mechanical interference with the detector and its small beam pipe, the dipole must be at least 20 cm away from the IP. In addition, to minimize perturbations to the detector magnetic field, all three lattice magnets are required to have a linear magnetic behavior, that is, any iron should be completely saturated or permanent magnetic materials should be used.

A very severe constraint to the design is that the intense synchrotron radiation must not hit the magnets. Because this could require the use of a warm bore, we have left 5 mm between the aperture radius and the coil inner radius.

In Table 3.10–2 we summarize some of the magnet parameters considered in the preliminary design. These iron-free magnets have been computed assuming the coils to have a circular sector shape with one wedge in order to eliminate the first three allowed multipole components. All the magnets have an overall current density of 450 A/mm^2 with a Cu-to-NbTi ratio of 1.3. To allow the maximum field at the ends (not yet designed) to be as high as 9 T, the magnets will be designed to operate at 2 K.

Table 3.10–2. Parameters of the B1, QF1 and QD2 superconducting magnets.

	B1	QF1	QD2
Coil inner radius [mm]	25	19	32.2
Coil outer radius [mm]	34	51.8	54
Overall current density (A/mm^2)	450	450	450
B_{max} in the cross section (T)	3.05	6.63	5.46
Radial space available (mm)	79	185	256

For the dipole, B1, spatial constraints dictate that the mechanical structure keeping the coils in compression must be efficient, for example a "ring and collet" design, whereas for the quadrupoles, collars can be used. As can be seen from Table 3.10–2, B1 has only 4.5 cm available radially around the coils. Assuming that

1.4 cm are used for insulation, support structure, and an outer shell, the cryostat will have only 2.2 cm available radially.

The dipole will have a central section of 10 cm and two end regions each 5 cm long, leading to a magnetic length of 15 cm, as required. Allowing 1 cm for the end shoes and the outer shell, 20 mm are available to the cryostat axially. Since the space to wind the coils is limited, it is likely that the ends will have large—and undesirable—field harmonics.

The separation between B1 and QF1 is 19.5 cm, and that between QF1 and QD2 is 22 cm. These separations are sufficient to provide space for the ends, the end plates, the electrical bus and the cooling pipes.

To verify the adequacy of the engineering design, the following points must be examined in detail:

- Synchrotron radiation masking
- Detailed cryostat design
- Magnetic analysis of the magnet ends in order to verify sufficient integral multipole field quality and a reasonable maximum field value in this region

These activities are already under way.

4. Major R&D Areas

Reaching, and eventually exceeding, the design luminosity of 3×10^{33} cm^{-2} s^{-1} will depend critically on successful R&D in a few major areas. These fall into two categories: technology issues and beam dynamics issues.

4.1. Technology R&D Issues

IR focusing optics. The required low-beta IR optics demands strong-focusing superconducting quadrupoles of special design in the low-energy ring. (Superconducting quadrupoles are also employed in the high-energy ring, but their parameters are rather similar to those of an existing design[33] at TRISTAN.) The quadrupole parameters call for a compact system with high pole-tip field (about 5 T). Permanent-magnet quadrupoles are often an attractive option, but are inadequate for this purpose. The individual focusing and defocusing quadrupoles in the IR are short, so the actual fields will be dominated by end effects. Design of such magnets will involve detailed three-dimensional field calculations. Afterwards, a careful analysis of the effects that the nonlinear fields produce on the particle orbits must be carried out.

It will be very desirable to build a prototype quadrupole and to test it both in the laboratory and (to examine its behavior in a high-radiation environment) under beam storage conditions in PEP. In addition to the standard approach with individual quadrupoles, it will be interesting to explore other alternatives. A simple and attractive solution may be the design of a superconducting doublet or triplet with continuous focusing in which the coils twist around azimuthally along the beam's path. The integrated focusing effect on the beam would be the same and such a design seems feasible.

RF system. The low-impedance rf system, which could be either room-temperature or superconducting, is another major area of R&D. Extensive electromagnetic field calculations and low and high power tests in an rf test stand would be required. Special emphasis must be placed on the design and testing of high-power rf windows, fundamental power couplers and HOM loading couplers. If power through the rf window were to turn out to be a significant limitation, one might envision an R&D program on *windowless* transmission of rf power through high-quality, high-vacuum waveguides (differentially pumped to

isolate the cavity from the klystrons) straight into the cavity. The choice between a specially designed room-temperature rf system and one based on superconducting cavities can only be made provisionally during the conceptual design stage; a final decision would most likely follow only from the results of these R&D studies.

For the superconducting rf scenario, there are a number of other issues that will have to be addressed:

- Behavior of the system in the high synchrotron radiation environment in both rings
- Stability of the rf system under a situation of essentially 100% beam loading
- Cost and complications of cryogenics, etc.

The first step in any of these studies would involve a careful engineering design, fabrication and testing of a single-cell rf unit at 353 MHz, with both power and HOM couplers, and windows. Two such studies would have to be performed—one each for the room-temperature and superconducting versions. It may also be worthwhile to consider alternative frequencies, closer to 500 MHz, to take advantage of ongoing development efforts on superconducting cavities at DESY and Cornell.

Feedback system. Careful designs of high-sensitivity, broadband pickups and kickers for the feedback systems would have to be made. A low-power feedback system is already in the works at PEP. This system utilizes an existing 800 MHz cavity, de-Qed to damp 18 bunches.[35] Following design and fabrication, a high-power feedback system could be tested in PEP in the following configurations:

- 7 GeV with 2.3 A
- 11 GeV with 0.32 A

Both these configurations would lead to a synchrotron radiation power of 3 MW, which is compatible with the present specifications for the PEP rf system installed power and also with the vacuum-chamber radiation-handling capability. The vacuum chamber need not be replaced for these tests, although that step will be required for the actual operation at a luminosity of 3×10^{33} cm^{-2} s^{-1}.

Crab cavity. If a finite-crossing-angle scenario were adopted for the final collider design, significant R&D would be required on the design and construction of a "crab cavity," which is necessary to eliminate the possibility of synchrobetatron resonances. Following a specific design, a small-angle and also a large-angle crab cavity would be built, and each tested both for its effectiveness and to measure whether the specified tolerances on amplitude and phase fluctuations have been achieved.

Vacuum chamber. Significant effort has to be spent on the design of high-quality vacuum chambers capable of handling large doses of synchrotron radiation power and of maintaining good vacuum in the presence of large beam currents. Special attention must be paid to improved cooling schemes and to the design of radiation outlet ports (e.g., for the very-high-power radiation from wigglers) that produce minimum electromagnetic disturbance (impedance) in the path of the beam.

IR design. The design of the small beam pipe at the IP (required for vertex detection) must be carefully studied, as must the issues of radiation masking and cooling—both in the immediate IP region and in the magnets that bracket it. Extreme care and some degree of conservatism need to be exercised in the final design of these components.

4.2. Beam Dynamics R&D Issues

The main beam dynamics issue would revolve around the physics of the "beam-beam limit" (as it enters into the luminosity) for asymmetric colliders. The role of damping decrements and the question of round *vs.* flat beams are the most important issues to be considered. R&D can proceed mainly via detailed computer simulations, but controlled beam dynamics experiments in PEP will also play a crucial role. The computer simulations should include such features as:

- The realistic thick-lens effect of finite-length bunches
- The non-Gaussian nature of the beams
- The possible coherent beam-beam modes, both high-frequency internal bunch modes and low-frequency bunch-to-bunch modes

It should be emphasized that our understanding of the beam-beam effect, as outlined in this report, is adequate for us to venture into a conceptual design of the collider. Indeed, it is likely that further detailed understanding will not come until after the collider is in operation. One exception to this, however, concerns the issue of round beams. *It will be crucial to devote PEP beam time to beam dynamics experiments to study the feasibility and the benefits of creating round beams in the high-energy APIARY ring.*

Round beams in PEP could most easily be achieved by adjusting the normal quadrupoles and possibly adding skew quadrupoles to the lattice, thus altering the coupling to give a round beam at the IP. Emittance coupling via a coupling resonance can also be pursued, to see whether the introduction of such a systematic resonance structure is favorable or unfavorable from a beam-beam point of view. Experiments at different beam energies in PEP would also elucidate the role of the damping decrement in achieving a high beam-beam tune-shift limit, and would address the energy dependence of the luminosity under conditions where the tune shift ξ is saturated.

Other beam dynamics efforts must focus on experimental investigations of multibunch instabilities and their cures, on the transverse mode-coupling instability, and on gymnastics with the PEP optics in general.

5. A Construction and Upgrade Program for a PEP-Based B-Factory

With an ultimate luminosity target of up to 10^{34} cm^{-2} s^{-1} in mind, we envision a stepwise, strategic scenario of design, R&D, and construction that will lead to an initial implementation (following its commissioning period) of a collider with 3×10^{33} cm^{-2} s^{-1} luminosity. Continuing R&D efforts, in parallel with construction of this initial configuration and during its subsequent operation, would then allow for a luminosity upgrade by replacing or upgrading specific hardware components in the machine; flexibility to accommodate these changes will have been built into the design. We outline here an example of one possible upgrade strategy.

The low-beta IR optics configuration is very strongly coupled to the design luminosity, and is not easily and smoothly tunable without significant changes. Therefore, the most important parameter that would define a "relaxed" startup ($\mathcal{L} = 3 \times 10^{33}$ cm^{-2} s^{-1}) would be the beam current; initially it would be reduced from the 3 A maximum current allowed by the vacuum chamber design. Reducing the beam current would cause a proportional reduction in all the effects that stem from synchrotron radiation and beam intensity—the root causes of the problems in cooling, vacuum, and rf systems that have pressed the technology the hardest.

Let us envision how we could achieve an initial luminosity of 3×10^{33} cm^{-2} s^{-1}. Because the low-energy ring will be installed in the PEP tunnel, it will be necessary to make major modifications to the PEP hardware from the outset. For example, all of the present magnet stands would need to be lowered to accommodate the new ring (which we would place atop of the existing PEP ring, as shown schematically in Fig. 3.6–3). In this case, it would be most efficient to make many of the longer-term modifications to PEP simultaneously.

To handle a beam current of up to 3 A, it may be necessary to reorient the PEP dipoles such that the open side of the C points towards the outside of the ring. Advances in vacuum system technology, however, could make this optional. In any case, a new vacuum system, specially designed to handle the heat load and gas-desorption vacuum load, would have to be installed. Our present estimates indicate that the vacuum chamber in the

straight sections between dipoles must also be specially constructed.

A new rf system would also be installed during this major installation shutdown. Probably, a room-temperature rf system would be installed; this could be replaced subsequently by a superconducting system if experience warranted it. Similarly, the feedback system installed initially would be a more modest system to handle only the $\mathcal{L} = 3 \times 10^{33}$ cm^{-2} s^{-1} case. If the components were all available in advance, the installation of the new ring and the upgrade of PEP would proceed in parallel and could be completed in about 3 years.

As a follow-up to the feasibility study presented in this report, a conceptual design effort has been launched. Such an effort will, after considering the pros and cons, arrive at a definitive decision on head-on collision *vs.* crossing "crabwise" at an angle. The choice between modified room-temperature rf and superconducting rf in PEP is not likely to be made at the conceptual design stage and would have to await further R&D. All during the construction phase, the effort on design and construction of a detector would proceed so it could be installed as soon as operation begans.

6. Conclusions and Outlook

In this report we have provided a feasible design scenario for an asymmetric B factory based on PEP at SLAC. The foundations of our approach are to utilize state-of-the-art storage ring technology, careful engineering, and a design philosophy that stresses flexibility. The concept outlined here permits the immediate design and subsequent construction of a collider capable of an initial luminosity of 3×10^{33} cm^{-2} s^{-1} (after its commissioning phase), without requiring any undeveloped technologies. Furthermore, the design has sufficient latitude for the collider to reach even higher luminosity with further development efforts.

The issues associated with the very high beam intensities required to achieve a high luminosity, such as synchrotron radiation heating and photodesorption, and designs of the rf and feedback systems, have been given a considerable amount of detailed attention.

Radiation-induced heating and gas desorption, which together place severe demands on the design of the vacuum system, are challenging, but are amenable to sophisticated engineering solutions.

We believe that the rf system could be either a specially designed room-temperature version or a superconducting design. The room-temperature design is simple and could be implemented immediately with some improvements in the power transmission capability of rf windows. A proof-of-principle cavity design for the superconducting cavity already exists, although some R&D would be required to validate it in a high-current application such as we are considering. Substantial engineering effort and attention to detail will be required in the design of the rf system in order to damp the higher-order modes down to a level where the growth times of coupled multibunch instabilities are no faster than 1 ms.

Assuming we are successful in damping the rf cavity modes to a sufficient level, the required feedback system, although demanding in terms of power, is quite feasible. We have explored a specific design for the feedback system, and have shown that it can be implemented. These two aspects—rf and feedback—will unquestionably require the utmost care in the construction of a B factory.

The required superconducting quadrupole triplet in the high-energy ring can already be designed following similar ones built for TRISTAN, and the superconducting doublet for the low energy ring is considered to be achievable as far as gradients are concerned. In the case of the low-energy doublet, however, the mechanical problem of close spacing between the quadrupoles and clearance for the detector solenoid would require detailed engineering. This effort is now under way.

The injection system requirements could be easily met by the present SLC injector complex.

Design of the interaction region to provide adequate beam separation has been shown to be feasible. At present, however, a means of handling the large amount of synchrotron radiation power in this region has not been demonstrated. Masking techniques adequate for a 3-cm beam pipe are difficult, but appear to be within reach. There are indications that many of these IR problems will be reduced, or eliminated, if flat-beam optics (with or without crab crossing) are employed. This option is being actively studied at present.

Given encouragement, support, and a dedicated team, we have every reason to have a good hope of success in completing such a challenging and potentially rewarding enterprise, which would be a major tool in a sustained B-physics program at SLAC.

References:

1. The Physics Program of a High-Luminosity Asymmetric B-Factory, SLAC-353, LBL PUB-5245, CALT-68-1588, October 2, 1989.

2. K. Berkelman, invited talk presented at the La Thuile Symposium, February 29-March 5, 1988.

3. F. Abe et al., "Proposal for Study of B-Physics by a Detector with Particle Identification and High Resolution Calorimetry at Tristan Accumulator Ring", KEK-Report 1988.

4. A. N. Dubrovin, A. N. Skrinsky, G. N. Tumaiki and A. A. Zholents, "Conceptual Design of a Ring Beauty Factory", EPAC Accelerator Conference, Rome, June 1988, vol. 1. p. 467.

5. "Proposal for an Electron Positron Collider for Heavy Flavor Particle Physics and Synchrotron Radiation," PR-88-09, July 1988, report from Paul Scherrer Institute, CH-5234 Villigen, Switzerland.

6. H. Nesemann, W. Schmidt-Parzefall and F. Willeke, "The Use of Petra as a B-Factory", EPAC Accelerator Conference, Rome, June 1988, vol. 1, p. 439.

7. D. Hitlin, "Requirements: High Luminosity Asymmetric B-Factory", Proc. Workshop On High Luminosity Asymmetric Storage Rings for B Physics, CALT-68-1552.

8. A. A. Garren et al., "An Asymmetric B-meson Factory at PEP", Proc. Particle Accelerator Conference, March 1989, Chicago; LBL-26982.

9. R. H. Siemann, "Simulations of Electron-Positron Storage Rings", CBN-89-4, May 1984. Invited paper at the Third Advanced ICFA Beam Dynamics Workshop on "Beam-Beam Effects in Circular Colliders", May 29-June 3, 1989, Novosibirsk, USSR.

10. S. Chattopadhyay et al., "On Damping Rings with Zero Momentum Compaction and Other Issues", Proc. ICFA Workshop on Low Emittance Beams, BNL, Upton, NY, March 20-28, 1987, BNL-52090.

11. C. Pellegrini, talk at the Workshop on B-Factories and Related Physics Issues, Blois, France, June 26-July 1, 1989.

12. K. Yokoya, private transmittal of Beam-Beam Simulation Code, written by himself, to our colleagues at LBL.

13. R. H. Siemann, "The Accelerator Physics Challenges of B-Factories", CLNS 89/938, August, 1989, Plenary talk at the XIV Int'l. Conf. High Energy Accelerators, Tsukuba, Japan, August 22-26, 1989.

14. H. Wiedemann, "Beam-Beam Effect and Luminosity in SPEAR", Proc. Beam-Beam Interaction Seminar, SLAC-PUB-2624, (1980).

15. S. Myers, Nonlinear Dynamics Aspects of Particle Accelerators (Berlin: Springer-Verlag, 1986, edited by J. M. Jowett, S. Turner and M. Month), p.176.

16. S. Chattopadhyay, "Physics and Design Issues of Asymmetric Storage Ring Colliders as B-Factories", invited Talk at XIV International Conference on High Energy Accelerators, August 22-26, 1989, Tsukuba, Japan. To be published in the proceedings.

17. M. A. Furman, "A Symplectic Coherent Beam-Beam Model", Proc. Third Advanced ICFA Beam Dynamics Workshop, May 29-June 3, 1989, Novosibirsk, USSR.

18. M. S. Zisman, S. Chattopadhyay, and J. Bisognano. 1986. ZAP User's Manual. Lawrence Berkeley Laboratory Report No. LBL-21270 (unpublished).

19. L. Z. Rivkin. 1987. Collective Effects in PEP. In Proc. of Workshop on PEP as a Synchrotron Radiation Source: 139-156. M. S. Zisman, 1987, *ibid.*:157-184.

20. M. S. Zisman, M. Borland, J. Galayda, A. Jackson, S. Kramer, & H. Winick. 1988. Study of Collective Effects for the PEP Low-Emittance Optics. Lawrence Berkeley Laboratory Report No. LBL-25582 and Stanford Synchrotron Radiation Laboratory Report No. ACD-Note 59 (unpublished). S. Kramer, L. M. Borland, J. Galayda. A. Jackson, H. Winick, & M. S. Zisman. 1989. Study of Collective Effects in a Low-Emittance PEP Lattice. In Proc. of 1989 Particle Accelerator Conference, Chicago, IL.

21. M. S. Zisman. 1988. Influence of Collective Effects on the Performance of High-Brightness Synchrotron Radiation Sources. In Proc. of JAERI-Riken Symposium on Accelerator Technology for the High-Brilliance synchrotron Radiation Sources, Tokyo, Japan: 311-346.

22. M. Sands. 1970. The Physics of Electron Storage Rings—An Introduction. Stanford Linear Accelerator Center Report No. SLAC-121. National Technical Information Service, Springfield, Virginia.

23. F. Porter. 1988. An Initial Parameter List for An Asymmetric e^+e^- Storage Ring B-Factory. California Institute of Technology Informal Note FCP-881130 (unpublished).

24. J. D. Jackson, Ed. 1986. Superconducting Super Collider Conceptual Design Report. SSC-SR-2020:168.

25. E. Haebel and J. Sekutowicz, "Higher Order Mode Coupler Studies at DESY", DESY M-86-06, July 1986.

26. D. Boussard et al., "Further Results From The Test of a 352 MHz Superconducting Cavity in the CERN SPS", CERN/EF/RF 88-3, 12 October, 1988.

27. D. Rubin, Talk on RF at the Workshop on B-Factories and Related Physics Issues, Blois, France, June 26-July 1, 1989.

28. G. Lambertson, "Electromagnetic Detectors", LBL-26075, 1989. Also presented at the Joint U.S.-CERN School on Particle Accelerators, Isola di Capri, Italy, Oct. 20-26, 1988.

29. G. Lambertson, private communication.

30. O. Gröbner et al., "Studies of Photon Induced Gas Desorption Using Synchrotron Radiation". Vacuum, vol. 33, p.397, 1983.

31. "1-2 GeV Synchrotron Radiation Source", Conceptual Design Report, July 1986, LBL publication, PUB-5172 Rev.

32. H. Schember and P. Bhandari, "An Investigation of Beam Pipe Cooling Techniques for a Proposed Particle Accelerator," Jet Propulsion Laboratory Report D-7151, February, 1990.

33. P. B. Wilson, "Future e+e- Linear Colliders and Beam-Beam Effects", SLAC-PUB-3985, May, 1986. Invited talk at the Stanford Linear Accelerator Conference, California, June 2-6, 1986.

34. K. Tsuchiya et al., "Superconducting Quadrupole Magnets for the Tristan Low-beta Insertion", 11th International Conference on Magnet Technology, Tsukuba, Japan, Sept. 25-29, 1989.

35. Internal note of PEP Feedback Group, "A Feedback System for PEP to Suppress Multibunch Instabilities", SSRL/SLAC, Version 1.1, June 13, 1989.

Appendix A
Energy Transparency Scaling Relations for IP Parameters

The choice of beam parameters is based on the simplifying assumptions that:

- Horizontal and vertical beam-beam tune shifts of both beams are all equal to a single specified value, ξ
- Both beams exactly overlap transversely at the IP

These assumptions lead to three important relations among energy, intensity, emittance, and β values, from which explicit expressions for emittance and luminosity can be obtained.

A.1. Equal-Energy Beams

The first assumption gives the relationship of the horizontal and vertical β function and emittance values. If the beams are identical, the tune shifts are given by

$$\Delta\nu_i = \frac{r_e \beta_i N}{2\pi \gamma \sigma_i (\sigma_x + \sigma_y)} ,$$

where $i = x, y$ and $\sigma_i = (\varepsilon_i \beta_i)^{1/2}$ (at the IP).

Equating the tune shifts in both transverse planes, $\Delta\nu_x = \Delta\nu_y$, gives the first rule:

$$\frac{\beta_y}{\beta_x} = \frac{\varepsilon_y}{\varepsilon_x} = \frac{\sigma_y}{\sigma_x} = r, \qquad \text{(A-1)}$$

where r is a constant.

A.2. Unequal Beams

Suppose that two unequal-energy beams, designated by the superscript $j = (+,-)$, have beam sizes given by

$\sigma_i^j = (\varepsilon_i^j \beta_i^j)^{1/2}$.

Setting $\sigma_i^+ = \sigma_i^-$ gives the second rule:

$$\frac{\beta_i^+}{\beta_i^-} = \frac{\varepsilon_i^-}{\varepsilon_i^+} = b, \qquad \text{(A-2)}$$

where b is a constant and again i = x,y. The tune shifts are given by

$$\Delta\nu_i^j = \frac{r_e \beta_i^j N^k}{2\pi \gamma^j \sigma_i^k \left(\sigma_x^k + \sigma_y^k\right)},$$

where j = (+, -) and k = (-, +).

Equating the four tune shifts, $\Delta\nu_i^+ = \Delta\nu_i^- = \xi$, gives the third rule:

$$b = \frac{\beta_i^+}{\beta_i^-} = \left(\frac{\gamma^+}{\gamma^-}\right)\left(\frac{N^+}{N^-}\right) \qquad \text{(A-3)}$$

A.3. Emittance

An explicit formula for emittance is obtained from the tune-shift formula by replacing σ_i^k with σ_i^j:

$$\begin{aligned} \varepsilon_x^j &= \frac{r_e N^k}{2\pi \xi \gamma^j (1 + r)} \\ \varepsilon_y^j &= r\, \varepsilon_x^j \end{aligned} \qquad \text{(A-4)}$$

A.4. Luminosity

For equal beam sizes, the luminosity is given by

$$\mathcal{L} = \frac{c N^+ N^-}{4\pi s_B \sigma_x \sigma_y},$$

where s_B is the bunch spacing. Substituting $\sigma_x\sigma_y = \beta_y\varepsilon_x$, and replacing N with the beam current, I (= ecN/s_B), we obtain the expression for the luminosity:

$$\mathcal{L} = \frac{\xi(1+r)}{2\,e\,r_e}\left(\frac{I\cdot E}{\beta_y^*}\right)_{+,-}$$
$$= 2.17\times 10^{34}\,\xi(1+r)\left(\frac{I\cdot E}{\beta_y^*}\right)_{+,-} \quad [\mathrm{cm^{-2}\,s^{-1}}] \qquad \text{(A-5)}$$

where I is in amperes, E is in GeV, and β_y is in cm. With the assumptions made here, the parenthetical expression in Eq. (A-5) can be evaluated with parameters appropriate to either beam.

Appendix B
Low-Energy Ring with Crab Crossing in the PEP Tunnel

Here we report on a preliminary design in which the two rings have the same circumference but the beams collide at an angle instead of head-on. To avoid synchrobetatron resonances in this scheme, the technique of "crab-crossing" is necessary.

As shown in Section 3, a head-on collision scheme poses some difficult (though not intractable) problems for the interaction region (IR) optics. For example, separation magnets must be placed close to the IR to peel the low-energy beam away from the high-energy beam before the high-energy beam enters its first strong focusing magnet; the low-energy beam cannot tolerate the focusing strength. This is a triple disadvantage: the separation fields cause synchrotron radiation to be emitted very close to the detector; the presence of the separation magnets forces the high-energy focusing quadrupoles to be placed further from the IP, making the beta functions and chromaticity larger; and, finally, the length of the separation system limits the closeness of the bunch spacing.

A crab-crossing design, in which the IR optics are decoupled by a finite crossing angle, escapes all these pitfalls. However, some penalties are incurred. The most obvious one is the requirement for large-angle crab cavities, with their unwanted impedances and their possibly difficult voltage tolerances. Another is the need to create a complicated horizontal crossing scheme, since vertical crossing would impose serious limitations on the cavity tolerances.

Several other penalties, which are interrelated, also come into play. In order to keep the weighted transverse impedance of the crab cavities within reasonable bounds, the beta function must be suppressed at the cavities; as a result, β_x at the IP has to be large and the beam must be flat. This loses the advantageous factor of two that is available for round beams, so β_y^* has to be reduced. This, in turn, forces a *very* short crab bunch and correspondingly high voltages. (A surprising consequence is that one needs significantly higher rf voltages in the low-energy ring than in the high-energy ring.)

Compensating advantages of the crab-crossing scheme are that the IR quadrupoles need not be superconducting and that the beams need not be excited vertically—the natural vertical emittance is acceptable and the collision process may behave in the way to which we have become acccustomed.

In the design presented here, both rings have the same circumference as PEP and would be installed in the PEP tunnel. The crossing plane is horizontal and the crab angle θ_x is about 1.4° (25 milliradians). The tune shifts adopted here ($\xi = 0.05$) are higher than those presently adopted for the round-beam design. The optics in the IR are not radical—they are of the familiar flat-beam type—and they can be realized easily with adequate dynamic aperture. Optically, it seems to be a comfortable design.

The rf system is another matter. The frequency is 706 MHz and every bucket is filled. We are compelled to abandon the familiar frequency of 353 MHz in the interests of closer bunch spacing with correspondingly lower bunch populations and shorter bunches. The klystrons will be physically smaller, but the power density at their windows (and the cavity windows) will be higher.

Table B-1 summarizes the major parameters of a design for a luminosity of 1×10^{34} cm^{-2} s^{-1}. The crossing configurations of the two beams in the horizontal plane (plan view) and in the vertical plane (elevation) are shown in Fig. B-1.

The lattice functions (square roots of the horizontal and vertical beta functions, and the dispersion $D_{x,y}$) for half of the low-energy ring are shown in Fig. B-2; the same functions are shown in Fig. B-3 for one-twelfth of the high-energy ring.

In the large low-energy ring, one has the normal FODO optics matched to the IP optics and a wiggler region around 720 m from the IP. A closer look at the optics in the low-energy ring near the IP is given in Fig. B-4.

Table B-1. Parameters of crossing angle design.

	Low-energy beam		High-energy beam
Energy, E [GeV]	3.1		9
Circumference, C [m]		2200.027	
Luminosity, $\mathcal{L}$ [cm^{-2} s^{-1}]		1×10^{34}	
Tune shifts, ξ_x/ξ_y		0.05/0.05	
Beta function at IP, β_x/β_y [cm]		50/1	
Current, I [A]	3.0		1.0
Natural bunch length, σ_ℓ [cm]		0.50	
Energy spread, σ_p/p	8.1×10^{-4}		6.0×10^{-4}
Bunch spacing, s_B [m]		0.42	
Particles/bunch, N_B	2.7×10^{10}		8.9×10^{9}
Emittance, $\varepsilon_x/\varepsilon_y$ [m-rad]		$1.3 \times 10^{-8}/2.7 \times 10^{-10}$	
Synchrotron tune, ν_s	0.170		0.047
Momentum compaction, α	3.1×10^{-3}		1.1×10^{-3}
Cavity rf voltage, V_{rf} (MV)	34.2		21.3
RF frequency, f_{rf} [MHz]		706	
Harmonic number, h		5184	
Longitudinal threshold, $\lvert Z/n \rvert_{eff}$ [Ω]	0.36		0.67
Energy damping decrement, T_0/τ_E		4×10^{-4}	
Crab angle, θ_x [mrad]		25	
Crab cavity frequency, f_x [MHz]		706	
Crab cavity voltage, V_x [MV]	1.4		2.5

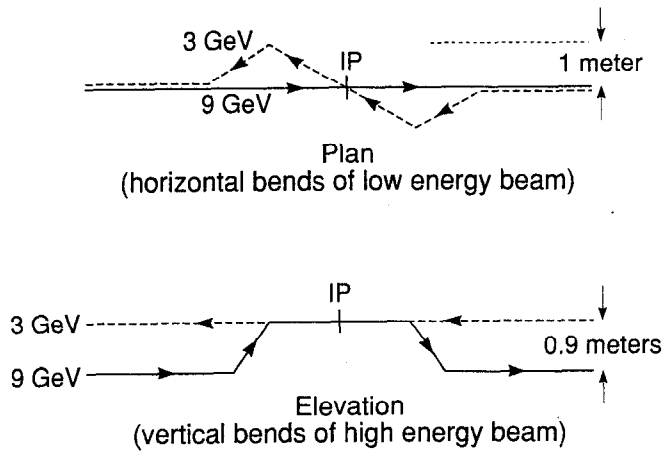

Fig. B–1. Crossing configuration of high and low energy beams in the horizontal plane (plan view) and vertical plane (elevation), respectively.

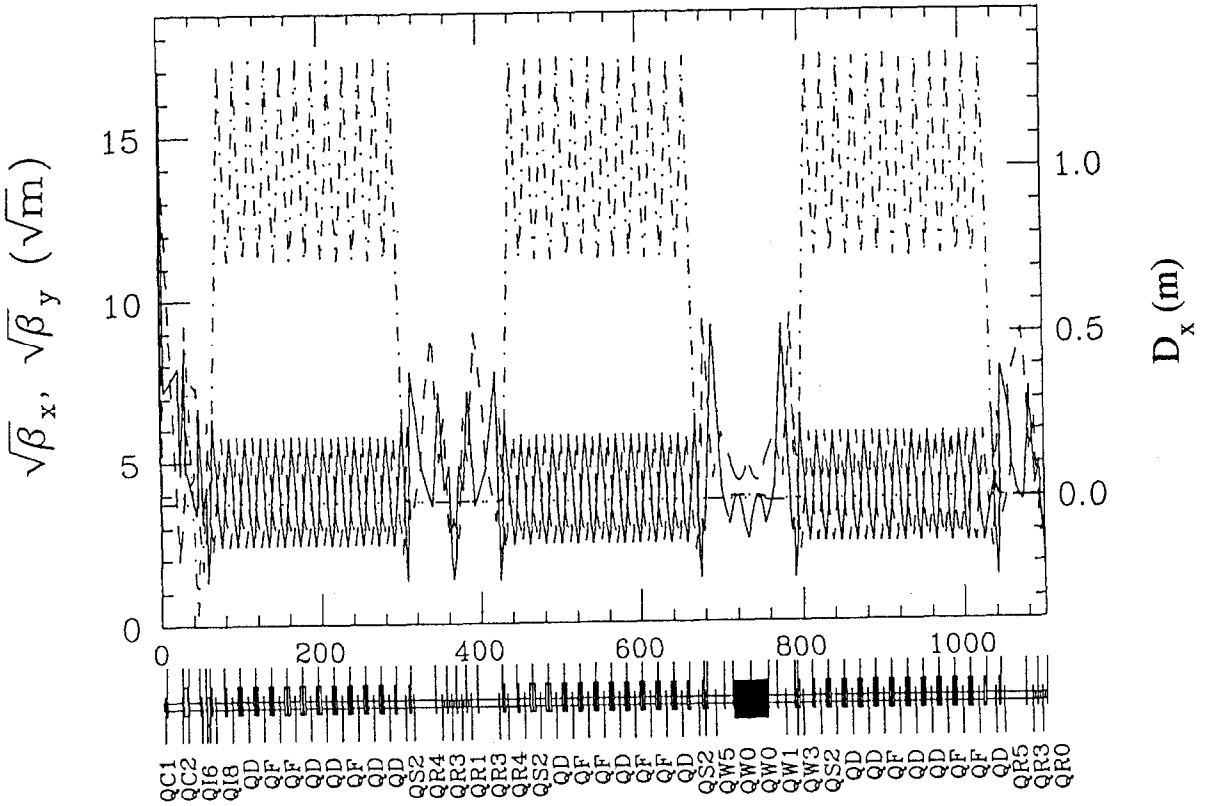

Fig. B-2. Lattice functions for one-half of the low-energy ring. Solid line: $\sqrt{\beta_y}$. Dashed line: $\sqrt{\beta_x}$. Dot-dashed line: D_x. Dotted line: D_y.

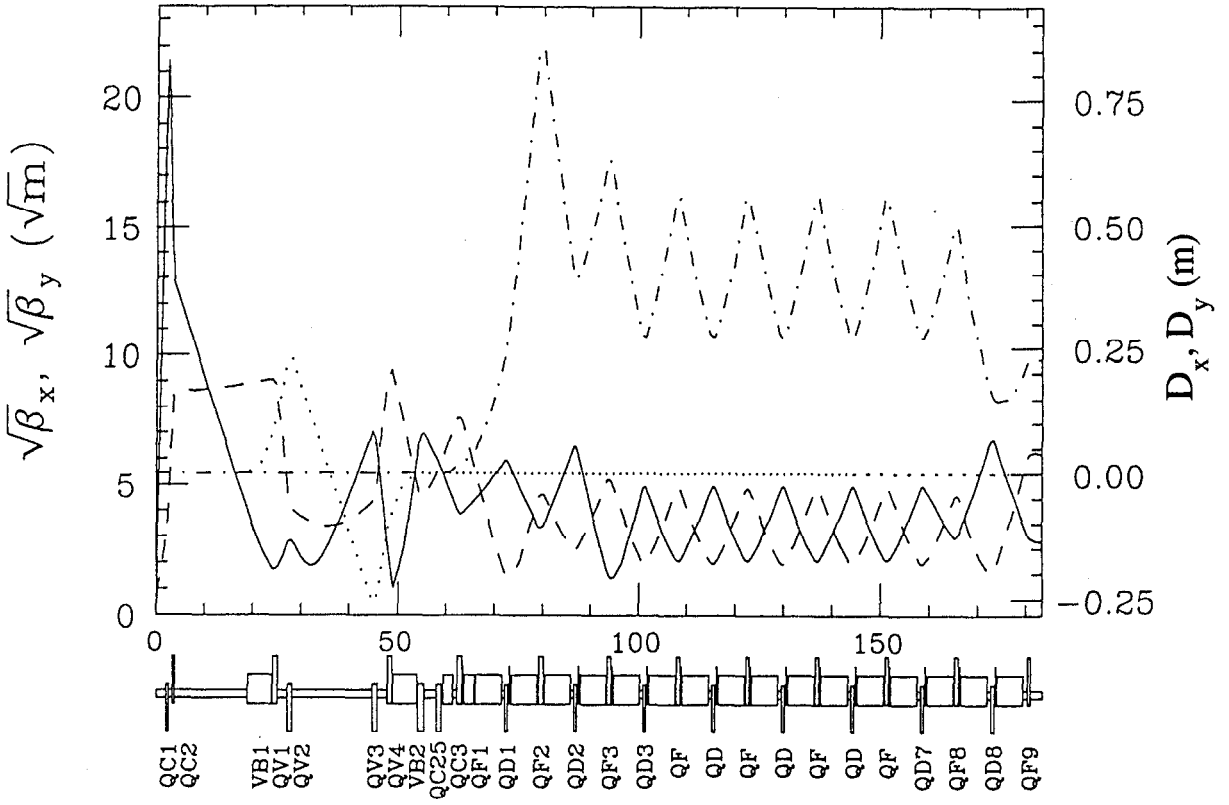

XBL 8910-7790

Fig. B-3. Lattice functions for one-twelfth of the high-energy ring. Solid line: $\sqrt{\beta_y}$. *Dashed line:* $\sqrt{\beta_x}$. *Dot-dashed line:* D_x. *Dotted line:* D_y.

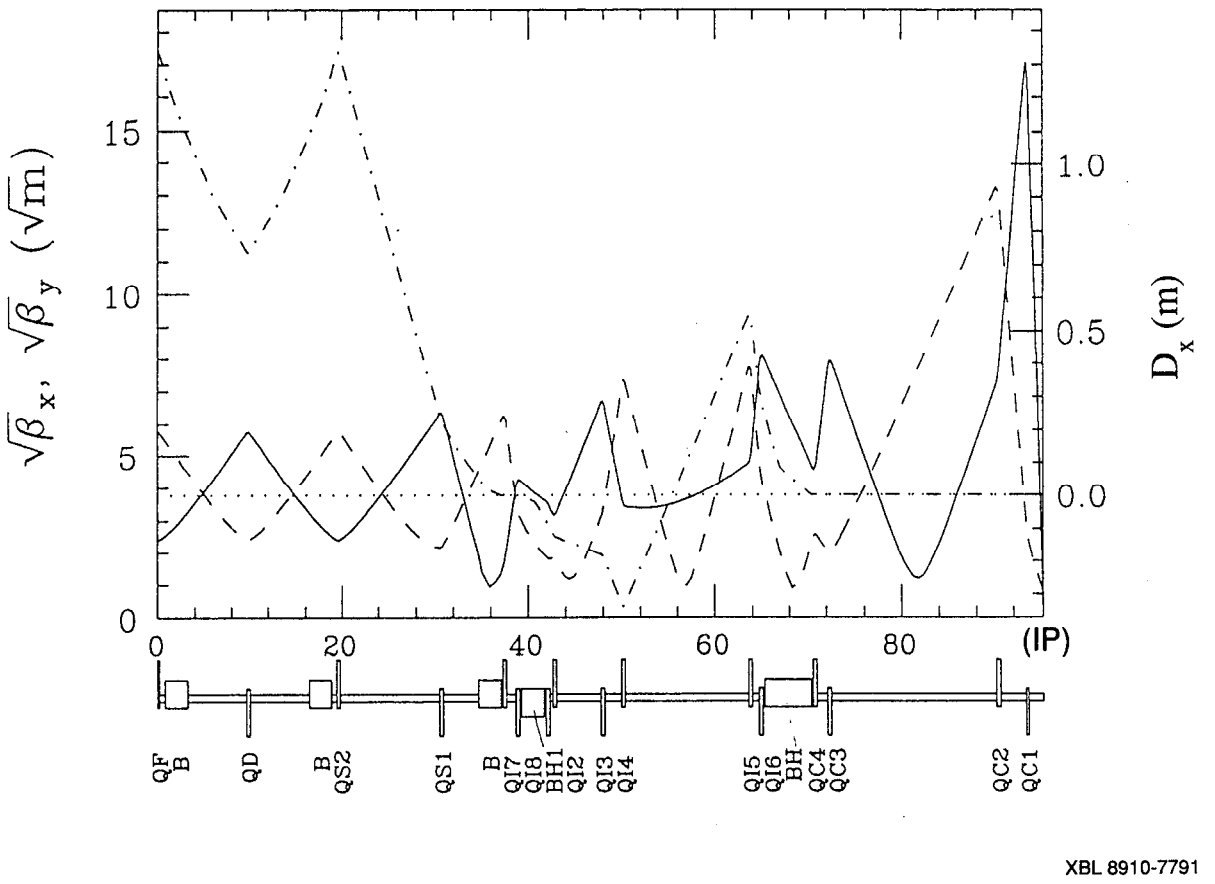

Fig. B-4. Optics in the low-energy ring near the IP. The bending magnets for the horizontal crossing are labeled BH and BH1. Solid line: $\sqrt{\beta_y}$ Dashed line: $\sqrt{\beta_x}$. Dot-dashed line: D_x. Dotted line: D_y.

Appendix C
Synchrotron Phase Damping

Consider coherent motion of the phase φ and energy deviation δE of the bunch centroid around φ_0 and ΔE_0:

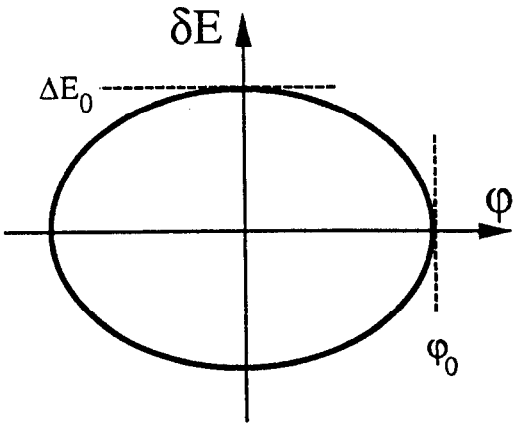

Equations of motion for phase and energy deviation, in the absence of feedback, are

$$\frac{d\varphi}{dt} = -\omega_s \frac{\varphi_0}{\Delta E_0} \delta E \qquad \text{(C-1)}$$

$$\frac{d(\delta E)}{dt} = \omega_s \frac{\Delta E_0}{\varphi_0} \varphi \qquad \text{(C-2)}$$

With feedback, we have an additional term

$$\frac{d(\delta E)}{dt} = \omega_s \frac{\Delta E_0}{\varphi_0} \varphi \qquad \text{(C-2)}$$

so the complete equation of motion in the presence of feedback is

$$\frac{d(\delta E)}{dt} = \frac{\omega_0}{2\pi} \beta\varphi + \omega_s \frac{\Delta E_0}{\varphi_0} \varphi \quad . \qquad \text{(C-4)}$$

In Eq. (C-4), β is the overall phase-to-energy gain of the feedback loop. Let the multibunch coherent motion be characterized by a complex frequency Ω, defined as $\Omega = \omega + ig$, such that

$$\delta E = E_0 e^{-i\Omega t} \quad . \tag{C-5}$$

From Eqs. (C-1), (C-4), and (C-5) we have

$$\Omega^2 = \omega_s^2 + \frac{\omega_s \omega_0}{2\pi} \frac{\varphi_0}{\Delta E_0} \beta \quad , \tag{C-6}$$

and

$$\omega^2 - g^2 + 2ig\omega = \omega_s^2 + \frac{\omega_s \omega_0}{2\pi} \frac{\varphi_0}{\Delta E_0} \left[\mathrm{Re}(\beta) + i\, \mathrm{Im}(\beta) \right] \tag{C-7}$$

For real β, there is no damping, but there is a coherent frequency shift of

$$\omega = \omega_s \left(1 + \frac{1}{2\pi} \frac{\omega_0}{\omega_s} \frac{\varphi_0}{\Delta E_0} \mathrm{Re}(\beta) \right)^{1/2} \tag{C-8}$$

The case of Re (β) < 0 corresponds to a phase delay. For Im (β) < 0, there is damping induced by the feedback, given approximately by:

$$\mathrm{Im}(\beta) \approx 2 \frac{g}{f_0} \frac{\Delta E_0}{\varphi_0} \tag{C-9}$$

Thus, the real energy gain per turn is given by:

$$\frac{d(\delta E)}{\mathrm{turn}} = \varphi_0 \, \mathrm{Im}(\beta) \approx 2 \frac{g}{f_0} \Delta E_0 \quad . \tag{C-10}$$